NASA
Technical
Paper
2306
C.3
May 1984

Aeropropulsive Characteristics of Nonaxisymmetric-Nozzle Thrust Reversers at Mach Numbers From 0 to 1.20

George T. Carson, Jr.,
Francis J. Capone,
and Mary L. Mason

NASA

NASA Technical Paper 2306

1984

Aeropropulsive Characteristics of Nonaxisymmetric-Nozzle Thrust Reversers at Mach Numbers From 0 to 1.20

George T. Carson, Jr.,
Francis J. Capone,
and Mary L. Mason

Langley Research Center
Hampton, Virginia

NASA
National Aeronautics
and Space Administration

Scientific and Technical Information Branch

SUMMARY

An investigation was conducted in the Langley 16-Foot Transonic Tunnel to determine the static and aeropropulsive performance of nonaxisymmetric-nozzle thrust reversers installed on a generic twin-engine fighter aircraft model. Percentages of reverser deployment and variation of reverser-port (passage) angle were investigated. Test data were obtained at static conditions and at Mach numbers from 0.15 to 1.20. Angle of attack was varied from -3° to 9° for selected configurations. High-pressure air was used to simulate jet flow, and the nozzle pressure ratio was varied from 1.0 (jet off) to 9.0.

Reverse-thrust levels of greater than 50 percent at static conditions and of greater than 30 percent at wind-on conditions were achieved with several of the reverser configurations. Internal reverser-port passage length was found to be very important in improving reverser performance. Increasing the port passage length improved reverse-thrust performance by as much as 28 percent at static conditions and by as much as 17 percent at Mach 1.20. Aft external doors improved reverser performance at static conditions and a nozzle pressure ratio of 2.5 by nearly 24 percent. Vectoring of the forward thrust while partially deploying reverse thrust was a more effective method of augmenting aircraft control during landing approach than was using top and bottom differential reverser-port angle.

INTRODUCTION

Recent studies have shown that thrust reversing has the potential to improve fighter aircraft operational characteristics (refs. 1 to 4). One major benefit is short take-off and landing (STOL) operation, which can allow the aircraft to operate from bomb-damaged runways. Thrust reversing could provide a shorter landing distance to match the short take-off distance inherent in a fighter aircraft with high thrust-to-weight ratio. At reverse-thrust levels of 50 percent of forward thrust, landing ground rolls of 350 to 500 m can be achieved.

Another major benefit is the ability to rapidly decelerate the aircraft in flight (compared with conventional speed brakes or reduced throttle settings) and thus gain another dimension in maneuverability. High throttle settings can be maintained, thereby taking advantage of the significant inlet momentum drag component in addition to the reversed gross thrust. Operation of this type of reverser eliminates the need to "spool up" the engine from an idle power setting and reduces time to reaccelerate to the desired speed. Although no definite requirements for in-flight reverse-thrust levels have been established, an in-flight reverse thrust of 30 percent of forward thrust was assumed in some early studies summarized in reference 1.

References 1 and 5 indicate that in-flight thrust reversing systems are particularly adaptive to twin-engine aircraft with nonaxisymmetric nozzles, because the inclusion of these systems can result in less weight penalty than with comparably equipped axisymmetric nozzles. The purpose of this investigation was to determine static and aeropropulsive performance of nonaxisymmetric-nozzle thrust reversers over a range of Mach numbers, nozzle pressure ratios, and angles of attack. Two main

nozzle-reverser design variables were investigated: percentage of reverser deployment and reverser-port exit angle. The nozzle design used to study the percentage of reverser deployment was based on a nozzle configuration from reference 6 and included a configuration which provided simultaneous thrust vectoring and reversing. Other nozzle variables investigated were internal port passage length, forward and aft external doors, sidewalls, and differential top and bottom port angles.

This investigation was conducted in the Langley 16-Foot Transonic Tunnel from static conditions to a free-stream Mach number of 1.20, from nozzle pressure ratios of 1.0 (jet off) to approximately 9.0, and from angles of attack of -3° to 9°.

SYMBOLS

Model forces and moments are referred to the stability-axis system with the model moment reference center located at $0.25\bar{c}$, the point which corresponds to fuselage station (FS) 104.30 cm at 4.45 cm above the model center line. All aerodynamic coefficients are nondimensionalized with respect to $q_\infty S$ or $q_\infty S\bar{c}$ except at static conditions, for which p_a is substituted for q_∞.

A_e nozzle exit area, cm^2 (see fig. 8)

A_{max} model cross-sectional area (maximum) at FS 113.67 cm, cm^2 (see fig. 8)

A_{seal} cross-sectional area enclosed by seal strip at FS 113.67 cm, cm^2 (see fig. 2)

A_t base-line nozzle throat area, cm^2 (see fig. 8)

AR nozzle throat aspect ratio, b_n/h_t (see fig. 8)

b_n width of nozzle throat, cm (see fig. 8)

$C_{(D-F)}$ drag-minus-thrust coefficient

C_F thrust coefficient

$C_{F,i}$ ideal isentropic gross thrust coefficient

C_L lift coefficient including thrust component

C_m pitching-moment coefficient including thrust component

$C_{m,n}$ nozzle pitching-moment coefficient

C_{m_δ} trim effectiveness, per degree

$C_{m_{\delta_h}}$ horizontal-tail effectiveness (excluding nozzles), per degree

$C_{m,n_{\delta_v}}$ thrust-vector effectiveness (nozzles only), per degree

$C_{m,n_{\delta_\theta}}$ differential reverser-port angle effectiveness (nozzles only), per degree

C_N normal-force coefficient

C_p pressure coefficient, $\frac{p_e - p_\infty}{q_\infty}$

$\bar{c}$ wing mean geometric chord, 44.42 cm

D total drag on metric portion of model, N

D_f skin-friction drag, N

F thrust measured along stability axis, N

F_A axial force, N

$F_{A,main}$ axial force measured with main balance, N

$F_{A,mom}$ momentum tare axial force due to bellows, N

F_g gross thrust in direction of the thrust vector, N

F_i ideal isentropic gross thrust, N

F_j thrust along body axis, N

h_b vertical distance from nozzle center line to upstream edge of reverser port

h_e exit height of base-line (forward-thrust) nozzle, cm

h_t nozzle throat height, cm

l_n length from nozzle throat to exit of the base-line (forward-thrust) nozzle, cm (see fig. 8)

M free-stream Mach number

$\dot{m}$ measured mass-flow rate, kg/sec

$\dot{m}_i$ ideal mass-flow rate, kg/sec

NPR nozzle pressure ratio, $p_{t,j}/p_a$ for $M = 0$ and $p_{t,j}/p_\infty$ for $M > 0$

N_j thrust normal force, N

p_a atmospheric pressure, Pa

p_e external afterbody and nozzle surface pressure, Pa

p_i internal static pressure, Pa

p_s average static pressure at external seal at FS 113.67 cm, Pa

$p_{t,j}$ jet total pressure, Pa

p_∞ free-stream static pressure, Pa

q_∞ free-stream dynamic pressure, Pa

R gas constant for air, 287.3 J/kg-K

S wing reference area, 4290.0 cm^2

s thrust-reverser-port passage uncontained length, cm (see fig. 13)

$T_{t,j}$ jet total temperature, K

v thrust-reverser-port passage contained length, cm (see fig. 13)

w_v width of reverser ports, cm (see fig. 13)

x axial distance from base-line (forward-thrust) nozzle throat, positive downstream, cm (see fig. 9)

y lateral distance measured from nozzle center line, positive to the right looking upstream, cm (see fig. 9)

α angle of attack, deg

γ ratio of specific heats, 1.3997 for air at 300 K

δ effective jet-turning angle, deg

δ_v geometric nozzle-turning angle, deg

θ reverser-port angle, deg

Λ_{le} leading-edge sweep angle, deg

Subscripts:

b bottom of reverser nozzle

F forward-thrust mode

R reverse-thrust mode

t top of reverser nozzle

Abbreviations:

ASME American Society of Mechanical Engineers

BL buttock line, cm

FS fuselage station, cm

LE leading edge

STOL short take-off and landing

TE trailing edge

WL water line, cm

2-D C-D two-dimensional convergent-divergent

APPARATUS AND PROCEDURE

Wind Tunnel

This investigation was conducted in the Langley 16-Foot Transonic Tunnel. This facility is a single-return, continuous-flow, exchange-air-cooled, atmospheric-pressure wind tunnel with an octagonal, slotted-throat test section. It has a continuously variable air speed up to a Mach number of 1.30. A detailed description of this wind tunnel is given in reference 7.

Models and Support System

Forward- or reverse-thrust nozzles were installed on a wing-tip-support model simulating a generic twin-engine fighter aircraft. The base-line (forward-thrust) nozzle of this investigation was the base-line dry-power nozzle of reference 8. A photograph of the wind-tunnel model with the base-line (forward-thrust) nozzle installed is shown in figure 1. A detailed sketch of the aircraft-nozzle model and support system without empennage surfaces is shown in figure 2. The support system consisted of three major components: the wing-tip support booms, the forebody, and the wing-centerbody combination. The forebody approximated the forward fuselage of a high-performance aircraft with faired-over inlets. The centerbody had a constant height and width of 12.70 cm and 25.40 cm and had rounded corners of a 2.54-cm radius, which gave a maximum cross-sectional area of 317.04 cm^2. The wing, whose half-span planform geometry is shown in figure 3, was mounted on the fuselage centerbody in a high position. (See fig. 1.) It has an aspect ratio of 2.40, a taper ratio of 0.43, and a cranked trailing edge. The NACA 64-series airfoil had a thickness ratio of 0.067 near the wing root to provide a realistic wake on the afterbody. However, outboard on the wing, from BL 27.94 to the support booms, it was necessary to increase the thickness ratio from 0.077 to 0.100 for structural support and for compressed air and instrumentation passages.

The metric portion of the model (aft of FS 113.67 cm), supported by the main force balance, consisted of the propulsion system, the afterbody, and the nozzles. The afterbody lines (boattail) were chosen to provide a length of constant cross section aft of the nonmetric centerbody and to enclose the force balance and jet simulation system apparatus while fairing smoothly downstream into the closely spaced nozzles. The afterbody shell from FS 122.56 cm to 168.28 cm was attached to a tandem force balance, which was attached to the main force balance (fig. 1). The main force balance in turn was grounded to the nonmetric wing-centerbody panel. The nozzles were attached directly to the thrust-minus-drag balance through the propulsion system piping. A clearance gap (metric break) was provided between the nonmetric and the individual metric portions (afterbody and nozzles) of the model to prevent fouling of the components on each other. A flexible plastic strip inserted into machined grooves in each component impeded flow into or out of the internal model cavity.

The location of the tail fins as mounted on the afterbody shell is shown in figure 4. Geometric details of the horizontal- and vertical-tail fins are given in figures 5 and 6.

Twin-Jet-Propulsion Simulation System

For jet-propulsion simulation, the Langley 16-Foot Transonic Tunnel is equipped with an external high-pressure air system which provides a continuous flow of clean, dry air at a nominal controlled temperature of 300 K ahead of the nozzle throat. Two remotely operated flow-regulating valves were used to balance the jet total pressure in the left- and right-hand nozzles. The airflow path can be traced using the sketch in figure 2. Compressed air flowed through the wing-tip support booms, then through each side of the wing into two flow-transfer bellows assemblies. The bellows assemblies, one of which is shown in figure 7, provided the means of transferring compressed air from the nonmetric to the metric portions of the model. In order to eliminate incoming axial momentum, air was discharged radially through eight equally spaced sonic nozzles. Two flexible metal convolutions (bellows) served as seals. The airflow then passed successively through a tailpipe, a circular-to-rectangular transition section, a choke plate, and an instrumentation section, and then expanded through the nozzle configuration being tested. (See fig. 2.)

Design Rationale of the Nozzle Models

Base-line (forward-thrust) nozzle.- The base-line (forward-thrust) nozzle shown in figure 8 is a nonaxisymmetric (two-dimensional), convergent-divergent nozzle simulating a dry-power operating mode with a design NPR $\approx$ 3.5. The nozzle expansion ratio was selected to be consistent with advanced mixed-flow turbofan engines. The following parameters were held constant for all nozzle configurations: A_t, b_n, h_t, AR, and $2A_t/A_{max}$. The sketch in figure 9 shows the base-line (forward-thrust) nozzle installed on the model as well as pressure orifice locations and the pressure orifice coordinate system used throughout this investigation.

Thrust-reverser deployment configurations.- The nozzle configurations used for the thrust-reverser deployment study are shown in the sketches in figure 10. This family of nozzle configurations simulates a single nozzle design with varying percentages of thrust-reverser deployment (nominal values of 25, 50, 75, and 100 percent) in which the percent deployment is the ratio of reverser-port area to total throat area of the base-line nozzle (0-percent reverser deployment) shown previously in figure 8. Increasing the percentage of reverser deployment (from 0 to 100 percent) represents conditions from forward cruise flight through various amounts of thrust modulation to full thrust reversing that can be used throughout the flight envelope of advanced fighter aircraft (refs. 1 and 3). This nozzle design was based on a realistic design shown in reference 6 (i.e., it contains actuators, structure, cooling, and so forth). The photographs in figure 11 show the 100-percent-deployed thrust-reverser nozzle installed on the model.

Combined thrust reversing and vectoring was investigated with the model which nominally had 50-percent thrust-reverser deployment (illustrated in fig. 12). This configuration retains approximately 50 percent of the forward thrust, which could be vectored upward or downward 15°. Although combined thrust reversing and vectoring could be used throughout the entire flight envelope for additional airplane trim and control power, it was tested only at static conditions and at $M = 0.15$, typical landing approach conditions. This reversing and vectoring mode of operation could be

used either for primary control or to augment aerodynamic controls while simultaneously modulating thrust for slower touchdown speeds.

Thrust-reverser-port angle configurations.- Four generic-type-nozzle thrust-reverser configurations were tested to investigate the effects of port exit angle θ, port passage length, and external doors and sidewalls. Configurations for three reverser-port angles (110°, 120°, and 130°) shown in figure 13 were designed to have ideal static reverse-thrust levels of 34 percent for $\theta = 110°$, 50 percent for $\theta = 120°$, and 64 percent for $\theta = 130°$. The magnitude of static reverse thrust obtained is primarily a function of $\cos \theta$. The top and bottom port areas were each equal to half the throat area of the base-line dry-power nozzle. (See fig. 8.) The photograph in figure 14 shows an upstream view of the reverser nozzle with $\theta = 110°$ installed on the model.

An alternate reverser configuration for $\theta = 110°$, which had a short internal passage length, was tested with and without forward and aft external doors and sidewalls, as shown in figure 15. This figure shows that the forward and aft external doors increased reverser-port passage length when installed. Note that the uncontained length of the passage s and the contained length of the passage v increased with the external doors installed and that the vertical distance from nozzle center line to upstream edge of reverser port h_b and the port width w_y remained the same with or without the external doors. (See figs. 13 and 15.) References 9 and 10 present results on the effects of varying external doors, sidewalls, and passage lengths at static conditions. This investigation extended that data base to wind-on conditions.

Differential variation of top and bottom port angles (different port angles on top and on bottom) as a trim device during landing approach ($M = 0.15$) was investigated using the models illustrated in figure 16. These configurations had a 130° reverser-port angle on top and either a 110° or a 120° reverser-port angle on the bottom. The configurations shown in figure 16 provided net upward thrust. In order to investigate net downward thrust, the top and bottom model parts were exchanged on each nozzle.

Instrumentation

Forces and moments on the metric portions of the model were measured with two six-component strain-gage balances. The main balance connected the nonmetric wing-centerbody combination and the metric aft-end model parts and measured forces and moments (external and internal) on the nozzles, the afterbody shell, and the tail surfaces. The second balance, which was rigidly connected to the main balance, measured forces and moments on the afterbody shell and tail surfaces only. This tandem balance arrangement allowed separation of nozzle forces and moments from the total forces and moments.

Eight static pressures were measured in the seal gap at the first metric break (FS 113.67 cm). All orifices were located on the nonmetric centerbody and spaced symmetrically around the model perimeter. An additional five orifices on the right side of the model measured seal gap pressures at the second metric break (FS 122.68 cm). A third set of pressures were measured with surface orifices near the third metric break (FS 168.28 cm). These orifices, used to approximate seal pressures in the gap which was too thin to accommodate pressure taps, also formed part of the afterbody pressure orifice system on the center line of the right nozzle

as shown in figures 2 and 9. Also, two internal pressures were measured at the fuselage stations where each of the metric breaks was located. All the aforementioned pressures were used for pressure-area corrections to the balances as described in the "Data Reduction" section.

Chamber pressure and temperature measured in the supply pipe upstream of the eight sonic nozzles (see fig. 7) were used to compute mass-flow rate. Jet exhaust conditions were measured in an instrumentation section upstream of each nozzle. Instrumentation consisted of a total-temperature probe and a total-pressure rake in each section. Each rake contained four total-pressure probes as shown in figure 8.

External static pressures on the base-line (forward-thrust) nozzle were measured with orifices located as shown in figure 9. Nozzle internal static pressures were not measured on the base-line nozzle during this investigation, since it was expected they were the same as those presented in reference 8. Internal and external surface pressures on the family of nozzles with varying thrust-reverser deployment were measured at orifices located as given in figure 10. Internal and external surface pressures on the family of nozzles with varying thrust-reverser-port angles were measured at orifices located as given in figure 13.

Data Reduction

All data from the instrumentation of the aircraft-nozzle model and the wind-tunnel facility were recorded simultaneously on magnetic tape. For each data point, 50 frames of data were taken over a period of 5 sec and the average value was used for computation.

The main balance (see fig. 2) measured total thrust and aerodynamic forces and moments on all metric portions (afterbody, nozzles, and tails) of the model. The drag balance measured aerodynamic and internal forces and moments on the afterbody shell and on the tails only. Force and moment interactions existed between the main balance and the bellows (flow-transfer) system because of the balance offset from the model center line. (See fig. 2.) Consequently, single and combined normal-force and pitching-moment calibrations were performed to determine these interactions with and without the jets operating. The determination of these interactions was similar to the method outlined in the appendix of reference 11.

Thrust minus axial force was computed from the main balance axial force using the following relationship:

$$F_j - F_A = F_{A,main} + (p_s - p_\infty)(A_{max} - A_{seal}) + (p_i - p_\infty)A_{seal} - F_{A,mom} + D_f$$

The first term, $F_{A,main}$, is the total axial force measured with the main balance and corrected for the bellows interaction discussed earlier. The second term, $(p_s - p_\infty)(A_{max} - A_{seal})$, is the correction for the pressure-area force in the first metric break gap at FS 113.67 cm. The third term, $(p_i - p_\infty)A_{seal}$, is the correction for the pressure-area force caused by differences in internal-cavity and free-stream pressure. The term $F_{A,mom}$, which ideally should be zero, is an exhaust flow momentum tare correction and is a function of the bellows internal pressure, which is a function of the chamber pressure in the supply pipes just ahead of the sonic nozzles. It was correlated with chamber pressure by static tests (M = 0) by using ASME standard calibration nozzles for which F_j/F_i was known over a wide range of chamber

pressure. The last term, D_f, is the computed skin-friction drag of the model afterbody section from FS 113.67 cm to FS 122.68 cm. This friction term was added to the main balance reading in order to have axial-force data for both balances start at the same fuselage station, that is, FS 122.68 cm.

Since the force balance was offset from the model center line, a similar adjustment was made to the pitching moment. This adjustment was necessary because the pressure-area tare force was assumed to act along the model center line. The pitching-moment tare was determined by multiplying the tare force by an appropriate moment arm and subtracting the value from the measured pitching moments.

Although afterbody force and moment data measured with the drag balance are not presented for this investigation, nozzle pitching-moment coefficient $C_{m,n}$ is presented. This coefficient was determined by subtracting afterbody pitching-moment coefficient (measured with the drag balance) from C_m.

The adjusted forces and moments measured with both balances were transferred from the body axis (which lies in the horizontal-tail chord) of the metric portion of the model to the stability axis. Attitude of the nonmetric forebody relative to gravity was determined from a calibrated attitude indicator located in the model nose. Angle of attack α, which is the angle between the afterbody center line and the relative wind, was determined by applying terms for afterbody deflection (caused when the model and balance bent under aerodynamic load) and a term for flow angularity to the angle measured with the attitude indicator. The flow angularity adjustment was 0.1°, which is the average angle measured in the Langley 16-Foot Transonic Tunnel.

The ideal isentropic gross thrust F_i, which was used to evaluate measured performance, is defined as

$$F_i = \dot{m}\left\{\frac{2\gamma}{\gamma - 1} RT_{t,j}\left[1 - \left(\frac{p_\infty}{p_{t,j}}\right)^{\frac{\gamma-1}{\gamma}}\right]\right\}^{1/2}$$

where $\dot{m}$ is the mass-flow rate measured at the sonic nozzles of the bellows assemblies. The base-line nozzle throat area was used to compute ideal mass-flow rate for all nozzle configurations. After assembly of each nozzle configuration, the actual throat areas were measured. These values are given in table 1.

For evaluation of a configuration which combined thrust modulation (partial thrust-reverser deployment) and thrust vectoring at static conditions (M = 0), gross thrust F_g and effective jet-turning angle δ were defined as

$$F_g = \left(F_j^2 + N_j^2\right)^{1/2}$$

and

$$\delta = \tan^{-1} \frac{N_j}{F_j}$$

Test Conditions

This investigation was conducted in the Langley 16-Foot Transonic Tunnel at static conditions (M = 0) and at free-stream Mach numbers from 0.15 to 1.20. The nozzle pressure ratio was varied from 1.0 (jet off) to 9.0, depending on free-stream Mach number. The angle of attack was varied from -3° to 9°. At M = 0.15 (free-stream velocity of about 100 knots), the ratio of jet dynamic pressure to free-stream dynamic pressure varied linearly from 45.2 at NPR = 2.0 to 87.1 at NPR = 3.8. For actual aircraft landing approach conditions, this ratio normally lies in the range from 40.0 to 70.0.

In accordance with the criteria of reference 12, boundary-layer transition strips were used to ensure a turbulent boundary layer over the afterbody and the nozzles. A 0.254-cm-wide strip of No. 120 silicon carbide grit, sparsely distributed in a lacquer film, was located 2.54 cm from the nose of the forebody and proportionally along the wing and tail-fin spans at 5 percent of the root chord and 10 percent of the tip chord. The average Reynolds number per meter varied from 7.0×10^6 to 13.5×10^6.

PRESENTATION OF RESULTS

The results of this investigation are presented graphically for selected conditions in figures 17 to 46. Figures 17 to 36 show force and moment data; figures 37 to 46 show pressure distribution data. An index relating the nozzle configurations to force, moment, and pressure distribution data figures is given in table 2. Force and moment data for all conditions are given in tables 3 and 4 for static and wind-on conditions, respectively.

DISCUSSION

Base-Line (Forward-Thrust) Nozzle

The static performance F_j/F_i and discharge coefficient $\dot{m}/\dot{m}_i$ of the base-line (forward-thrust) nozzle are shown in figure 17, and the aeropropulsive performance at Mach numbers of 0.15, 0.60, 0.90, and 1.20 is shown in figure 18. The base-line static performance obtained during this investigation is typical of other nonaxisymmetric convergent-divergent nozzles (refs. 11 and 13). The variation of ideal thrust coefficient with nozzle pressure ratio for the base-line (forward-thrust) nozzle is shown in figure 19 for static and wind-on conditions.

Thrust-Reverser Deployment Configurations

Static performance.- The effect on static performance and discharge coefficient of varying reverser deployment from 25 to 100 percent is shown in figure 20. The 0-percent reverser deployment configuration (base line) was presented previously in figure 17. Reference 1 has indicated that for landing operations, reverse-thrust levels of 50 percent of the ideal thrust are desirable for effective ground-roll reduction. Although this was not achieved for this nozzle design, an improvement in reversing performance is probably possible by redesign of the reverser ports. No improvement in reverse-thrust performance was achieved by addition of port sidewalls to the configuration with 100-percent reverser deployment. The sidewalls and sidewall locations were the same as for the configuration shown in figure 15. The data obtained from testing this configuration are not presented since they were coincident with the configuration without sidewalls.

Deployment of a nozzle thrust reverser requires consideration of the resulting discharge coefficient $\dot{m}/\dot{m}_i$. If the reverse-thrust mode discharge coefficient is significantly lower or higher than the forward-thrust mode discharge coefficient, engine operation can be adversely affected unless the port area is increased or decreased to compensate. The variation of $\dot{m}/\dot{m}_i$ because of reverser deployment shown in figure 20(b) is small, being less than ± 8 percent from the base-line nozzle. Since small variations of $\dot{m}/\dot{m}_i$ do not significantly affect engine flow rate and back pressure, no change of port area for a full-scale nozzle should be necessary.

Discharge coefficients for some of the configurations exceeded unity (see fig. 20(b)) apparently for two reasons: the effective throat area probably exceeded the geometric throat area as a result of skewed and curved normal shock fronts, and some geometric throat areas were larger than the reference throat areas (used to compute $\dot{m}_i$) of the base-line nozzle (as previously discussed in the "Data Reduction" section). The data of figure 20(b) can be corrected for throat area variations by multiplying by $A_t/A_{t,R}$ as shown by the solid symbols of figure 20(b). This correction adjusts the discharge coefficients of the various deployed reverser configurations to values which are closer (within ± 4 percent) to the discharge coefficient of the base-line nozzle.

Aeropropulsive performance.- The aeropropulsive performance for the thrust-reverser deployment configurations at $M = 0.15$, 0.60, 0.90, and 1.20 is presented in figure 21. Base-line (forward-thrust) nozzle aeropropulsive performance was presented previously in figure 18. As indicated in reference 1, reverse thrust equal to 30 percent of ideal thrust may be sufficient for improved deceleration capabilities at all flight conditions. The data of figure 21 indicate that reverse-thrust levels of this magnitude and considerably greater can be generated with the current nozzle design at typical operating nozzle pressure ratios when the reverser is deployed 75 to 100 percent, depending on Mach number. A schedule of typical operating nozzle pressure ratios with Mach number is given in table 5. These values are also indicated with arrows on the figures presenting aeropropulsive data. The small effect of Mach number on discharge coefficient for each of the reverser deployments shown in figure 21(e) indicates little or no external flow suppression on nozzle internal flow.

Thrust-reverser effectiveness.- Thrust-reverser effectiveness at forward speeds can be expressed as the ratio $(F - D)_R/(F - D)_F$. Results from the present investigation are compared with other nonaxisymmetric nozzles (refs. 13 and 14) and with an

axisymmetric nozzle (ref. 15) in figure 22. This figure shows that the nonaxisymmetric nozzles generally have better reversing effectiveness than the axisymmetric nozzle of reference 15 for deployments up to about 85 percent. Typically, aeropropulsive reversing effectiveness is approximately twice the static (M = 0) reversing performance at a thrust-reverser deployment of 100 percent (ref. 10). This improvement in effectiveness is due to base drag developed on the rear of reverser panels at forward speeds. The NPR values used for the comparison in figure 22 are the maximum NPR values available for the axisymmetric nozzle.

Thrust reversing and vectoring.- It is possible to augment airplane pitch control during partial thrust-reverser deployment (during landing approach, for example) by vectoring that portion of jet exhaust flow which passes through the normal nozzle throat. During the present investigation, thrust-vector angles of $\pm 15°$ were tested on the 50-percent-deployed thrust-reverser configuration. (See fig. 12.) The basic static performance parameters are shown in figure 23. It should be noted that F_g is the gross thrust in the direction of the thrust vector and F_j is the thrust in the body axis (and thus includes geometric turning losses). As indicated in figure 23(b), the resultant effective jet-turning angles δ were significantly different from the geometric nozzle-turning angles δ_v. For example, at $\delta_v = 0°$, the effective jet-turning angle varied from about -21° to -10° depending on nozzle pressure ratio. The skewed turning characteristics may be caused by asymmetry of the model or by different top and bottom exit areas. (See table 1.) Aeropropulsive characteristics were determined at typical landing approach conditions (M = 0.15) and are presented in figure 24. These data show a slight improvement in reversing performance when thrust vectoring is simultaneously used.

In order to show the effects of thrust vectoring, nozzle pitching-moment coefficient is presented in figure 25 at static conditions and at M = 0.15. Nozzle pitching-moment coefficient is the difference between total pitching-moment coefficient measured with the main balance (thrust included) and the pitching-moment coefficient measured with the afterbody balance (no thrust). Pitching-moment coefficients for the wind-on condition were larger than at static conditions because of the relative levels of p_a and q_∞. Figure 26 shows that nozzle pitching-moment coefficients did not vary significantly with angle of attack. The nonlinear variation of nozzle pitching-moment coefficient with δ_v at either constant nozzle pressure ratio at $\alpha = 0°$ or at constant angle of attack at NPR = 2.6 probably results from the model asymmetries or from different top and bottom exit areas, as previously discussed. The effectiveness of thrust vectoring for control is compared with horizontal-tail effectiveness in a subsequent section.

Thrust-Reverser-Port Angle Configurations

Static performance.- The effects of varying reverser-port angle on static performance and discharge coefficient are shown in figure 27. This figure shows that each of the three nozzles either achieved or exceeded their design goals (as defined by $\cos \theta$) at nozzle pressure ratios up to 2.5, which are typical static operating nozzle pressure ratios.

It is apparent that the discharge coefficient, which decreases with increasing reverser-port angle, is low (compared with the base-line nozzle) for this family of thrust-reverser designs. The reduction in discharge coefficient was probably caused by flow separation around the sharp lip at the entrance of the reverser port, which results in a much reduced effective port throat area. Also, reference 16 shows the existence of a highly skewed sonic line in the port, which can contribute to the

large losses experienced by this reverser. Even with low discharge coefficients, effective reversing is achieved.

Aeropropulsive performance.- Figure 28 shows the aeropropulsive performance for this family of reverser-thrust nozzles at $M = 0.15$, 0.60, 0.90, and 1.20. These results indicate that $(F - D)/F_i = -0.3$ in-flight deceleration was easily obtainable for the three configurations at all Mach numbers because of the increasing amount of base drag as Mach number increased.

Effect of port passage length.- An alternate nozzle configuration (fig. 15) with a reverser-port angle θ of 110° and a short internal passage length was tested with and without external doors and sidewalls. The main rationale for this configuration was to reduce the sharp reverser-port-entrance lip and its associated separation loss. The purpose of the external doors and sidewall was to provide the same port internal passage length as the basic 110° reverser-port nozzle but at a different vertical location. However, because of the vertical displacement of the port, nozzle internal geometry was also different. The external doors also simulated possible full-scale hardware which could be used to open the reverser port during thrust-reverser operation. Previous studies (refs. 10 and 13) have shown that reverser-port sidewalls can improve thrust-reverser performance.

Figure 29 shows that the alternate reverser configuration with the short internal passage length ($v/w_v = 0.03$) had poorer static performance compared with the basic 110° reverser configuration ($v/w_v = 1.42$). Decreases in reverser thrust levels range from about -87 percent at $NPR = 2.0$ to about -46 percent at $NPR = 7.0$. The average reverse-thrust level for the alternate configuration indicates a resultant flow angle of about 98° compared with 109° for the long internal passage length design, which implies reduced flow-turning capability for short internal passage length reverser ports. The reverse-thrust performance for the configuration with the external doors and sidewalls is about 7 percent less than the basic configuration, even though both configurations had the same port internal passage length (fig. 29). The difference in performance between these two configurations is attributed to the difference in length of the uncontained forward passage wall (difference in s/w_v). The reverser-port exit geometry is similar to a single expansion ramp nozzle in that the forward (free-expansion) surface outside the passage is pressurized by the port exhaust flow (ref. 9) and develops a force component in the forward-thrust direction at higher nozzle pressure ratios. This force component in the forward-thrust direction varies with nozzle pressure ratio in the same manner as the normal-force component on the external portion of the ramp of a single expansion ramp nozzle (refs. 11 and 13). It is expected that the magnitude of the vector will increase with nozzle pressure ratio and uncontained forward passage wall length s (see fig. 13), resulting in a decrease in reverse-thrust performance. The increase in discharge coefficient $\dot{m}/\dot{m}_i$ for the configurations with the short internal passage length or with sidewalls and external doors is probably due to reduced internal flow separation, since the lip angle on the alternate configurations is smaller than on the basic configuration.

The aeropropulsive performance for the basic and alternate configurations is presented in figure 30 and shows that the configurations with the long internal passage length ($v/w_v = 1.42$) gave better reversing performance than those with the short internal passage length ($v/w_v = 0.03$). This would be expected because of the reduced turning capability of the short internal length port discussed previously for the static data. These figures show that increasing port passage length improved reverse-thrust performance by as much as 28 percent at static conditions with $NPR = 2.5$ and by as much as 17 percent at $M = 1.20$ with $NPR = 7.0$.

The effects of forward speed on the two configurations with the same passage lengths ($v/w_v = 1.42$) are also illustrated in figure 30. Reverse-thrust levels were about equal at $M = 0.15$, even though reverse thrust for the basic configuration at $M = 0$ was larger. At $M = 0.60$, the alternate configuration (short internal passage length) had better performance. This crossover in performance from static conditions to forward speeds is probably caused by an increase in base drag on the rear door. Addition of these doors increased base area approximately 45 percent over the basic reverser.

Effect of external doors and sidewalls.- The alternate nozzle of figure 14 was tested with various combinations of external doors and sidewalls. The static performance and discharge coefficient are shown in figure 31. Highest reverse-thrust performance was obtained by use of aft external doors (resulting in an uncontained aft wall) with sidewalls. As discussed previously, an uncontained port wall (similar to a vertically oriented single expansion ramp nozzle) tends to be pressurized by the jet exhaust flow. However, opposite to the effect discussed previously for an uncontained forward port wall, the force vector on an uncontained aft port wall is in the reverse-thrust direction and results in an increase in reverse-thrust performance relative to the configurations without the aft doors. Aft external doors improved reverser performance at static conditions and a nozzle pressure ratio of 2.5 by nearly 24 percent.

The following observations of the effects of combinations of doors on reverser static performance are evident from figure 31. As previously discussed, poor reverser performance was obtained for the configuration without doors because of the short passage length. Addition of forward and aft doors improved reverser performance at low nozzle pressure ratios because of the longer passage length. However, some penalties occurred at high nozzle pressure ratio because of the uncontained forward wall. Addition of just the forward door was beneficial at low nozzle pressure ratios (up to about 3.5), but large penalties occurred at high nozzle pressure ratios because of the long uncontained forward wall. With just the aft door, reverse-thrust levels at $NPR \approx 2.0$ were nearly the same as with both the forward and aft doors. However, the advantage of the uncontained aft wall is obvious as there was a significant improvement in reverser performance as nozzle pressure ratio was increased.

When sidewalls were installed on the nozzle with either the forward or aft door, an additional improvement in reverse-thrust static performance was realized (fig. 31). This improvement in reverser performance was probably caused by a reduction in the lateral spreading of the reverser plume. For the configuration with only the aft external door, addition of the sidewalls resulted in a 2- to 4-percent increase in reverser performance over the range of nozzle pressure ratios tested. The sidewalls were very effective with the forward door, for which a 10-percent improvement in performance was obtained at $NPR = 2.5$. However, for the reverser configurations without doors and with both doors (forward and aft), addition of the sidewalls caused a decrease in reverser performance.

Effect of differential reverser-port angles.- Differential top and bottom reverser-port angles for use as a pitch control were investigated by testing four configurations with different top and bottom port angles. Two of these configurations are shown in figure 16. The other two configurations were formed by exchanging top and bottom components of the two configurations shown in this figure. The static and aeropropulsive characteristics for these configurations are shown in figures 32 and 33. Since these configurations were tested to determine trim capability during landing approach, wind-on data were obtained only at $M = 0.15$. The nozzle pitching-

moment coefficients for differential top and bottom reverser-port angles are given in figure 34 for static conditions and for $M = 0.15$. Figure 35 shows that nozzle pitching moment for each of the differential top and bottom port angle combinations is nearly independent of angle of attack at $M = 0.15$.

Differential reverser-port angle effectiveness $C_{m,n_{\delta_\theta}}$ and thrust-vector effectiveness $C_{m,n_{\delta_v}}$ (from the present study) and conventional horizontal-tail effectiveness $C_{m_{\delta_h}}$ (from ref. 17) are summarized and compared in figure 36. Thrust-vector effectiveness and differential reverser-port angle effectiveness were derived from this investigation using only the absolute maximum deflection data. Results shown in figure 36 indicate that thrust vectoring a partially deployed thrust reverser (see fig. 12) is a more effective pitch trim system than using differential top and bottom reverser-port angles. The effectiveness of this thrust-vectoring system appears to be directly proportional to nozzle pressure ratio, and thus it is more effective than the horizontal-tail trim with reverse thrust for $NPR > 2.4$ and more effective than the horizontal-tail trim with forward thrust for $NPR > 3.6$. (See fig. 36(a).)

Trim effectiveness is nearly independent of angle of attack for all trim systems except for horizontal-tail trim with reverse thrust. (See fig. 36(b).) Apparently, the improvement in trim effectiveness is caused by a reduction in external flow between the vertical tails because of reverser exhaust plume blockage. This would result in an increase in velocity and dynamic pressure around the outside of the vertical tails and over the horizontal tails which would result in an increase in horizontal-tail lift (ref. 17).

Internal Pressure Distribution

The internal pressures obtained during this investigation were too sparse to depict a meaningful representation of flow conditions within the reverser nozzles. As expected, stagnation was indicated at the center and choked flow was indicated near the exit ports. Reference 16 is a source of internal pressure distributions obtained from closely spaced orifices in a reverser nozzle. This reference indicates a smooth decay in pressure from stagnation to choked flow. Although the data of reference 16 were obtained at static conditions, no significant effect of external flow should be expected to propagate past the choked exit ports, as previously indicated by discharge coefficients in figure 21(e).

External Pressure Distribution

Base-line (forward-thrust) nozzle.- External pressure distributions on the base-line configuration at Mach numbers of 0.60, 0.90, and 1.20 are shown in figure 37. Data at a Mach number of 0.15 are not presented, since the low-pressure loading in this speed regime would not have yielded useful design information. Also, since the measurement of external surface pressure near the nozzle edges ($y/(b_n/2) = \pm 0.838$) did not show any significant difference from the center line ($y/(b_n/2) = 0$) values, lateral pressure distributions are not presented. Nozzle pressure ratio values near unity signify jet-off conditions. This nozzle has excellent pressure recovery at subsonic speeds. (See fig. 37.) At $M = 1.20$, there is minor expansion at the start

of the nozzle boattail (see fig. 37(c)), which is dependent on nozzle pressure ratio. Otherwise, the base-line nozzle appears independent of nozzle pressure ratio.

Thrust-reverser deployment nozzles.- The external pressure distributions for 25-, 50-, 75-, and 100-percent thrust-reverser deployments at Mach numbers of 0.60, 0.90, and 1.20 are shown in figures 38 to 41. Again, there were no significant differences between the center-line and the edge ($y/(b_n/2) = \pm 0.836$) pressure distributions and, consequently, only the center-line data are presented. For the 25-, 50-, and 75-percent deployed nozzles (figs. 38 to 40), external pressures were measured only at locations upstream of the reverser port. For the 100-percent deployed nozzle (fig. 41), external pressures were measured both upstream and downstream of the reverser port. Afterbody and nozzle surfaces upstream of the reverser port were pressurized by deployment (operation) as is typical of any thrust reverser. On the nozzle surface aft of the reverser port (measured on the 100-percent reverser, fig. 41), thrust-reverser deployment caused large negative base pressure coefficients on the aft face of the nozzle flaps. These large negative pressure coefficients are apparently caused by reverser flap (blocker) deployment rather than the reverse-thrust plume, since they are relatively independent of nozzle pressure ratio except for an initial pressure rise at $M = 1.20$. It is these large negative base pressures which greatly enhance thrust-reverser performance at wind-on conditions because of increased drag.

Thrust-reverser-port angle nozzles.- The external pressure distributions for nozzles with reverser-port angles of 110°, 120°, and 130° at Mach numbers of 0.60, 0.90, and 1.20 are shown in figures 42 to 44. External pressure distributions for the alternate 110° reverser-port angle nozzle with short internal passage lengths without and with sidewalls and aft external doors are shown in figures 45 and 46. Ahead of the reverser port, the surface pressure increased with nozzle pressure ratio. No clear trend between pressure coefficient and reverser-port angle could be determined. Surface pressure aft of the reverser port was more sensitive to nozzle pressure ratio than the 100-percent deployed reverser nozzle. All these nozzles exhibited low base pressures which could be expected to enhance reverser performance. However, for the 120° and 130° reverser-port nozzles at $M = 1.20$, an initial pressure rise dependent on nozzle pressure ratio was observed on the rear panel.

CONCLUDING REMARKS

An investigation has been conducted in the Langley 16-Foot Transonic Tunnel to determine the performance of nonaxisymmetric-nozzle thrust reversers installed on a generic twin-engine fighter aircraft model. This investigation was conducted at static conditions ($M = 1.0$) and at Mach numbers from 0.15 to 1.20 over a nozzle pressure ratio range from 1.0 (jet off) to 9.0 and over an angle-of-attack range from -3° to 9°. The results of this investigation indicate the following:

1. All thrust-reverser configurations investigated exceeded an in-flight thrust-reversing goal of 30 percent at typical operating nozzle pressure ratios.

2. At static conditions, a reverser-port turning angle of 120° or 130° was required to achieve 50-percent reverse thrust at nozzle pressure ratios up to 2.5.

3. Thrust-reverser performance was improved by increasing the percentage of reverser deployment, the reverser-port angle, or the reverser-port internal passage length. For example, increasing the port passage length improved reverse-thrust performance by as much as 28 percent at static conditions and by as much as 17 percent at Mach 1.20.

4. When external reverser-port doors were used for mechanical or aerodynamic reasons, significant improvements in reverser performance could be obtained with an aft door only or with an aft door longer than the forward door. This produced a force vector on a surface in the drag or reverse-thrust direction, whereas a forward door produced a force vector in the forward-thrust direction.

5. Vectoring of the forward thrust while partially deploying reverse thrust was a more effective method of augmenting aircraft control during landing approach than the use of top and bottom differential reverser-port angles.

6. A significant contribution to wind-on thrust-reverser performance was the external drag on the aft surface of the reverser flaps.

7. Increasing reverser-port angle caused significant decreases in discharge coefficient relative to the forward-thrust nozzle because of flow separation around the sharp lip at the entrance of the reverser port.

Langley Research Center
National Aeronautics and Space Administration
Hampton, VA 23665
April 16, 1984

REFERENCES

1. Capone, Francis J.: The Nonaxisymmetric Nozzle - It Is for Real. AIAA Paper 79-1810, Aug. 1979.

2. Banks, D. W.; Quinto, P. F.; and Paulson, J. W., Jr.: Thrust-Induced Effects on Low-Speed Aerodynamics of Fighter Aircraft. AIAA-81-2612, Dec. 1981.

3. Nelson, B. D.; and Nicolai, L. M.: Application of Multi-Function Nozzles to Advanced Fighters. AIAA-81-2618, Dec. 1981.

4. Bowers, Douglas L.; and Laughrey, James A.: Application of Advanced Exhaust Nozzles for Tactical Aircraft. ICAS Proceedings - 1982, Volume 1, B. Laschka and R. Staufenbiel, eds., Aug. 1982, pp. 132-141. (Available as ICAS-82-4.1.1.)

5. Wallace, Hoyt W.; and Bowers, Douglas L.: Advanced Nozzle Integration for Air Combat Fighter Application. AIAA-82-1135, June 1982.

6. Stevens, H. L.; Thayer, E. B.; and Fullerton, J. F.: Development of the Multi-Function 2-D/C-D Nozzle. AIAA-81-1491, July 1981.

7. Peddrew, Kathryn H., compiler: A User's Guide to the Langley 16-Foot Transonic Tunnel. NASA TM-83186, 1981.

8. Yetter, Jeffery A.; and Leavitt, Laurence D.: Effects of Sidewall Geometry on the Installed Performance of Nonaxisymmetric Convergent-Divergent Exhaust Nozzles. NASA TP-1771, 1980.

9. Re, Richard J.; and Leavitt, Laurence D.: Static Internal Performance Including Thrust Vectoring and Reversing of Two-Dimensional Convergent-Divergent Nozzles. NASA TP-2253, 1984.

10. Capone, Francis J.; Re, Richard J.; and Bare, E. Ann: Thrust Reversing Effects on Twin-Engine Aircraft Having Nonaxisymmetric Nozzles. AIAA-81-2639, Dec. 1981.

11. Capone, Francis J.: Static Performance of Five Twin-Engine Nonaxisymmetric Nozzles With Vectoring and Reversing Capability. NASA TP-1224, 1978.

12. Braslow, Albert L.; Hicks, Raymond M.; and Harris, Roy V., Jr.: Use of Grit-Type Boundary-Layer-Transition Trips on Wind-Tunnel Models. NASA TN D-3579, 1966.

13. Capone, Francis J.; and Berrier, Bobby L.: Investigation of Axisymmetric and Nonaxisymmetric Nozzles Installed on a 0.10-Scale F-18 Prototype Airplane Model. NASA TP-1638, 1980.

14. Capone, Francis J.; and Maiden, Donald L.: Performance of Twin Two-Dimensional Wedge Nozzles Including Thrust Vectoring and Reversing Effects at Speeds up to Mach 2.20. NASA TN D-8449, 1977.

15. Maiden, Donald L.; and Mercer, Charles E.: Performance Characteristics of a Single-Engine Fighter Model Fitted With an In-Flight Thrust Reverser. NASA TN D-6460, 1971.

16. Putnam, Lawrence E.; and Strong, Edward G.: Internal Pressure Distributions for a Two-Dimensional Thrust-Reversing Nozzle Operating at a Free-Stream Mach Number of Zero. NASA TM-85655, 1983.

17. Capone, Francis J.; Mason, Mary L.; and Carson, George T., Jr.: Thrust Reversing Effects on Horizontal Tail Effectiveness of Twin-Engine Fighter Aircraft. AIAA-83-0086, Jan. 1983.

TABLE 1.- MEASURED NOZZLE THROAT AREAS

[All areas are in square centimeters]

Nozzle configuration	Throat location	Left nozzle	Right nozzle	Total of left and right nozzles
Base line (forward thrust)	Total	17.12	17.12	34.24
25-percent deployment	Top	2.13	2.13	
	Center	13.10	13.19	
	Bottom	1.87	1.88	
	Total	17.10	17.20	34.30
50-percent deployment	Top	4.60	5.00	
	Center	8.74	8.60	
	Bottom	4.53	4.64	
	Total	17.87	18.24	36.11
75-percent deployment	Top	7.00	6.95	
	Center	4.43	4.26	
	Bottom	6.89	6.80	
	Total	18.32	18.01	36.33
100-percent deployment	Top	8.90	8.86	
	Bottom	8.83	8.86	
	Total	17.73	17.72	35.45
50-percent deployment with forward thrust vectored downward 15°	Top	4.54	4.68	
	Center	8.31	8.32	
	Bottom	4.48	4.51	
	Total	17.33	17.51	34.84
50-percent deployment with forward thrust vectored upward 15°	Top	4.64	4.72	
	Center	8.21	8.21	
	Bottom	4.66	4.66	
	Total	17.51	17.59	35.10
110° reverser-port angle	Top	8.65	8.56	
	Bottom	8.52	8.50	
	Total	17.17	17.06	34.23
120° reverser-port angle	Top	8.57	8.59	
	Bottom	8.57	8.49	
	Total	17.14	17.08	34.22
130° reverser-port angle	Top	8.59	8.60	
	Bottom	8.79	8.67	
	Total	17.38	17.27	34.65

TABLE 1.- Concluded

Nozzle configuration	Throat location	Left nozzle	Right nozzle	Total of left and right nozzles
110° reverser-port angle (short internal passage length)	Top Bottom Total	8.75 8.32 17.07	8.67 8.64 17.31	34.38
130° top/110° bottom reverser-port angles	Top Bottom Total	8.72 8.64 17.36	8.80 8.64 17.44	34.80
130° top/120° bottom reverser-port angles	Top Bottom Total	8.68 8.64 17.32	8.66 8.80 17.46	34.78
110° top/130° bottom reverser-port angles	Top Bottom Total	8.71 8.67 17.38	8.62 8.79 17.41	34.79
120° top/130° bottom reverser-port angles	Top Bottom Total	8.85 8.60 17.45	8.89 8.56 17.45	34.90

TABLE 2.- INDEX TO DATA FIGURES

Nozzle configuration	Figure for -	
	Force and moment data	Pressure distribution data
Base line (forward thrust)	17 to 19	37
25-percent deployment	20 to 22	38
50-percent deployment	20 to 22	39
75-percent deployment	20 to 22	40
100-percent deployment	20 to 22	41
50-percent deployment with forward thrust vectored downward 15°	23 to 26, 36	
50-percent deployment with forward thrust vectored upward 15°	23 to 26, 36	
110° reverser-port angle	27 to 31	42
120° reverser-port angle	27, 28	43
130° reverser-port angle	27, 28	44
110° reverser-port angle (short internal passage length)	29 to 31	45
110° reverser-port angle (short internal passage length) with forward external doors	31	
110° reverser-port angle (short internal passage length) with sidewalls	31	
110° reverser-port angle (short internal passage length) with aft external doors	31	
110° reverser-port angle (short internal passage length) with forward external doors and sidewalls	31	

TABLE 2.- Concluded

Nozzle configuration	Figure for -	
	Force and moment data	Pressure distribution data
110° reverser-port angle (short internal passage length) with forward and aft external doors	31	
110° reverser-port angle (short internal passage length) with forward and aft external doors and sidewalls	29 to 31	
110° reverser-port angle (short internal passage length) with aft external doors and sidewalls	29 to 31	46
130° top/110° bottom reverser-port angles	32 to 36	
130° top/120° bottom reverser-port angles	32 to 36	
110° top/130° bottom reverser-port angles	32 to 36	
120° top/130° bottom reverser-port angles	32 to 36	

TABLE 3.- STATIC FORCE AND MOMENT DATA FOR NOZZLE CONFIGURATIONS

NPR	F_j/F_i	C_N	C_F	C_m
Base line (forward thrust)				
1.00	0.000	0.0001	0.0003	-0.0000
2.00	.957	-.0010	-.0115	.0018
2.49	.973	-.0008	-.0165	.0018
3.50	.991	-.0008	-.0272	.0027
4.00	.993	-.0010	-.0325	.0032
5.00	.991	-.0012	-.0431	.0043
6.00	.986	-.0014	-.0538	.0055
6.97	.980	-.0016	-.0643	.0066
25-percent deployment				
1.00	0.000	0.0000	0.0003	-0.0000
2.01	.649	-.0004	-.0074	.0008
2.52	.654	-.0007	-.0107	.0013
3.99	.653	-.0013	-.0204	.0027
5.03	.646	-.0018	-.0273	.0038
6.05	.634	-.0015	-.0339	.0037
7.02	.626	-.0020	-.0404	.0047
50-percent deployment				
1.00	0.000	-0.0001	-0.0001	0.0000
2.00	.233	-.0013	-.0029	.0017
2.00	.228	-.0009	-.0028	.0011
2.53	.252	-.0017	-.0045	.0023
3.52	.252	-.0014	-.0072	.0016
4.02	.250	-.0016	-.0086	.0018
5.00	.246	-.0020	-.0112	.0024
6.02	.242	-.0023	-.0139	.0028
6.63	.238	-.0026	-.0154	.0030
75-percent deployment				
1.00	0.000	-0.0001	0.0001	0.0000
2.01	-.047	-.0008	.0006	.0002
2.52	-.047	-.0011	.0009	.0003
3.54	-.050	-.0016	.0015	.0007
4.05	-.053	-.0017	.0019	.0006
5.01	-.054	-.0023	.0025	.0012
6.03	-.054	-.0027	.0032	.0011
6.66	-.057	-.0027	.0038	.0008

TABLE 3.- Continued

NPR	F_j/F_i	C_N	C_F	C_m
100-percent deployment				
1.00	0.000	-0.0001	-0.0002	0.0000
2.00	-.273	-.0007	.0034	-.0001
2.51	-.297	-.0009	.0054	-.0002
3.51	-.312	-.0015	.0092	-.0001
4.00	-.316	-.0021	.0111	.0005
5.02	-.322	-.0032	.0152	.0015
6.02	-.321	-.0030	.0190	.0006
6.05	-.321	-.0028	.0192	.0003
50-percent deployment with forward thrust vectored downward 15°				
1.00	0.000	-0.0000	-0.0002	0.0000
2.01	.235	-.0029	-.0029	.0048
2.49	.241	-.0037	-.0041	.0060
3.51	.239	-.0041	-.0067	.0064
4.01	.237	-.0044	-.0079	.0069
5.01	.233	-.0056	-.0104	.0086
6.01	.229	-.0067	-.0128	.0103
6.78	.223	-.0076	-.0146	.0117
50-percent deployment with forward thrust vectored upward 15°				
1.00	0.000	-0.0000	-0.0000	0.0000
2.00	.177	-.0006	-.0021	.0003
2.50	.189	.0008	-.0032	-.0019
3.52	.201	.0018	-.0056	-.0037
4.02	.201	.0022	-.0067	-.0044
5.00	.204	.0030	-.0090	-.0057
6.01	.204	.0037	-.0113	-.0069
7.02	.203	.0043	-.0137	-.0079
110° reverser-port angle				
1.00	0.000	-0.0001	-0.0000	0.0000
2.07	-.418	-.0006	.0036	-.0002
2.50	-.368	-.0007	.0044	-.0002
3.51	-.318	-.0010	.0062	-.0003
4.01	-.365	-.0011	.0085	-.0005
5.03	-.320	-.0014	.0100	-.0005
5.97	-.290	-.0017	.0112	-.0005
6.99	-.269	-.0021	.0125	-.0004

TABLE 3.- Continued

NPR	F_j/F_i	C_N	C_F	C_m
120° reverser-port angle				
1.00	0.000	0.0001	0.0001	-0.0001
2.01	-.694	.0007	.0056	-.0020
2.48	-.501	-.0006	.0058	-.0001
3.49	-.426	-.0009	.0082	-.0005
4.00	-.431	-.0010	.0099	-.0007
5.00	-.469	-.0013	.0144	-.0011
6.00	-.428	-.0015	.0165	-.0012
7.00	-.401	-.0019	.0185	-.0013
130° reverser-port angle				
1.00	0.000	-0.0001	-0.0000	0.0000
2.00	-.726	.0002	.0055	-.0013
2.51	-.703	.0004	.0079	-.0020
3.50	-.568	-.0015	.0104	.0006
4.01	-.537	-.0012	.0118	-.0004
5.02	-.556	-.0018	.0163	-.0004
5.98	-.563	-.0018	.0205	-.0012
7.01	-.529	-.0021	.0233	-.0013
110° reverser-port angle (short internal passage length)				
1.00	0.000	-0.0001	0.0000	0.0000
2.00	-.055	-.0006	.0005	.0001
2.51	-.091	-.0007	.0012	.0001
3.50	-.136	-.0011	.0031	.0001
4.00	-.153	-.0014	.0042	.0001
5.00	-.181	-.0017	.0066	.0000
6.01	-.164	-.0020	.0076	.0001
7.01	-.149	-.0024	.0083	.0001
110° reverser-port angle (short internal passage length) with forward external doors				
1.00	0.000	-0.0000	-0.0000	-0.0000
2.08	-.200	-.0005	.0020	-.0001
2.50	-.267	-.0006	.0037	-.0002
3.51	-.327	-.0010	.0076	-.0005
3.98	-.291	-.0011	.0080	-.0004
5.01	-.213	-.0015	.0078	-.0002
6.03	-.155	-.0019	.0072	.0001
6.98	-.118	-.0022	.0065	.0003

TABLE 3.- Continued

NPR	F_j/F_i	C_N	C_F	C_m
110° reverser-port angle (short internal passage length) with sidewalls				
1.00	0.000	-0.0001	-0.0000	0.0000
2.00	-.058	-.0005	.0005	.0002
2.50	-.088	-.0007	.0012	.0002
3.52	-.130	-.0011	.0030	.0003
3.98	-.145	-.0013	.0039	.0003
4.98	-.170	-.0017	.0062	.0002
5.91	-.154	-.0021	.0069	.0004
110° reverser-port angle (short internal passage length) with aft external doors				
1.00	0.000	-0.0000	-0.0001	0.0000
2.01	-.303	-.0004	.0027	-.0002
2.51	-.323	-.0007	.0043	-.0002
3.50	-.435	-.0010	.0097	-.0006
4.03	-.457	-.0012	.0123	-.0008
5.04	-.478	-.0015	.0171	-.0011
6.01	-.494	-.0020	.0220	-.0012
7.00	-.509	-.0025	.0274	-.0012
110° reverser-port angle (short internal passage length) with forward external doors and sidewalls				
1.00	0.000	0.0001	-0.0001	-0.0000
2.01	-.175	-.0004	.0016	-.0001
2.51	-.357	-.0005	.0050	-.0004
3.51	-.384	-.0010	.0089	-.0005
3.98	-.323	-.0011	.0088	-.0004
4.98	-.232	-.0015	.0085	-.0002
5.99	-.171	-.0019	.0078	.0001
6.98	-.124	-.0022	.0068	.0003
7.96	-.089	-.0026	.0057	.0007
110° reverser-port angle (short internal passage length) with forward and aft external doors				
1.00	0.000	-0.0001	-0.0001	0.0000
2.01	-.314	-.0005	.0030	-.0001
2.51	-.300	-.0006	.0041	-.0002
3.50	-.282	-.0009	.0063	-.0004
4.01	-.306	-.0011	.0082	-.0005
5.02	-.276	-.0015	.0098	-.0005
5.99	-.255	-.0018	.0113	-.0005
7.00	-.240	-.0021	.0129	-.0005

TABLE 3.- Continued

NPR	F_j/F_i	C_N	C_F	C_m
110° reverser-port angle (short internal passage length) with forward and aft external doors and sidewalls				
1.00	0.000	-0.0000	-0.0001	-0.0000
1.99	-.327	-.0005	.0031	-.0002
2.52	-.300	-.0007	.0041	-.0002
3.51	-.275	-.0010	.0061	-.0003
4.00	-.288	-.0012	.0076	-.0003
5.00	-.245	-.0016	.0086	-.0003
6.00	-.216	-.0019	.0095	-.0003
7.00	-.197	-.0022	.0105	-.0003
110° reverser-port angle (short internal passage length) with aft external doors and sidewalls				
1.00	0.000	-0.0000	-0.0002	-0.0000
1.99	-.315	-.0005	.0028	-.0001
2.50	-.346	-.0007	.0046	-.0003
3.50	-.456	-.0010	.0102	-.0007
3.99	-.479	-.0011	.0128	-.0009
5.02	-.503	-.0015	.0180	-.0012
6.00	-.522	-.0020	.0233	-.0013
6.99	-.535	-.0024	.0288	-.0017
130° top/110° bottom reverser-port angles				
1.00	0.000	-0.0001	0.0003	0.0000
1.98	-.711	.0028	.0056	-.0054
2.01	-.712	.0029	.0057	-.0056
2.51	-.657	.0045	.0078	-.0083
3.51	-.456	.0012	.0088	-.0038
4.00	-.460	.0008	.0106	-.0036
5.01	-.475	.0023	.0146	-.0065
6.02	-.448	.0022	.0173	-.0070
7.02	-.415	.0018	.0193	-.0070
130° top/120° bottom reverser-port angles				
1.00	0.000	0.0000	0.0002	-0.0000
2.02	-.730	.0008	.0058	-.0024
1.99	-.733	.0007	.0057	-.0023
2.50	-.699	.0032	.0080	-.0064
3.51	-.524	.0011	.0100	-.0038
4.00	-.505	.0003	.0115	-.0030
4.99	-.533	.0004	.0161	-.0040
5.98	-.514	.0007	.0194	-.0052

TABLE 3.- Concluded

NPR	F_j/F_i	C_N	C_F	C_m
110° top/130° bottom reverser-port angles				
1.00	0.000	0.0001	-0.0001	-0.0000
2.02	-.527	-.0026	.0043	.0038
2.50	-.481	-.0039	.0057	.0057
3.51	-.427	-.0027	.0083	.0028
4.00	-.438	-.0028	.0102	.0025
4.99	-.433	-.0045	.0133	.0047
5.98	-.416	-.0053	.0160	.0051
7.03	-.388	-.0058	.0182	.0051
120° top/130° bottom reverser-port angles				
1.00	0.000	-0.0001	-0.0001	0.0000
2.01	-.705	.0001	.0056	-.0010
2.51	-.570	-.0028	.0066	.0039
3.49	-.499	-.0032	.0095	.0039
4.02	-.494	-.0027	.0113	.0023
5.01	-.513	-.0034	.0156	.0026
6.01	-.491	-.0041	.0187	.0030
7.00	-.462	-.0045	.0212	.0029

TABLE 4.- AEROPROPULSIVE FORCE AND MOMENT DATA
FOR NOZZLE CONFIGURATIONS

M	α, deg	NPR	$\frac{F - D}{F_i}$	C_L	$C_{(D-F)}$	C_m	$C_{m,n}$
Base line (forward thrust)							
0.15	-0.03	1.00	0.000	0.0169	-0.0090	-0.0173	0.0005
.15	-.03	2.00	.962	-.0221	-.7360	.0836	.1028
.15	-.04	2.61	.979	-.0062	-1.1270	.0876	.1098
.15	-.05	3.01	.984	-.0041	-1.3771	.1025	.1235
.15	-.03	3.79	.988	-.0154	-1.9008	.1517	.1759
.15	-3.02	1.00	.000	.0111	-.0094	.0051	-.0021
.15	-.08	1.00	.000	.0344	-.0044	-.0231	-.0056
.15	2.92	1.00	.000	.0591	.0107	-.0538	-.0104
.15	5.92	1.00	.000	.1044	.0227	-.0921	-.0206
.15	8.96	1.00	.000	.1326	.0381	-.1380	-.0222
.15	-2.99	2.61	.971	-.0708	-1.1218	.1113	.1045
.15	.14	2.61	.968	.0219	-1.1121	.0739	.0949
.15	2.99	2.62	.963	.1027	-1.1161	.0417	.0918
.15	5.97	2.62	.952	.1992	-1.0879	.0012	.0852
.15	8.95	2.62	.934	.2871	-1.0816	-.0431	.0828
.60	-.03	1.05	.000	.0080	.0073	-.0154	.0023
.60	-.05	2.01	.820	.0066	-.0389	-.0092	.0082
.60	-.04	3.02	.907	.0096	-.0805	-.0104	.0090
.60	-.04	3.51	.925	.0098	-.1003	-.0091	.0106
.60	-.04	5.02	.947	.0087	-.1634	-.0029	.0164
.60	-3.03	1.04	.000	-.0072	.0077	.0066	.0012
.60	-.03	1.05	.000	.0104	.0088	-.0158	.0018
.60	2.98	1.04	.000	.0291	.0119	-.0394	.0027
.60	5.97	1.04	.000	.0592	.0164	-.0763	.0006
.60	8.97	1.05	.000	.0886	.0264	-.1183	.0032
.60	-3.04	3.49	.925	-.0180	-.0986	.0202	.0118
.60	-.03	3.51	.913	.0110	-.0979	-.0100	.0094
.60	2.96	3.52	.880	.0414	-.0955	-.0411	.0073
.60	5.95	3.51	.821	.0791	-.0895	-.0808	.0030
.60	8.97	3.52	.733	.1136	-.0798	-.1227	-.0004
.90	-.02	1.10	.000	.0156	.0130	-.0242	.0023
.90	-.03	1.99	.394	.0091	-.0079	-.0170	.0070
.90	-.05	3.00	.672	.0095	-.0257	-.0169	.0077
.90	-.03	5.03	.831	.0095	-.0633	-.0142	.0111
.90	-.03	6.97	.881	.0093	-.1011	-.0112	.0141
.90	-.04	7.01	.883	.0094	-.1025	-.0111	.0139
.90	-3.02	1.10	.000	.0010	.0114	-.0085	.0045
.90	-.04	1.09	.000	.0114	.0128	-.0224	.0039
.90	2.96	1.09	.000	.0200	.0143	-.0335	.0061
.90	5.95	1.08	.000	.0315	.0170	-.0500	.0074
.90	8.96	1.10	.000	.0702	.0253	-.1013	.0029
.90	-3.03	5.00	.850	-.0064	-.0646	.0004	.0125
.90	-.03	5.00	.836	.0085	-.0633	-.0137	.0114
.90	2.97	5.01	.813	.0260	-.0617	-.0307	.0103
.90	5.97	5.00	.771	.0461	-.0587	-.0557	.0100
.90	8.93	5.02	.651	.0886	-.0494	-.1051	.0057

TABLE 4.- Continued

M	α, deg	NPR	$\frac{F - D}{F_i}$	C_L	$C_{(D-F)}$	C_m	$C_{m,n}$
Base line (forward thrust)							
1.20	0.06	0.89	0.000	-0.0147	0.0276	0.0158	0.0048
1.20	.07	3.01	-.237	-.0153	.0056	.0167	.0071
1.20	.07	5.02	.379	-.0120	-.0159	.0115	.0030
1.20	.09	7.02	.585	-.0086	-.0375	.0077	.0019
1.20	.06	9.02	.694	-.0084	-.0605	.0092	.0031
1.20	-2.93	.90	.000	-.0547	.0312	.0690	.0075
1.20	.07	.89	.000	-.0129	.0283	.0111	.0052
1.20	3.07	.87	.000	.0366	.0320	-.0481	.0051
1.20	6.08	.86	.000	.0779	.0406	-.1009	-.0058
1.20	9.06	.82	.000	.1091	.0535	-.1452	-.0077
1.20	-2.93	6.99	.538	-.0565	-.0343	.0681	.0061
1.20	.08	7.04	.588	-.0068	-.0378	.0051	.0018
1.20	3.09	7.00	.518	.0520	-.0330	-.0621	-.0063
1.20	6.06	7.01	.374	.0914	-.0237	-.1074	-.0111
1.20	9.06	7.00	.171	.1296	-.0106	-.1581	-.0173
25-percent deployment							
0.15	0.01	1.00	0.000	-0.0087	-0.0103	-0.0126	0.0078
.15	.01	2.02	.614	-.0396	-.4525	.0493	.0616
.15	-.01	2.62	.624	-.0454	-.6945	.0698	.0833
.15	-.03	3.02	.625	-.0507	-.8467	.0860	.1009
.15	-.00	3.83	.625	-.0592	-1.1639	.1153	.1324
.15	-3.02	2.63	.616	-.0985	-.6894	.0997	.0859
.15	-.01	2.62	.617	-.0327	-.6852	.0670	.0793
.15	3.00	2.62	.616	.0246	-.6818	.0360	.0760
.15	6.02	2.62	.613	.0844	-.6893	.0065	.0780
.15	9.01	2.62	.602	.1492	-.6764	-.0266	.0744
.60	-.00	1.01	.000	.0070	.0115	-.0167	.0011
.60	-.00	2.02	.333	.0052	-.0148	-.0126	.0034
.60	-.01	3.03	.455	.0045	-.0383	-.0103	.0052
.60	-.01	3.53	.481	.0041	-.0499	-.0092	.0065
.60	-.03	5.04	.520	.0017	-.0858	-.0041	.0099
.60	-2.99	3.52	.477	-.0203	-.0500	.0191	.0055
.60	.00	3.53	.472	.0055	-.0489	-.0101	.0052
.60	3.03	3.52	.447	.0317	-.0465	-.0398	.0041
.60	6.00	3.51	.393	.0643	-.0411	-.0770	-.0008
.60	8.98	3.52	.320	.0937	.0333	-.1138	-.0022
.90	-.04	1.05	.000	.0107	.0144	-.0255	.0018
.90	.00	2.00	-.078	.0106	.0020	-.0246	.0008
.90	-.02	2.89	.232	.0138	-.0083	-.0273	-.0007
.90	-.02	5.01	.400	.0149	-.0290	-.0278	.0006
.90	-.03	7.05	.450	.0134	-.0499	-.0245	.0031
.90	-3.02	5.03	.416	.0009	-.0308	-.0119	.0024
.90	.00	5.03	.398	.0166	-.0292	-.0291	-.0001
.90	3.00	5.04	.373	.0310	-.0272	-.0461	-.0017

TABLE 4.- Continued

M	α, deg	NPR	$\frac{F - D}{F_i}$	C_L	$C_{(D-F)}$	C_m	$C_{m,n}$
25-percent deployment							
0.90	6.01	5.01	0.321	0.0517	-0.0233	-0.0760	-0.0025
.90	9.00	5.07	.198	.0949	-.0144	-.1299	-.0089
1.20	-.02	.88	.000	-.0128	.0273	.0112	.0004
1.20	-.01	3.03	-.500	-.0129	.0110	.0108	-.0008
1.20	-.01	5.05	.053	-.0130	-.0018	.0097	-.0007
1.20	-.02	7.03	.255	-.0136	-.0156	.0104	.0002
1.20	-.02	9.06	.363	-.0137	-.0305	.0109	.0015
1.20	-3.00	7.06	.196	-.0586	-.0120	.0694	.0065
1.20	-.01	7.03	.251	-.0125	-.0154	.0087	-.0002
1.20	2.97	7.10	.195	.0443	-.0120	-.0584	-.0055
1.20	5.98	7.05	.054	.0841	-.0030	-.1058	-.0112
1.20	8.96	7.05	-.144	.1247	.0094	-.1613	-.0174
50-percent deployment							
0.15	-0.03	1.00	0.000	-0.0050	-0.0223	-0.0131	0.0033
.15	.01	2.00	.215	-.0444	-.1683	.0161	.0311
.15	-.00	2.61	.203	-.0595	-.2413	.0366	.0487
.15	-.00	3.02	.206	-.0758	-.3028	.0544	.0655
.15	-.01	3.81	.210	-.1017	-.4222	.0875	.0978
.15	-3.02	2.62	.199	-.0921	-.2365	.0665	.0545
.15	.01	2.61	.199	-.0518	-.2359	.0319	.0478
.15	3.01	2.62	.196	-.0154	-.2325	.0009	.0385
.15	6.02	2.61	.193	.0258	-.2315	-.0320	.0412
.15	9.01	2.61	.183	.0769	-.2181	-.0812	.0208
.60	-.01	1.03	.000	.0069	.0111	-.0162	.0007
.60	-.01	2.01	-.081	.0017	.0044	-.0107	.0020
.60	-.00	3.02	.054	-.0037	-.0046	-.0038	.0053
.60	-.01	3.51	.089	-.0052	-.0096	-.0024	.0076
.60	-.00	5.03	.146	-.0101	-.0259	.0034	.0089
.60	-3.01	3.53	.080	-.0246	-.0086	.0246	.0031
.60	.02	3.50	.084	-.0015	-.0092	-.0060	.0050
.60	2.99	3.51	.063	.0189	-.0066	-.0312	.0018
.60	6.00	3.52	.024	.0458	-.0024	-.0634	.0003
.60	8.99	3.53	-.026	.0668	.0034	-.0901	.0013
.90	.00	1.07	.000	.0087	.0146	-.0219	.0026
.90	-.02	2.05	-.415	.0113	.0096	-.0259	-.0026
.90	-.01	3.01	-.128	.0122	.0056	-.0262	-.0031
.90	.01	5.03	.044	.0017	-.0031	-.0124	.0031
.90	.01	7.06	.099	-.0039	-.0117	-.0059	.0060
.90	-3.01	5.02	.047	-.0092	-.0034	.0025	.0036
.90	.01	5.01	.039	.0024	-.0027	-.0128	.0019
.90	3.00	5.03	.030	.0126	-.0020	-.0261	.0023
.90	5.99	5.05	-.029	.0398	.0027	-.0644	-.0010
.90	9.01	5.06	-.117	.0731	.0099	-.1048	.0041
1.20	-.02	.90	.000	-.0126	.0274	.0111	.0010
1.20	-.02	3.03	-.735	-.0140	.0172	.0122	-.0005

TABLE 4.- Continued

M	α, deg	NPR	$\frac{F - D}{F_i}$	C_L	$C_{(D-F)}$	C_m	$C_{m,n}$
50-percent deployment							
1.20	0.02	5.06	-0.235	-0.0126	0.0109	0.0085	-0.0001
1.20	.01	7.08	-.058	-.0128	.0043	.0083	.0005
1.20	.01	9.06	.030	-.0138	-.0023	.0097	.0018
1.20	-3.00	7.07	-.113	-.0604	.0081	.0738	.0072
1.20	-.02	7.05	-.065	-.0122	.0048	.0073	.0003
1.20	2.99	7.06	-.126	.0448	.0089	-.0624	-.0044
1.20	5.98	7.05	-.269	.0848	.0186	-.1123	-.0112
1.20	8.99	7.06	-.468	.1254	.0322	-.1687	-.0164
75-percent deployment							
0.15	-0.01	1.00	0.000	0.0107	0.0039	-0.0145	0.0054
.15	-.01	2.01	-.108	.0032	.0880	-.0508	-.0110
.15	-.00	2.62	-.111	-.0267	.1390	-.0373	-.0096
.15	-.00	3.01	-.106	-.0610	.1622	-.0112	.0109
.15	.00	3.81	-.099	-.1049	.2092	.0222	-.0229
.15	-3.01	2.61	-.115	-.0566	.1422	.0019	.0091
.15	-.01	2.62	-.115	-.0336	.1434	-.0327	-.0033
.15	3.00	2.62	-.118	-.0155	.1461	-.0696	-.0063
.15	6.01	2.61	-.120	.0031	.1486	-.1021	-.0146
.15	9.00	2.62	-.126	.0233	.1570	-.1419	-.0167
.60	-.01	1.04	.000	.0061	.0129	-.0134	.0014
.60	.01	2.02	-.394	.0114	.0205	-.0241	-.0064
.60	.06	3.00	-.248	.0009	.0239	-.0120	-.0003
.60	.02	3.51	-.217	.0066	.0259	-.0214	-.0071
.60	-.05	5.04	-.162	.0210	.0307	-.0456	-.0112
.60	-2.99	3.50	-.214	-.0103	.0255	.0020	-.0087
.60	.10	3.52	-.212	.0032	.0257	-.0151	-.0022
.60	2.97	3.52	-.232	.0214	.0280	-.0407	-.0021
.60	4.97	3.53	-.251	.0332	.0303	-.0564	-.0026
.60	6.03	3.53	-.248	.0305	.0298	-.0523	-.0002
.60	9.02	3.53	-.263	.0328	.0317	-.0555	.0073
.90	-.03	1.10	.000	.0102	.0154	-.0187	.0008
.90	.02	2.02	-.725	.0200	.0165	-.0343	-.0077
.90	-.02	3.00	-.435	.0268	.0187	-.0456	-.0134
.90	-.05	5.02	-.259	.0287	.0219	-.0510	-.0146
.90	-.03	7.07	-.182	.0212	.0236	-.0422	-.0120
.90	-2.98	5.06	-.239	.0116	.0206	-.0262	-.0113
.90	-.01	5.03	-.261	.0286	.0221	-.0512	-.0175
.90	2.96	5.03	-.223	-.0121	.0190	.0060	.0072
.90	5.98	5.02	-.332	.0493	.0281	-.0854	-.0117
.90	8.99	5.03	-.320	.0407	.0271	-.0653	.0056
1.20	.00	.96	.000	-.0135	.0267	.0134	.0026
1.20	.01	3.02	-.941	-.0125	.0227	.0084	-.0008
1.20	.02	5.04	-.462	-.0125	.0219	.0072	.0002
1.20	-.01	7.06	-.294	-.0146	.0213	.0093	-.0002

TABLE 4.- Continued

M	α, deg	NPR	$\frac{F - D}{F_i}$	C_L	$C_{(D-F)}$	C_m	$C_{m,n}$
75-percent deployment							
1.20	0.01	9.01	-0.214	-0.0170	0.0207	0.0117	-0.0006
1.20	-3.01	7.03	-.348	-.0571	.0251	.0681	.0052
1.20	-.00	7.04	-.299	-.0136	.0216	.0084	-.0007
1.20	3.00	7.03	-.353	.0413	.0253	-.0602	-.0053
1.20	5.98	7.05	-.490	.0830	.0352	-.1144	-.0139
1.20	8.98	7.04	-.676	.1226	.0482	-.1698	-.0186
100-percent deployment							
0.15	-0.01	1.00	0.000	-0.0100	-0.0339	-0.0089	-0.0101
.15	.00	2.01	-.363	-.0475	.2866	-.0359	-.0330
.15	-.00	2.62	-.375	-.0681	.4575	-.0428	-.0837
.15	-.01	3.01	-.375	-.0814	.5612	-.0408	-.0886
.15	-.01	3.82	-.367	-.1099	.7641	-.0459	-.1077
.15	-3.00	2.60	-.383	-.0529	.4576	-.0245	-.0829
.15	-.02	2.60	-.382	-.0559	.4556	-.0442	-.0834
.15	3.00	2.60	-.380	-.0578	.4550	-.0723	-.0388
.15	5.98	2.60	-.382	-.0485	.4581	-.1082	-.0559
.15	9.01	2.60	-.385	-.0467	.4590	-.1380	-.0616
.60	-.01	1.05	.000	.0018	.0119	-.0097	.0007
.60	.01	2.01	-.560	.0006	.0279	-.0139	-.0028
.60	.00	3.04	-.462	-.0047	.0443	-.0110	-.0044
.60	.01	3.53	-.454	-.0065	.0538	-.0106	-.0047
.60	.01	5.03	-.429	-.0109	.0807	-.0108	-.0065
.60	-2.99	3.52	-.454	-.0256	.0533	.0212	-.0054
.60	.00	3.52	-.462	-.0039	.0540	-.0121	-.0033
.60	3.01	3.52	-.474	.0200	.0553	-.0463	-.0089
.60	9.00	3.52	-.536	.0570	.0628	-.0989	-.0109
.90	-.01	2.03	-.900	.0107	.0201	-.0269	-.0044
.90	.01	3.01	-.596	.0042	.0251	-.0187	-.0023
.90	.00	5.01	-.442	-.0030	.0366	-.0126	-.0026
.90	.02	7.06	-.386	-.0075	.0487	-.0106	-.0033
.90	-3.03	5.03	-.458	.0182	.0383	.0138	-.0011
.90	-.01	5.02	-.446	-.0022	.0371	-.0132	-.0034
.90	3.02	5.05	-.467	.0095	.0391	-.0326	-.0067
.90	5.98	5.03	-.512	.0269	.0430	-.0581	-.0067
.90	8.99	5.02	-.591	.0621	.0492	-.1047	-.0109
1.20	-.00	1.00	.000	-.0157	.0257	.0151	.0017
1.20	-.02	3.03	-1.134	-.0102	.0268	.0026	-.0029
1.20	-.02	5.01	-.676	-.0105	.0313	.0018	-.0028
1.20	-.00	7.04	-.507	-.0126	.0357	.0032	-.0036
1.20	.00	9.02	-.425	-.0170	.0402	.0076	-.0052
1.20	-3.02	7.03	-.553	-.0547	.0390	.0623	.0044
1.20	-.01	7.08	-.510	-.0127	.0361	.0035	-.0033
1.20	3.02	7.05	-.559	.0410	.0395	-.0639	-.0102
1.20	6.00	7.03	-.704	.0813	.0492	-.1158	-.0173
1.20	8.99	7.05	-.879	.1175	.0619	-.1671	-.0225

TABLE 4.- Continued

M	α, deg	NPR	$\frac{F - D}{F_i}$	C_L	$C_{(D-F)}$	C_m	$C_{m,n}$
50-percent deployment with forward thrust vectored downward 15°							
0.15	0.03	1.00	0.000	0.0162	0.0124	-0.0275	-0.0026
.15	.05	2.01	.171	-.0931	-.1288	.1412	.1581
.15	.06	2.60	.179	-.1454	-.2044	.2208	.2265
.15	.06	3.00	.184	-.1730	-.2562	.2570	.2589
.15	.06	3.80	.188	-.2281	-.3642	.3321	.3231
.15	-3.04	3.00	.172	-.2069	-.2398	.2841	.2585
.15	-3.04	2.61	.166	-.1806	-.1896	.2494	.2290
.15	.01	2.61	.172	-.1463	-.1972	.2166	.2182
.15	3.05	2.61	.178	-.1134	-.2045	.1864	.2182
.15	6.02	2.61	.180	-.0794	-.2044	.1571	.2133
.15	9.02	2.61	.183	-.0438	-.2104	.1181	.2071
50-percent deployment with forward thrust vectored upward 15°							
0.15	0.01	1.00	0.000	-0.0110	0.0051	-0.0013	0.0073
.15	-.00	2.00	.118	.0383	-.0865	-.1286	-.1462
.15	.00	2.63	.138	.0692	-.1590	-.1864	-.2020
.15	.01	3.01	.146	.0883	-.2046	-.2176	-.2240
.15	.01	3.84	.163	.1078	-.3139	-.2511	-.2675
.15	-3.01	2.61	.142	.0485	-.1592	-.1604	-.1966
.15	-.00	2.61	.136	.0836	-.1535	-.1957	-.2067
.15	2.99	2.61	.132	.1122	-.1499	-.2216	-.2070
.15	6.01	2.62	.121	.1440	-.1378	-.2506	-.2104
.15	9.00	2.61	.107	.1853	-.1208	-.2902	-.2135
110° reverser-port angle							
0.15	-0.00	1.00	0.000	-0.0155	-0.0444	-0.0081	0.0053
.15	-.02	2.00	-.482	-.0290	.2474	-.0578	-.0303
.15	-.02	2.61	-.433	-.0381	.3479	-.0582	-.0309
.15	.01	3.02	-.397	-.0575	.3984	-.0446	-.0276
.15	.00	3.81	-.419	-.0677	.5784	-.0632	-.0793
.15	-3.01	2.61	-.443	-.0356	.3554	-.0291	-.0518
.15	-.01	2.61	-.443	-.0317	.3562	-.0573	-.0366
.15	2.98	2.61	-.448	-.0221	.3563	-.0904	-.0359
.15	6.00	2.61	-.450	-.0116	.3573	-.1232	-.0438
.15	9.00	2.61	-.459	.0047	.3650	-.1664	-.0530
.60	-.02	1.01	.000	.0070	.0084	-.0162	.0019
.60	-.00	2.01	-.701	.0046	.0222	-.0168	-.0024
.60	.01	3.02	-.543	.0009	.0347	-.0143	-.0022
.60	.01	3.50	-.550	-.0018	.0429	-.0125	-.0038
.60	.01	5.02	-.430	-.0045	.0534	-.0122	-.0044
.60	-3.01	3.52	-.569	-.0243	.0447	.0240	-.0022
.60	-.01	3.51	-.563	-.0001	.0439	-.0133	-.0040
.60	2.98	3.50	-.600	.0255	.0470	-.0501	-.0078
.60	6.01	3.50	-.650	.0441	.0510	-.0745	-.0093

TABLE 4.- Continued

M	α, deg	NPR	$\frac{F - D}{F_i}$	C_L	$C_{(D-F)}$	C_m	$C_{m,n}$
110° reverser-port angle							
0.60	8.99	3.52	-0.733	0.0678	0.0572	-0.1082	-0.0139
.90	-.01	1.05	.000	.0099	.0116	-.0238	.0047
.90	-.00	1.99	-1.299	.0134	.0170	-.0297	-.0032
.90	-.00	2.01	-1.276	.0136	.0171	-.0299	-.0034
.90	.00	3.01	-.828	.0109	.0235	-.0271	-.0038
.90	.03	5.01	-.522	.0029	.0287	-.0176	-.0021
.90	-.01	7.03	-.399	-.0009	.0333	-.0143	-.0020
.90	-3.02	5.03	-.525	-.0100	.0290	.0040	-.0018
.90	-3.00	5.01	-.529	-.0104	.0292	.0046	-.0017
.90	-.00	5.00	-.533	.0037	.0295	-.0181	-.0025
.90	3.00	4.99	-.566	.0181	.0312	-.0392	-.0056
.90	6.00	5.01	-.643	.0379	.0354	-.0690	-.0068
.90	8.98	5.01	-.774	.0731	.0428	-.1158	-.0118
1.20	.00	.85	.000	-.0118	.0258	.0114	.0015
1.20	-.01	3.03	-1.695	-.0105	.0273	.0050	-.0036
1.20	.00	5.02	-.915	-.0101	.0285	.0025	-.0018
1.20	-.00	7.01	-.631	-.0107	.0295	.0025	-.0020
1.20	.01	8.98	-.487	-.0111	.0305	.0028	-.0022
1.20	-2.99	7.02	-.699	-.0551	.0327	.0640	.0027
1.20	-.00	6.99	-.637	-.0105	.0296	.0019	-.0021
1.20	3.00	7.00	-.722	.0451	.0336	-.0675	-.0068
1.20	5.99	7.02	-.934	.0843	.0436	-.1188	-.0146
1.20	8.99	7.02	-1.208	.1230	.0564	-.1747	-.0200
120° reverser-port angle							
0.15	-0.01	1.00	0.000	-0.0074	-0.0368	-0.0086	0.0078
.15	-.01	2.00	-.638	.0014	.3195	-.0927	-.0405
.15	.01	2.60	-.574	-.0094	.4465	-.1025	-.0471
.15	-.00	3.00	-.539	-.0239	.5254	-.0985	-.0513
.15	.00	3.79	-.502	-.0569	.6766	-.0783	-.0766
.15	-.00	3.80	-.503	-.0532	.6816	-.0841	-.0863
.15	-3.00	2.61	-.579	.0126	.4509	-.0832	-.0461
.15	.01	2.60	-.585	.0124	.4563	-.1161	-.0583
.15	2.99	2.60	-.587	.0241	.4584	-.1520	-.0636
.15	5.98	2.60	-.597	.0255	.4633	-.1839	-.0702
.15	9.01	2.60	-.607	.0208	.4749	-.2159	-.0772
.60	-.02	1.01	.000	.0075	.0086	-.0166	.0023
.60	-.00	2.00	-.921	.0008	.0291	-.0129	-.0026
.60	.00	3.02	-.666	-.0014	.0417	-.0125	-.0020
.60	.00	3.50	-.645	-.0032	.0500	-.0117	-.0025
.60	-.00	5.01	-.579	-.0049	.0711	-.0147	-.0067
.60	-3.00	3.50	-.657	-.0212	.0506	.0186	-.0031
.60	.01	3.50	-.659	-.0009	.0507	-.0131	-.0033
.60	2.98	3.50	-.690	.0220	.0528	-.0463	-.0072
.60	6.00	3.50	-.729	.0414	.0561	-.0724	-.0105
.60	8.99	3.51	-.804	.0610	.0620	-.1004	-.0092

TABLE 4.- Continued

M	α, deg	NPR	$\frac{F - D}{F_i}$	C_L	$C_{(D-F)}$	C_m	$C_{m,n}$
120° reverser-port angle							
0.90	-0.01	1.06	0.000	0.0104	0.0123	-0.0243	0.0042
.90	.00	2.01	-1.457	.0135	.0190	-.0298	-.0041
.90	-.01	3.00	-.945	.0094	.0264	-.0248	-.0026
.90	.02	5.02	-.661	.0008	.0361	-.0159	-.0022
.90	.01	6.98	-.529	-.0028	.0434	-.0135	-.0020
.90	-3.00	5.01	-.673	-.0131	.0368	.0079	-.0011
.90	-.01	5.02	-.672	.0013	.0366	-.0163	-.0025
.90	2.99	5.00	-.703	.0144	.0385	-.0367	-.0052
.90	5.98	5.00	-.777	.0331	.0424	-.0642	-.0065
.90	8.98	5.02	-.904	.0668	.0494	-.1091	-.0107
1.20	-.00	.85	.000	-.0111	.0254	.0110	.0008
1.20	.00	3.02	-1.838	-.0094	.0291	.0036	-.0036
1.20	-.00	5.00	-1.036	-.0094	.0316	.0021	-.0024
1.20	.01	7.02	-.740	-.0096	.0342	.0013	-.0025
1.20	.00	8.98	-.590	-.0120	.0366	.0038	-.0026
1.20	.00	8.99	-.590	-.0121	.0366	.0040	-.0027
1.20	-3.00	7.01	-.815	-.0538	.0375	.0623	.0014
1.20	-.00	7.01	-.744	-.0096	.0344	.0010	-.0027
1.20	2.99	7.03	-.832	.0452	.0387	-.0677	-.0076
1.20	5.99	7.03	-1.059	.0835	.0486	-.1181	-.0148
1.20	8.97	7.02	-1.348	.1221	.0618	-.1742	-.0196
130° reverser-port angle							
0.15	0.01	1.00	0.000	-0.0168	-0.0415	-0.0097	0.0053
.15	-.02	2.01	-.784	.0405	.3765	-.1267	-.0230
.15	-.01	2.61	-.663	-.0021	.4962	-.1200	-.0500
.15	-.01	3.02	-.663	-.0165	.6256	-.1229	-.0570
.15	.00	3.80	-.606	-.0616	.7941	-.0870	-.0882
.15	-3.02	2.62	-.675	.0121	.5071	-.0982	-.0511
.15	.02	2.61	-.673	.0159	.5023	-.1319	-.0605
.15	3.02	2.61	-.676	.0107	.5044	-.1628	-.0681
.15	5.98	2.62	-.678	.0066	.5077	-.1931	-.0697
.15	8.99	2.61	-.682	.0028	.5138	-.2207	-.0758
.60	-.00	1.00	.000	.0075	.0070	-.0172	.0017
.60	-.00	2.00	-1.067	.0028	.0325	-.0155	-.0021
.60	.00	3.00	-.814	-.0027	.0485	-.0118	-.0029
.60	.00	3.52	-.753	-.0040	.0559	-.0116	-.0058
.60	.01	4.99	-.720	-.0044	.0839	-.0174	-.0098
.60	-2.98	3.50	-.769	-.0224	.0565	.0193	-.0054
.60	-.02	3.51	-.765	-.0023	.0560	-.0125	-.0056
.60	3.00	3.51	-.792	.0186	.0578	-.0434	-.0079
.60	5.98	3.50	-.837	.0395	.0613	-.0720	-.0104
.60	9.00	3.51	-.887	.0527	.0646	-.0909	-.0084
.90	-.00	1.05	.000	.0111	.0121	-.0257	.0038
.90	.01	2.12	-1.373	-.0007	.0199	-.0118	-.0046

TABLE 4.- Continued

M	α, deg	NPR	$\frac{F - D}{F_i}$	C_L	$C_{(D-F)}$	$C_{\bar{m}}$	$C_{m,n}$
130° reverser-port angle							
0.90	-0.06	2.01	-1.535	0.0081	0.0194	-0.0232	-0.0037
.90	-.04	3.01	-1.089	.0067	.0291	-.0216	-.0022
.90	.02	4.99	-.802	-.0004	.0411	-.0149	-.0016
.90	.04	7.01	-.656	-.0045	.0512	-.0123	-.0029
.90	-2.99	5.01	-.824	-.0139	.0426	.0098	-.0011
.90	.02	5.01	-.813	.0003	.0421	-.0152	-.0026
.90	2.99	5.01	-.839	.0114	.0435	-.0338	-.0053
.90	5.99	4.99	-.909	.0287	.0471	-.0592	-.0058
.90	9.01	5.01	-1.026	.0611	.0531	-.1019	-.0093
1.20	-.00	.83	.000	-.0132	.0258	.0106	.0015
1.20	-.01	3.02	-2.025	-.0114	.0304	.0039	-.0021
1.20	-.01	5.02	-1.176	-.0111	.0343	.0026	-.0010
1.20	.01	7.01	-.867	-.0120	.0380	.0030	-.0012
1.20	.03	9.02	-.702	-.0137	.0414	.0046	-.0027
1.20	-3.00	7.00	-.951	-.0548	.0416	.0626	.0030
1.20	.00	6.98	-.877	-.0113	.0382	.0023	-.0016
1.20	.00	7.02	-.875	-.0110	.0383	.0019	-.0020
1.20	2.97	7.01	-.959	.0430	.0419	-.0662	-.0070
1.20	6.00	7.01	-1.189	.0828	.0522	-.1188	-.0142
1.20	8.98	7.01	-1.478	.1198	.0644	-.1728	-.0189
110° reverser-port angle (short internal passage length)							
0.15	-0.04	1.00	0.000	0.0248	-0.0212	-0.0162	-0.0016
.15	-.04	1.99	-.164	-.0077	.0970	-.0158	-.0029
.15	-.03	2.59	-.185	-.0196	.1731	-.0209	-.0076
.15	-.03	3.00	-.195	-.0303	.2274	-.0207	-.0402
.15	-.03	3.81	-.208	-.0509	.3455	-.0267	-.0549
.15	-3.05	2.61	-.192	-.0322	.1804	.0094	-.0333
.15	-.03	2.61	-.193	-.0202	.1822	-.0188	-.0381
.15	2.94	2.61	-.199	.0029	.1788	-.0539	-.0090
.15	5.97	2.61	-.200	.0299	.1784	-.0906	-.0179
.15	8.95	2.61	-.214	.0505	.1925	-.1315	-.0220
.60	-.06	1.01	.000	.0099	.0084	-.0178	.0017
.60	-.04	2.01	-.387	.0081	.0140	-.0176	-.0011
.60	-.06	2.99	-.272	.0037	.0192	-.0136	-.0008
.60	-.05	3.50	-.253	.0019	.0225	-.0124	-.0010
.60	-.05	5.00	-.245	-.0042	.0354	-.0081	-.0006
.60	-3.05	3.51	-.266	-.0194	.0236	.0192	.0004
.60	-.06	3.50	-.264	.0027	.0235	-.0129	-.0013
.60	2.93	3.50	-.306	.0290	.0272	-.0483	-.0067
.60	5.95	3.49	-.361	.0551	.0321	-.0805	-.0090
.60	8.96	3.50	-.443	.0810	.0392	-.1179	-.0126
.90	-.05	1.05	.000	.0107	.0129	-.0228	.0033
.90	-.03	2.02	-.919	.0156	.0143	-.0296	-.0040
.90	-.05	3.00	-.511	.0164	.0159	-.0309	-.0059
.90	-.06	5.02	-.303	.0077	.0193	-.0206	-.0029

TABLE 4.- Continued

M	α, deg	NPR	$\frac{F - D}{F_i}$	C_L	$C_{(D-F)}$	C_m	$C_{m,n}$
110° reverser-port angle (short internal passage length)							
0.90	-0.03	7.00	-0.268	0.0003	0.0263	-0.0125	0.0000
.90	-3.07	5.03	-.294	-.0060	.0189	-.0002	.0002
.90	-.06	5.01	-.308	.0081	.0198	-.0209	-.0026
.90	2.94	5.03	-.341	.0216	.0217	-.0404	-.0055
.90	5.96	5.02	-.426	.0452	.0270	-.0770	-.0075
.90	8.94	5.00	-.555	.0844	.0354	-.1283	-.0134
1.20	-.06	.84	.000	-.0105	.0268	.0103	.0001
1.20	-.06	3.02	-1.305	-.0101	.0229	.0067	-.0027
1.20	-.06	5.02	-.651	-.0080	.0233	.0017	-.0033
1.20	-.04	7.01	-.456	-.0082	.0250	.0012	-.0025
1.20	-.06	9.00	-.348	-.0103	.0260	.0043	-.0016
1.20	-3.05	7.02	-.517	-.0534	.0285	.0642	.0029
1.20	-.04	7.02	-.462	-.0065	.0254	-.0010	-.0025
1.20	2.95	7.00	-.543	.0498	.0299	-.0707	-.0075
1.20	5.94	7.00	-.730	.0889	.0400	-.1221	-.0156
1.20	8.94	7.04	-.986	.1286	.0538	-.1797	-.0205
110° reverser-port angle (short internal passage length) with forward and aft external doors and sidewalls							
0.15	-0.00	1.00	0.000	0.0094	-0.0077	-0.0156	0.0049
.15	-.01	1.99	-.493	-.0083	.2916	-.0539	-.0262
.15	-.01	2.60	-.430	-.0308	.3883	-.0492	-.0563
.15	-.01	2.99	-.403	-.0406	.4523	-.0506	-.0609
.15	-.00	3.80	-.390	-.0601	.6074	-.0546	-.0747
.15	-2.99	2.61	-.442	-.0167	.4053	-.0323	-.0576
.15	.00	2.61	-.442	-.0245	.4079	-.0535	-.0591
.15	3.01	2.61	-.439	-.0172	.4022	-.0864	-.0345
.15	5.98	2.61	-.443	-.0057	.4062	-.1215	-.0392
.15	9.01	2.62	-.446	-.0032	.4119	-.1548	-.0410
.60	.00	.96	.000	.0155	.0177	-.0206	-.0019
.60	.00	2.04	-.989	.0057	.0382	-.0156	-.0029
.60	-.00	3.01	-.734	-.0002	.0528	-.0128	-.0038
.60	-.02	3.51	-.686	-.0014	.0603	-.0132	-.0051
.60	-.01	5.01	-.498	-.0050	.0697	-.0123	-.0059
.60	-3.01	3.49	-.703	-.0222	.0614	.0210	-.0054
.60	.00	3.51	-.696	-.0026	.0609	-.0124	-.0045
.60	2.99	3.51	-.726	.0232	.0635	-.0491	-.0093
.60	6.01	3.50	-.764	.0406	.0674	-.0736	-.0122
.60	8.99	3.49	-.841	.0608	.0742	-.1048	-.0123
110° reverser-port angle (short internal passage length) with aft external doors and sidewalls							
0.15	-0.04	1.00	0.000	0.0081	-0.0178	-0.0076	0.0028
.15	-.02	1.99	-.486	-.0153	.2682	-.0446	-.0210
.15	-.02	2.60	-.483	-.0256	.4337	-.0631	-.0309

TABLE 4.- Continued

M	α, deg	NPR	$\frac{F - D}{F_i}$	C_L	$C_{(D-F)}$	C_m	$C_{m,n}$
110° reverser-port angle (short internal passage length) with aft external doors and sidewalls							
0.15	-0.02	3.00	-0.514	-0.0351	0.5831	-0.0748	-0.0748
.15	-.01	3.79	-.545	-.0485	.8724	-.0964	-.1033
.15	-3.02	2.59	-.491	-.0098	.4390	-.0418	-.0607
.15	-.03	2.60	-.490	-.0157	.4382	-.0659	-.0337
.15	2.99	2.60	-.496	-.0034	.4420	-.1037	-.0426
.15	5.99	2.60	-.494	.0048	.4418	-.1449	-.0498
.15	8.99	2.60	-.500	.0049	.4460	-.1753	-.0534
.60	-.01	1.07	.000	.0104	.0153	-.0127	-.0010
.60	-.01	2.00	-.999	.0091	.0330	-.0178	-.0033
.60	-.01	3.00	-.705	.0022	.0487	-.0139	-.0032
.60	-.02	3.49	-.692	-.0014	.0602	-.0120	-.0041
.60	.01	4.48	-.676	-.0020	.0834	-.0174	-.0083
.60	-3.01	3.51	-.700	-.0196	.0609	.0173	-.0057
.60	-.01	3.51	-.699	-.0013	.0608	-.0124	-.0045
.60	2.98	3.51	-.727	.0207	.0633	-.0449	-.0079
.60	5.99	3.51	-.765	.0390	.0670	-.0703	-.0108
.60	8.98	3.51	-.837	.0613	.0736	-.1039	-.0108
130° top/110° bottom reverser-port angles							
0.15	0.01	1.00	0.000	-0.0017	0.0293	-0.0108	0.0027
.15	.03	2.00	-.825	.6043	.4319	-.8487	-.2394
.15	.01	2.62	-.603	.0958	.4841	-.2625	-.1734
.15	-.05	3.01	-.575	.1182	.5711	-.3085	-.2073
.15	-.01	3.80	-.543	.0805	.7456	-.2920	-.2062
.15	-2.98	2.61	-.605	.1065	.4853	-.2417	-.1661
.15	.01	2.60	-.617	.1081	.4905	-.2713	-.1805
.15	3.02	2.60	-.625	.1087	.4977	-.3122	-.1780
.15	5.99	2.61	-.635	.1167	.5081	-.3498	-.1898
.15	9.01	2.60	-.646	.1141	.5142	-.3810	-.1941
130° top/120° bottom reverser-port angles							
0.15	-0.02	1.00	0.000	-0.0053	0.0090	-0.0071	0.0079
.15	-.01	2.01	-.853	.5324	.4371	-.7938	-.1605
.15	-.00	2.60	-.644	.0744	.5030	-.2178	-.1222
.15	-.01	3.00	-.624	.0928	.6028	-.2643	-.1526
.15	-.01	3.82	-.572	.0524	.7783	-.2480	-.1628
.15	-3.02	2.61	-.650	.0738	.5036	-.1872	-.1106
.15	.02	2.61	-.654	.0704	.5049	-.2156	-.1123
.15	3.01	2.61	-.661	.0733	.5127	-.2563	-.1277
.15	6.00	2.61	-.667	.0811	.5169	-.2988	-.1381
.15	9.01	2.61	-.675	.0693	.5264	-.3208	-.1389

TABLE 4.- Concluded

M	α, deg	NPR	$\frac{F - D}{F_i}$	C_L	$C_{(D-F)}$	C_m	$C_{m,n}$
110° top/130° bottom reverser-port angles							
0.15	-0.00	1.00	0.000	0.0087	0.0003	-0.0211	0.0044
.15	.01	2.00	-.663	-.4012	.3346	.5832	.1238
.15	-.01	2.60	-.572	-.0907	.4563	.0805	.0663
.15	.00	2.99	-.543	-.1306	.5340	.1247	.0900
.15	-.00	3.81	-.518	-.1446	.7178	.1058	.0679
.15	-3.00	2.61	-.583	-.0838	.4669	.1010	.0663
.15	.02	2.60	-.569	-.0895	.4547	.0734	.0509
.15	3.01	2.60	-.561	-.0913	.4493	.0442	.0484
.15	6.02	2.61	-.554	-.1025	.4437	.0234	.0457
.15	9.01	2.61	-.548	-.1045	.4375	-.0056	.0452
120° top/130° bottom reverser-port angles							
0.15	0.00	1.00	0.000	0.0188	0.0088	-0.0222	0.0009
.15	-.00	2.00	-.714	-.3264	.3640	.4713	.0767
.15	-.00	2.61	-.636	-.0475	.5130	-.0034	-.0031
.15	.01	3.01	-.607	-.0835	.5969	.0408	.0227
.15	-.00	3.80	-.566	-.1170	.7695	.0563	.0201
.15	-3.01	2.61	-.636	-.0367	.4938	.0127	.0084
.15	-.01	2.60	-.630	-.0458	.4927	-.0098	-.0105
.15	3.01	2.60	-.625	-.0521	.4866	-.0419	-.0096
.15	5.99	2.61	-.619	-.0573	.4799	-.0682	-.0155
.15	9.00	2.61	-.614	-.0722	.4798	-.0902	.0126

TABLE 5.- NOZZLE PRESSURE RATIO VARIATION WITH MACH NUMBER

M	Typical operating NPR
0.15	2.6
.60	3.5
.90	5.0
1.20	7.0

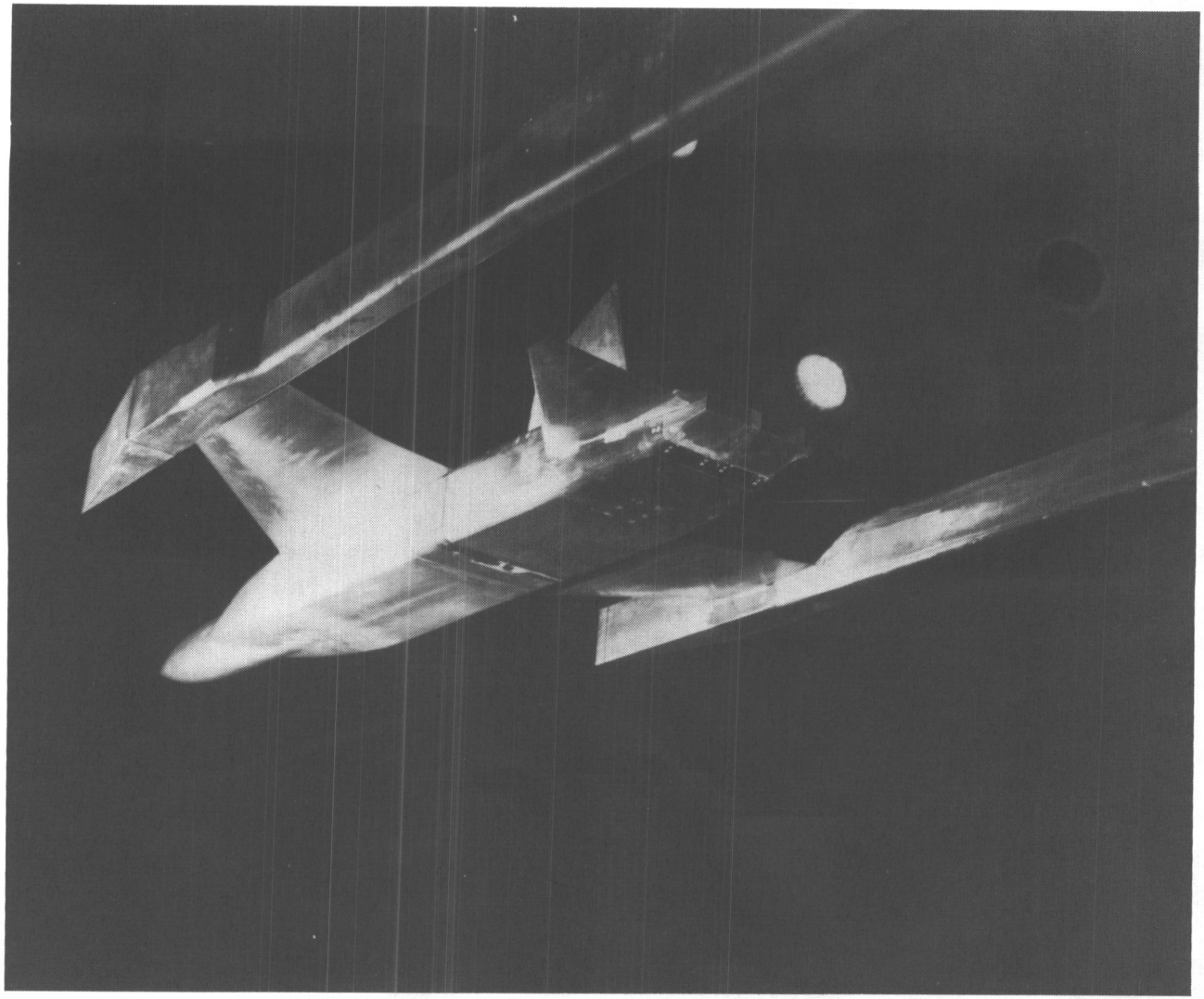

L-82-1374

Figure 1.- Generic twin-engine fighter aircraft model with base-line (forward-thrust) nozzle.

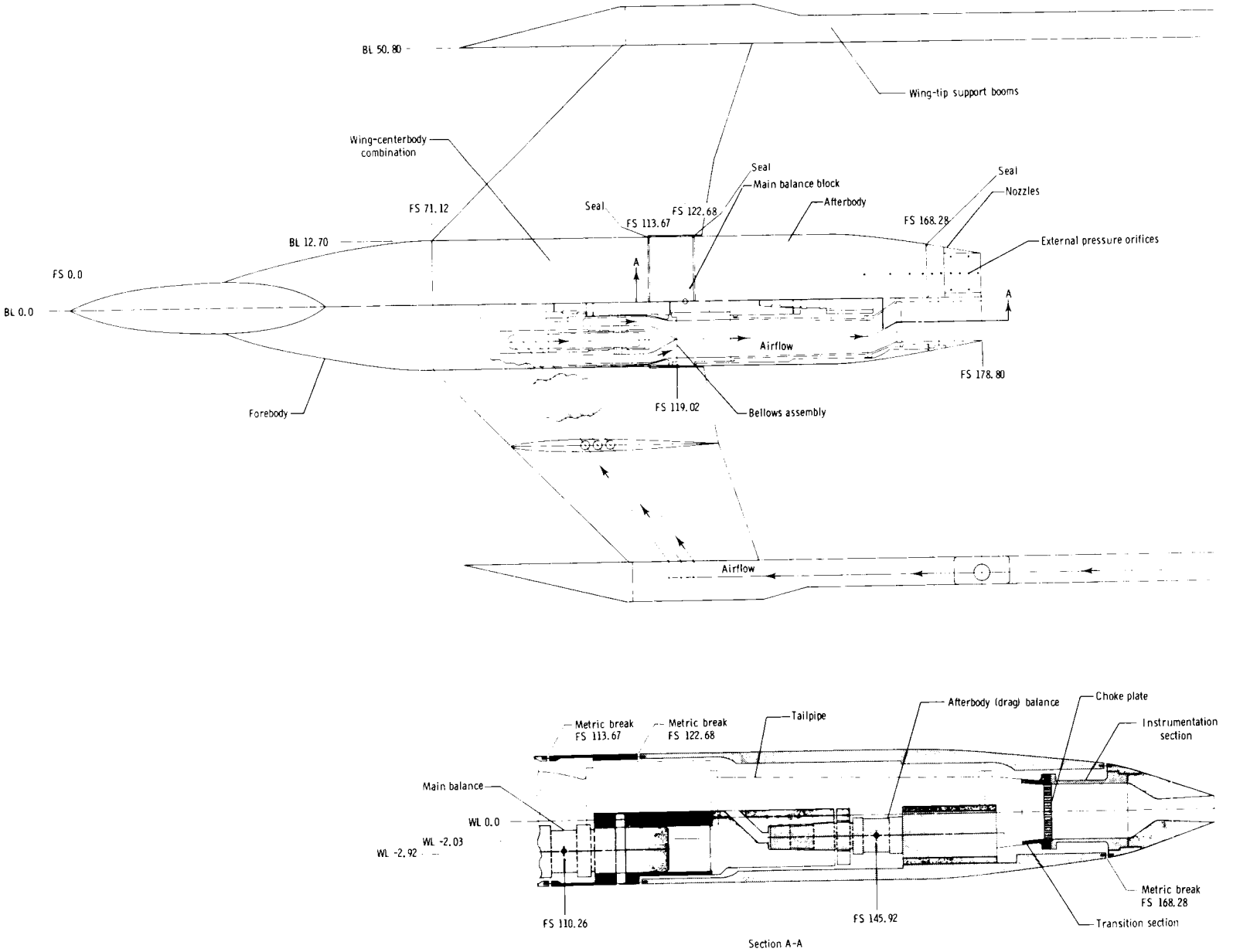

Figure 2.- Wing-tip supported model with base-line (forward-thrust) nozzle showing jet simulation system and balance arrangement. Dimensions in centimeters.

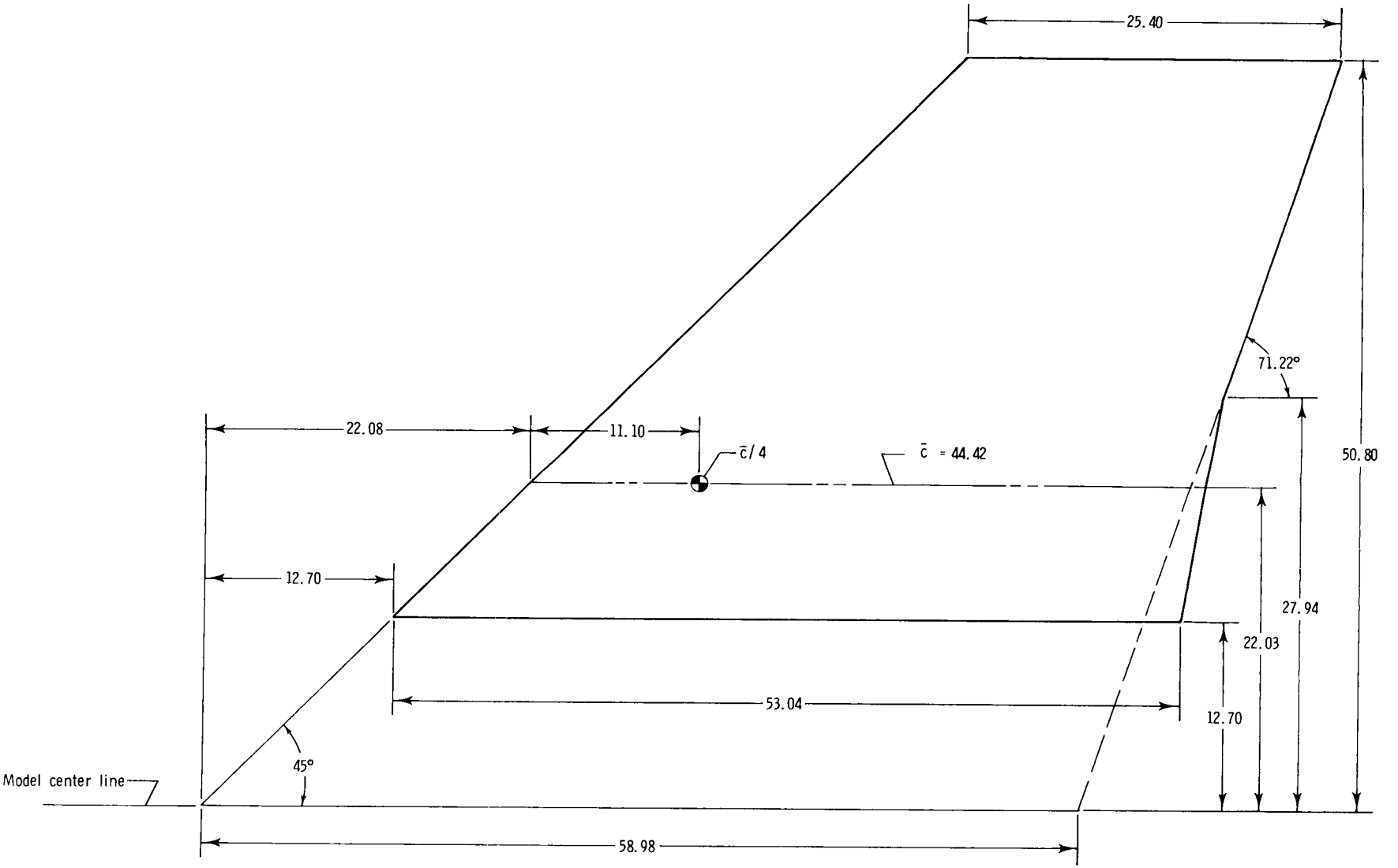

Figure 3.- Wing planform geometry. All linear dimensions in centimeters.

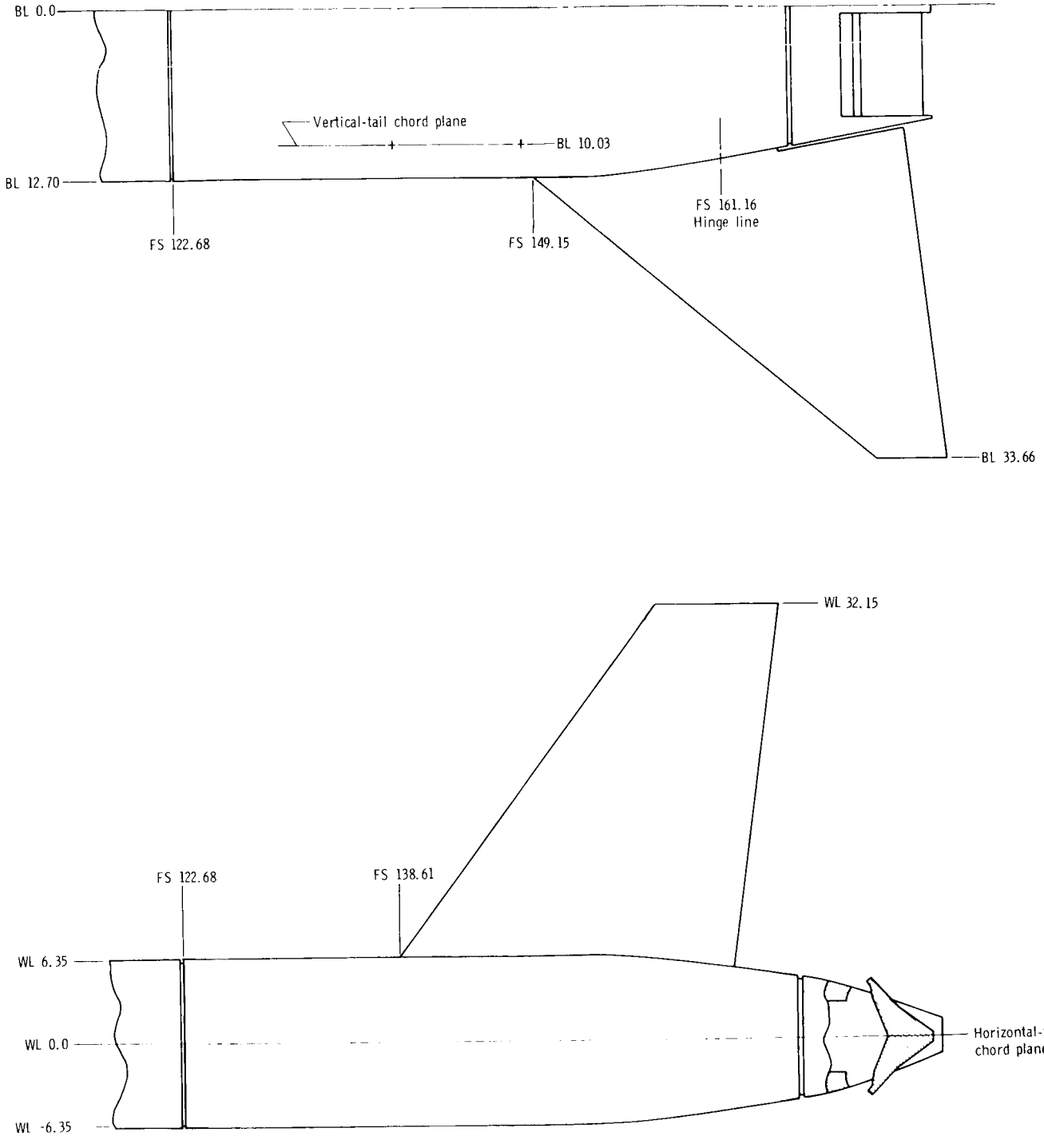

Figure 4.- Location of horizontal and vertical tails. Cutaway view of the 100-percent deployment nozzle is depicted installed on aircraft model. All linear dimensions in centimeters.

Horizontal-Tail Geometry

Airfoil sections:	
Tip	NACA 64-002.5
Root	NACA 64-005.5
Tip chord, cm	5.08
Root chord, cm	28.96
Taper ratio	.175
Span, cm	67.51
Planform area (one side exposed, filler excluded), m^2	.0372
Aspect ratio (exposed, filler excluded)	2.564
Λ_{le}, deg	50.0

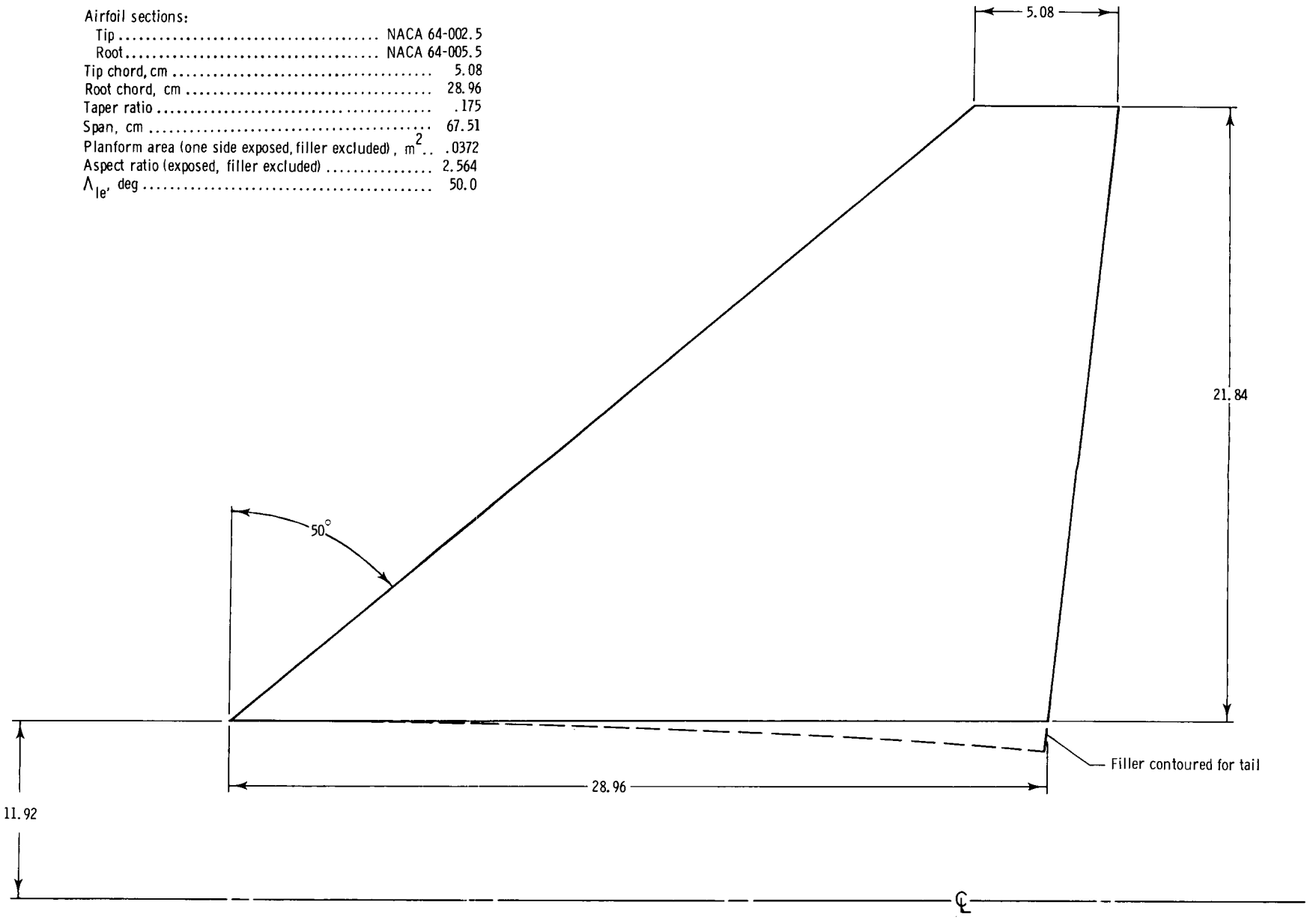

Figure 5.- Horizontal-tail geometry. All linear dimensions in centimeters.

Twin Vertical-Tail Geometry

Airfoil sections:	
Tip	NACA 64-003.5
Root	NACA 64-005
Tip chord, cm	9.14
Root chord, cm	24.38
Taper ratio	.375
Tail height (root to tip), cm	25.40
Planform area (one side exposed, filler excluded), m^2	.0426
Aspect ratio (exposed, filler excluded)	1.514
Λ_{le}, deg	36.52

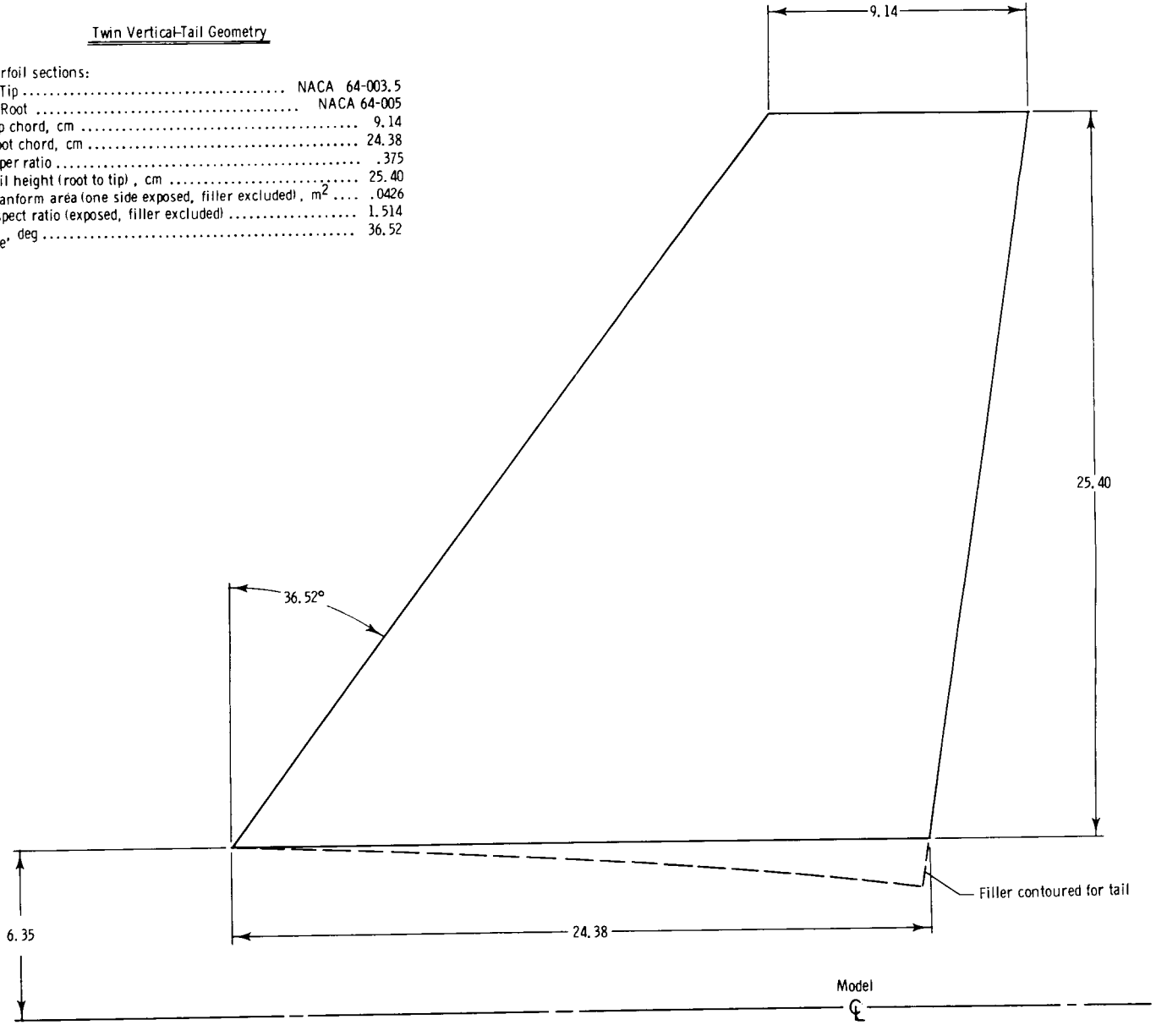

Figure 6.- Vertical-tail geometry. All linear dimensions in centimeters.

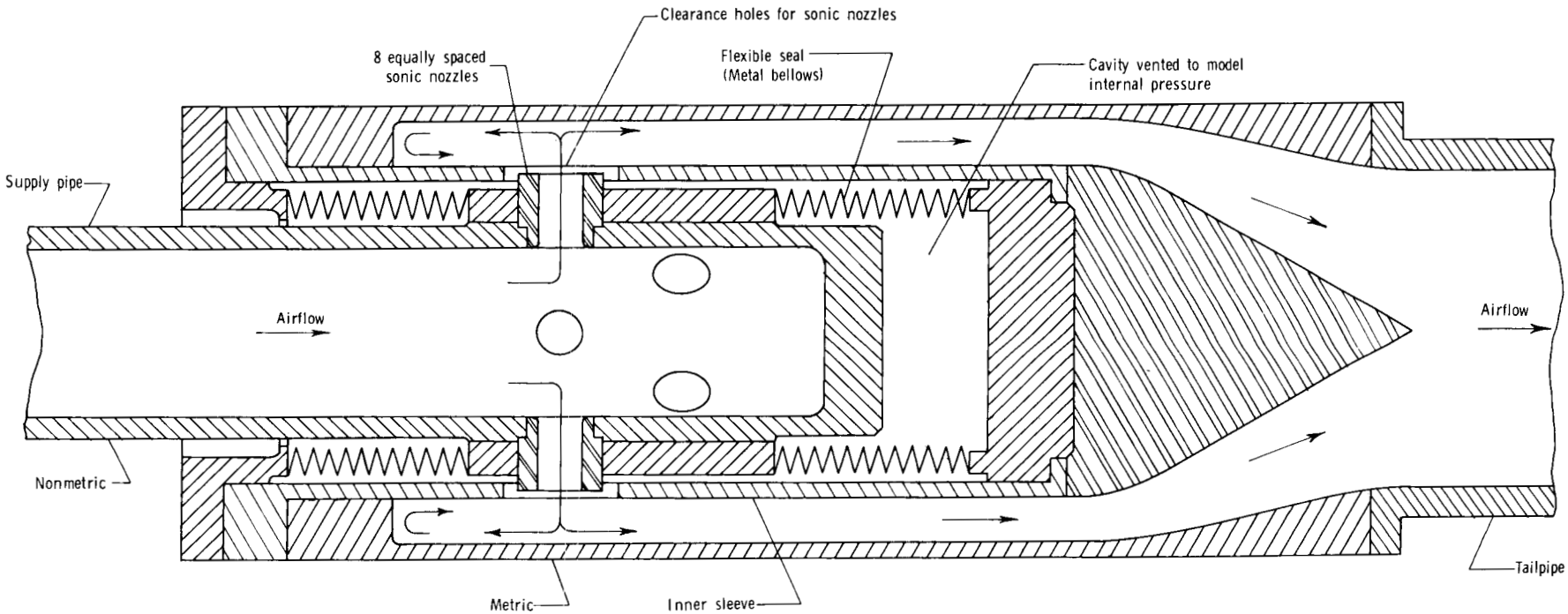

Figure 7.- Details of bellows assemblies used to transfer air from nonmetric to metric portions of model.

A_t, cm^2	A_e, cm^2	A_e/A_t	AR	$2A_t/A_{max}$
17.12	20.05	1.15	3.45	0.11

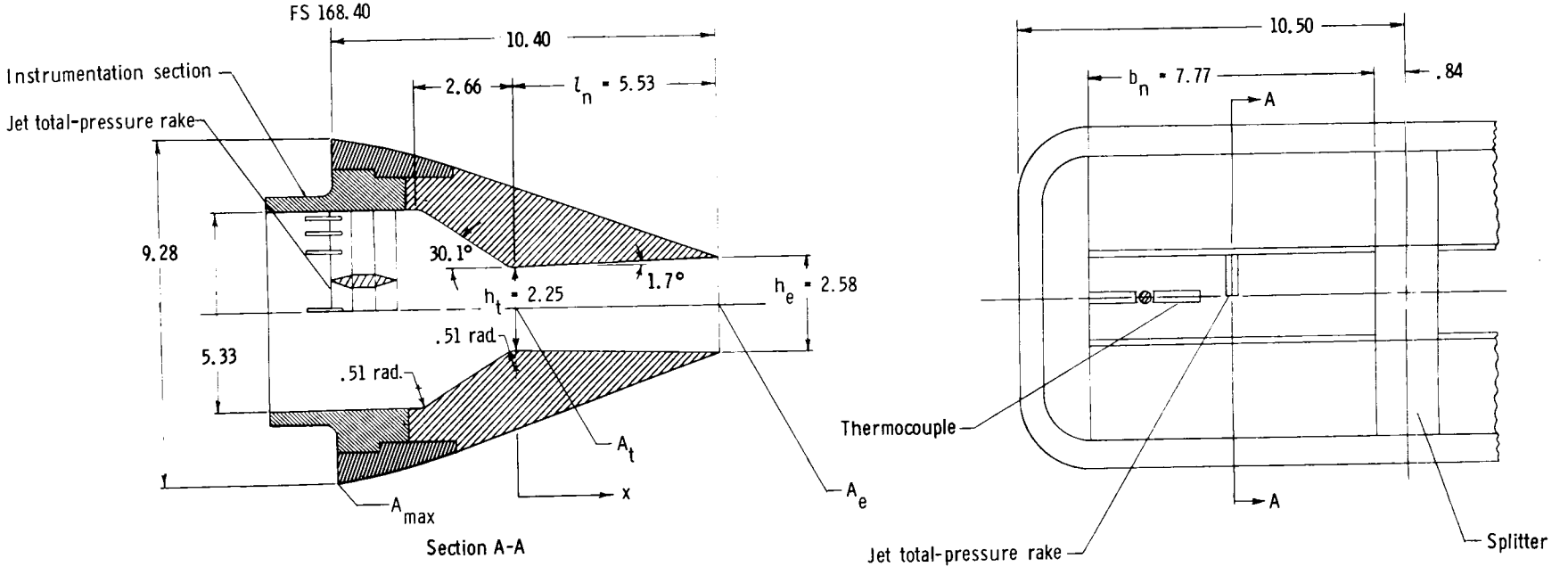

Figure 8.- Base-line (forward-thrust) nozzle geometry. All linear dimensions in centimeters.

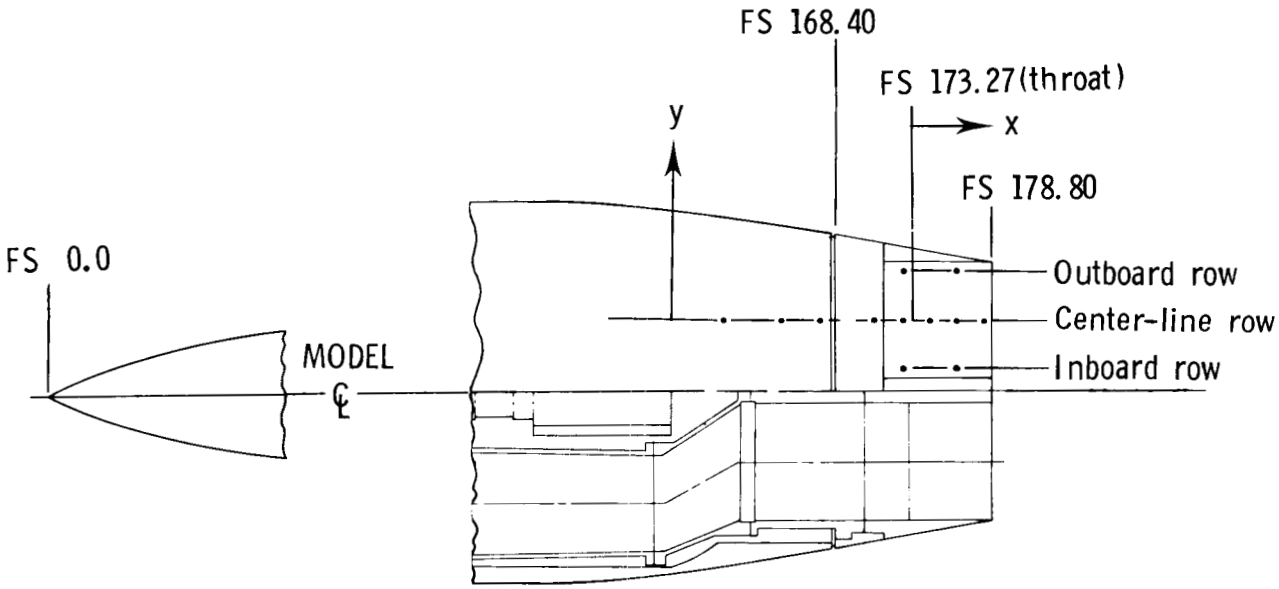

Pressure orifice locations

x/l_n	$y/(b_n/2)$
-2.200	0.00
-1.521	
-1.069	
-.423	
-.067	
.257	
.580	
.902	
-.067	.838
.580	
-.067	-.838
.580	

Figure 9.- External static-pressure orifice locations for base-line (forward-thrust) nozzle.

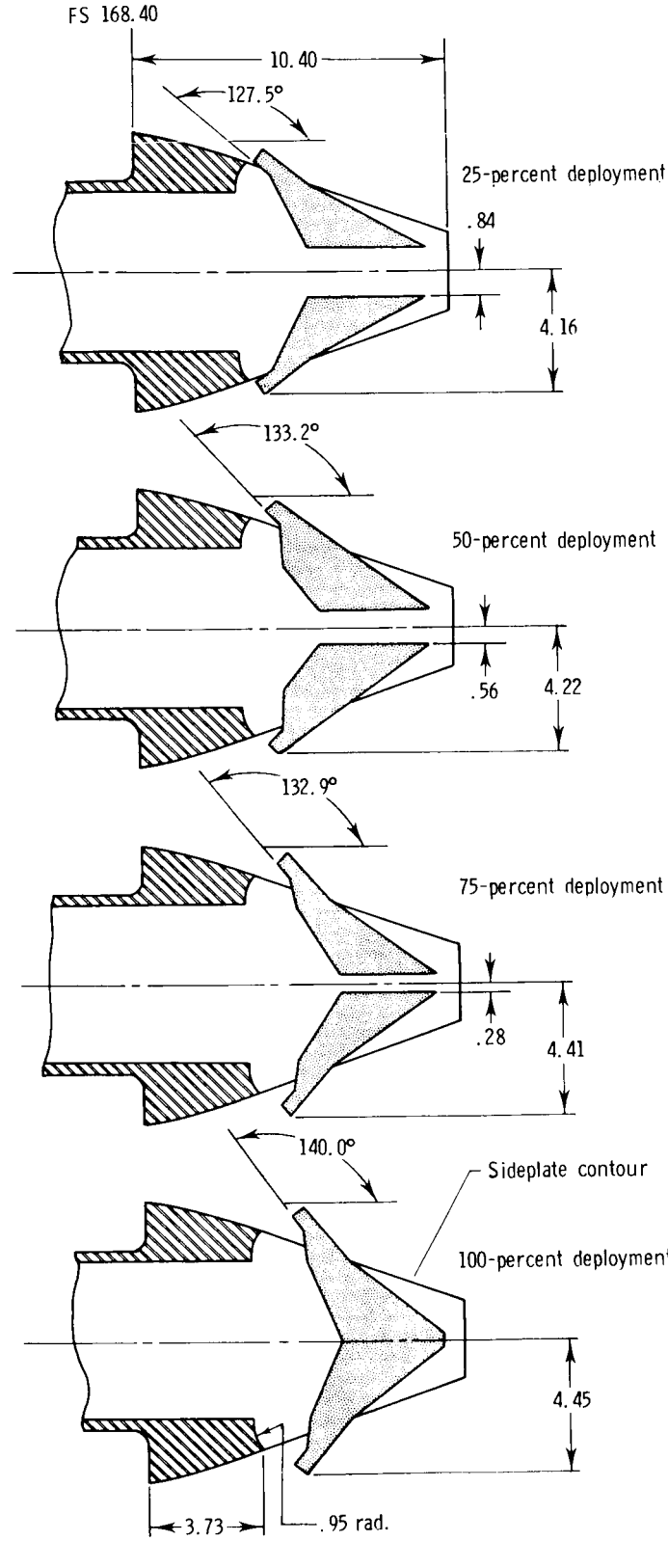

Pressure orifice locations for 100-percent deployment

External		Internal	
x/l_n	$y/(b_n/2)$	x/l_n	$y/(b_n/2)$
0.163	0.0	0.070	0.0
.374	↓	.094	↓
.608	↓	.167	↓
.723	↓	.230	↓
.875	↓	.070	.836
.723	.836	.167	↓
.875	↓	.167	-.836
.163	-.836		
.608	↓		

Figure 10.- Thrust-reverser port deployment nozzles. Nozzle width is 7.77 cm. All linear dimensions in centimeters.

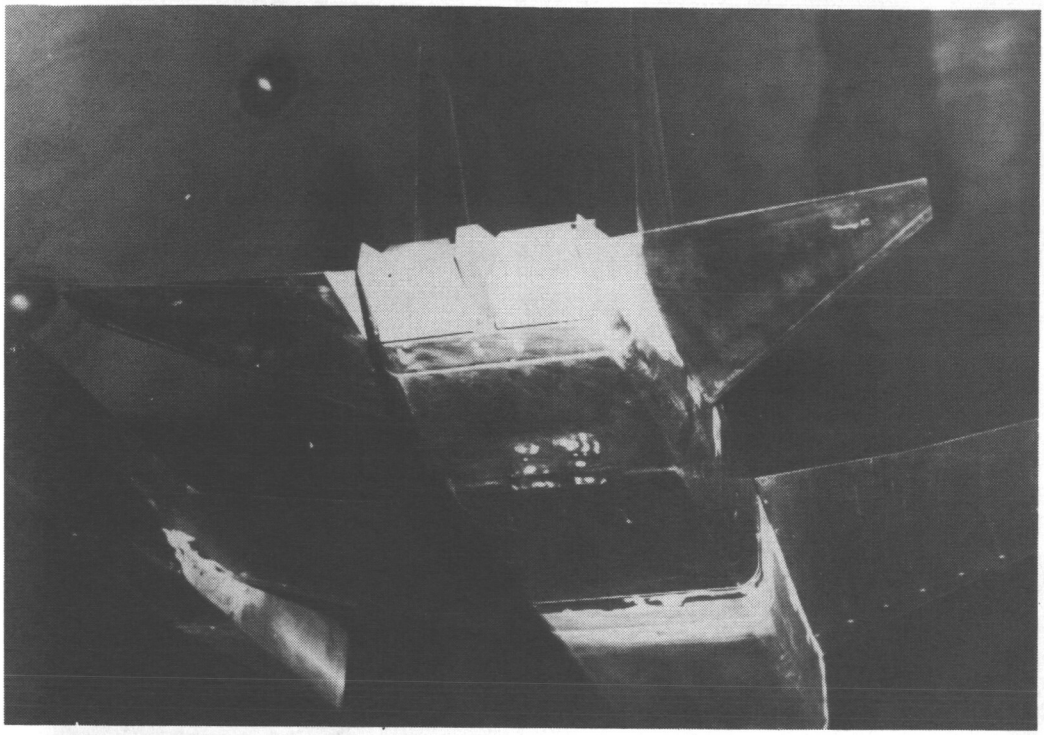

L-82-1294

(a) View upstream.

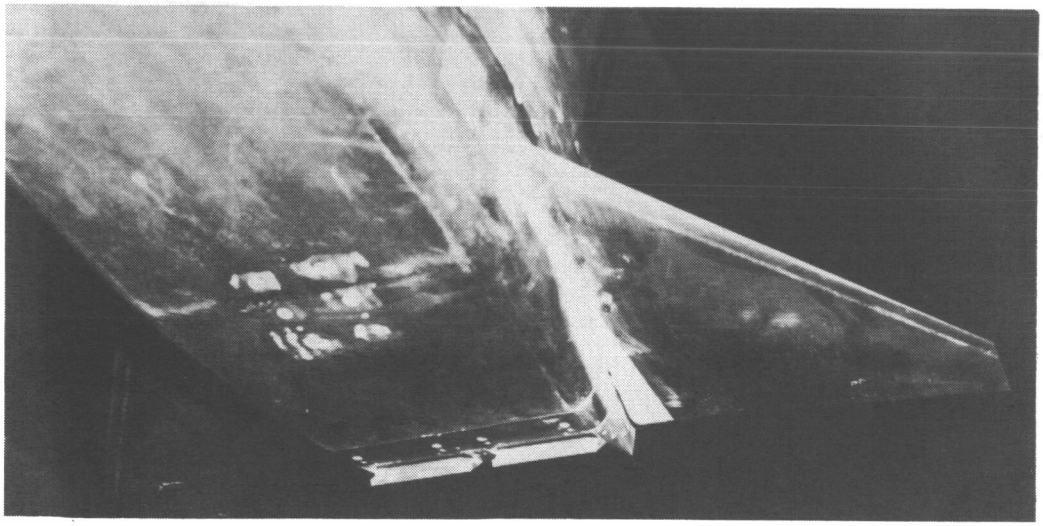

L-82-1298

(b) View downstream.

Figure 11.- Thrust-reverser nozzle deployed 100 percent installed on aircraft model.

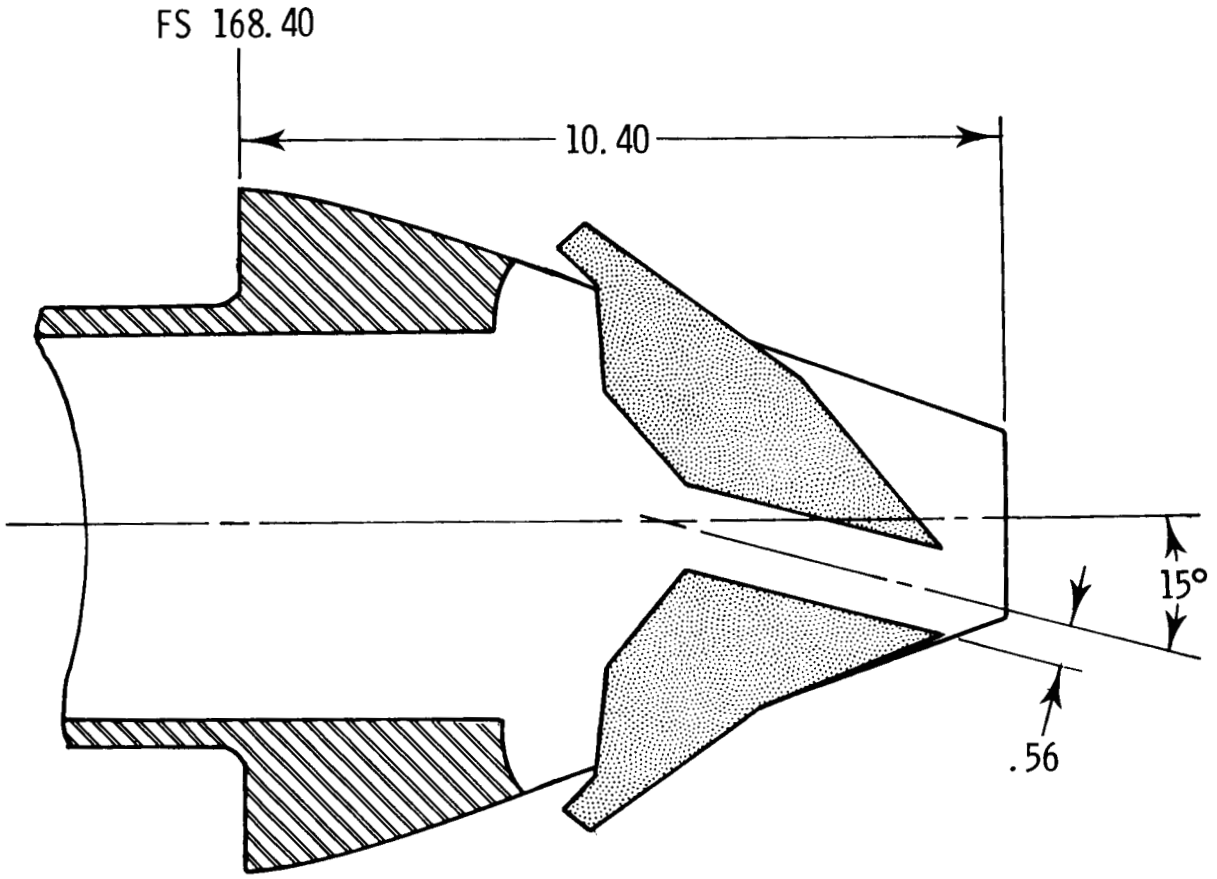

Figure 12.- Reverser deployed 50 percent with 15° thrust vectoring.
All linear dimensions in centimeters.

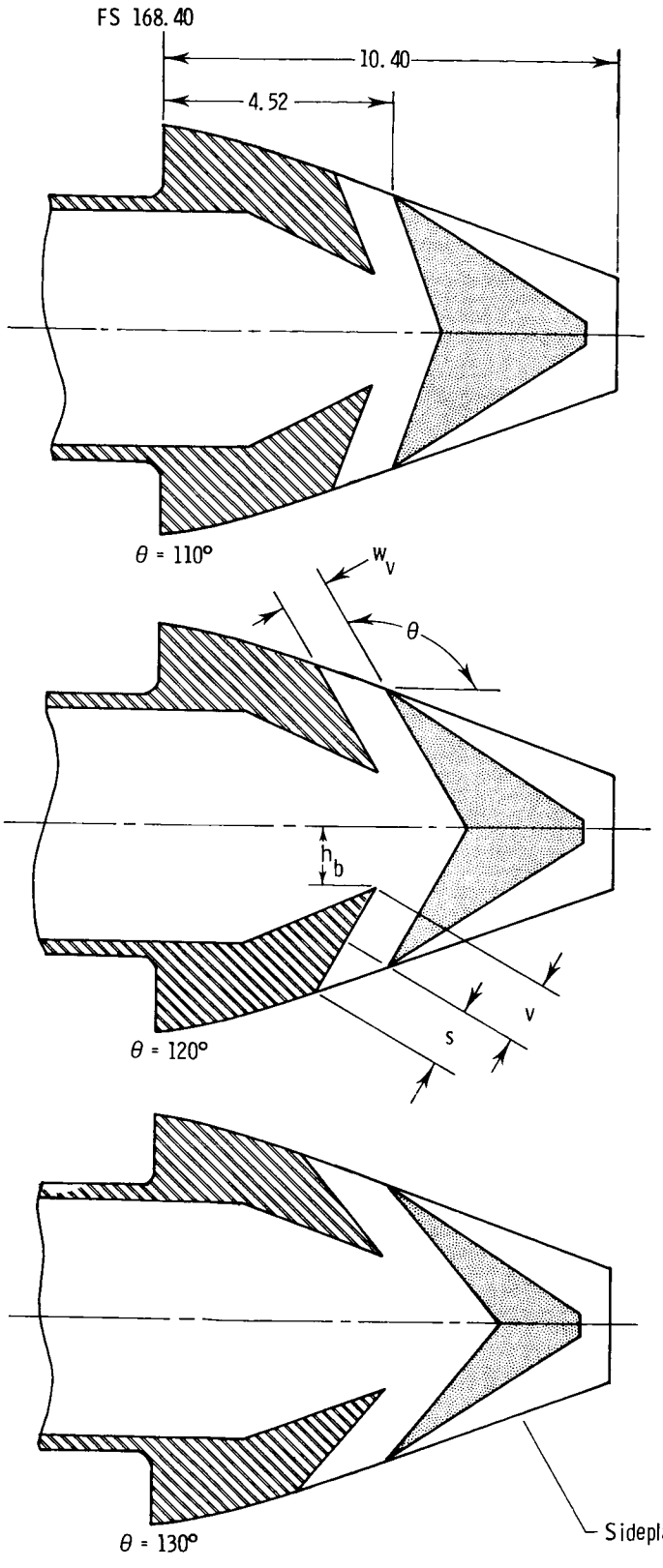

θ, deg	v	s	w_v	h_b	v/w_v	s/w_v
110	1.61	0.92	1.13	1.43	1.42	0.81
120	1.42	1.30	↓	1.35	1.26	1.15
130	1.22	1.88	↓	1.23	1.08	1.66

External pressure orifice locations

θ = 110°, 120°, 130°	
x/l_n	$y/(b_n/2)$
0.200	0.00
.316	↓
.587	↓
.703	↓
.860	↓
.703	.836
.860	↓
.200	-.836
.703	↓

Internal pressure orifice locations

θ = 110°		θ = 120°		θ = 130°	
x/l_n	$y/(b_n/2)$	x/l_n	$y/(b_n/2)$	x/l_n	$y/(b_n/2)$
0.098	0.00	0.128	0.00	0.164	0.00
.136	↓	.188	↓	.253	↓
.226	↓	.331	↓	.460	↓
.252	↓	.373	↓	.521	↓
.098	.836	.128	.836	.164	.836
.226	↓	.331	↓	.460	↓
.226	-.836	.331	-.836	.460	-.836

Figure 13.- Thrust-reverser-port angle configurations. Nozzle width is 7.77 cm. All linear dimensions in centimeters.

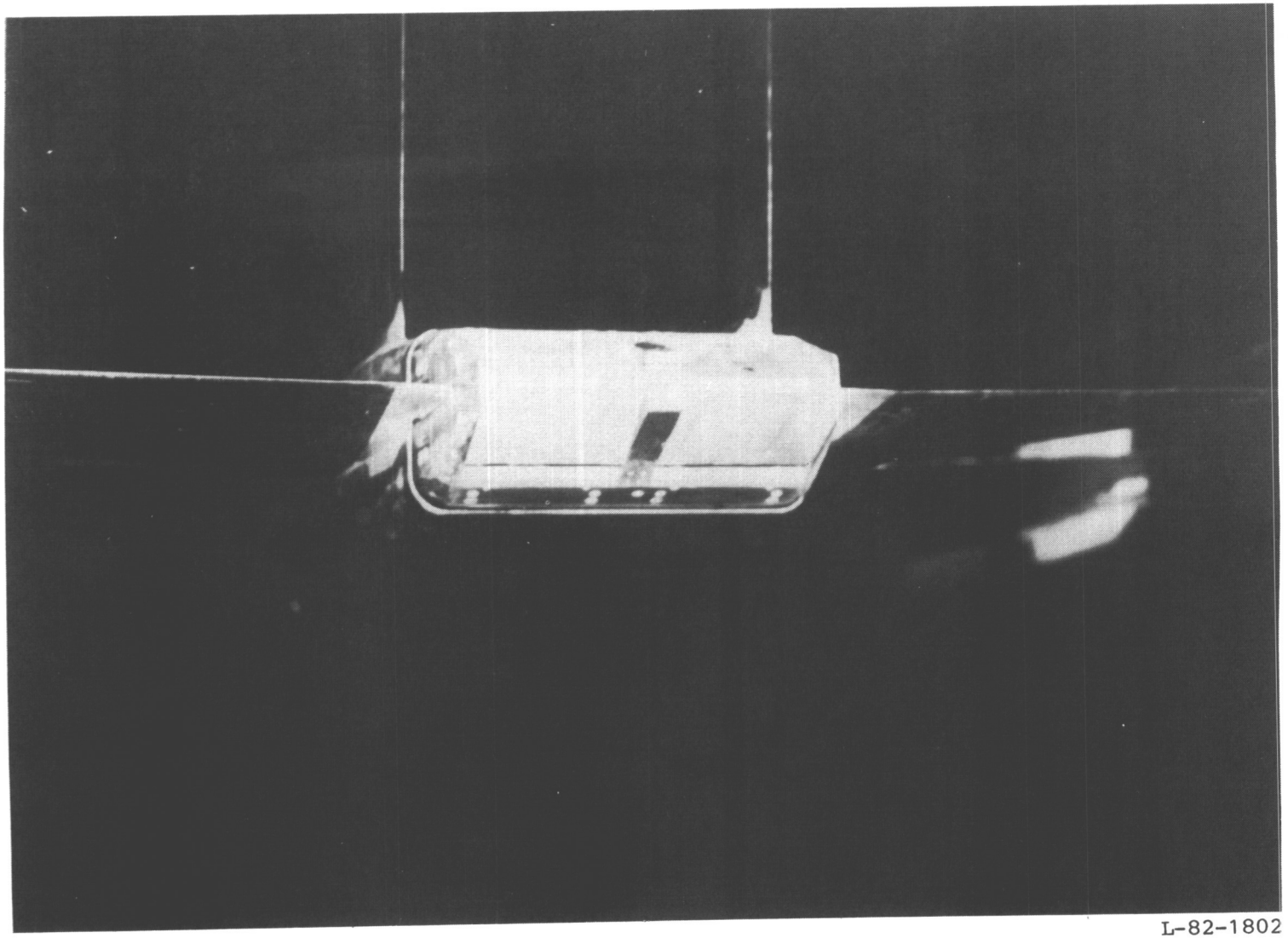

L-82-1802

Figure 14.- Reverser nozzle installed on the aircraft model. $\theta = 110°$.

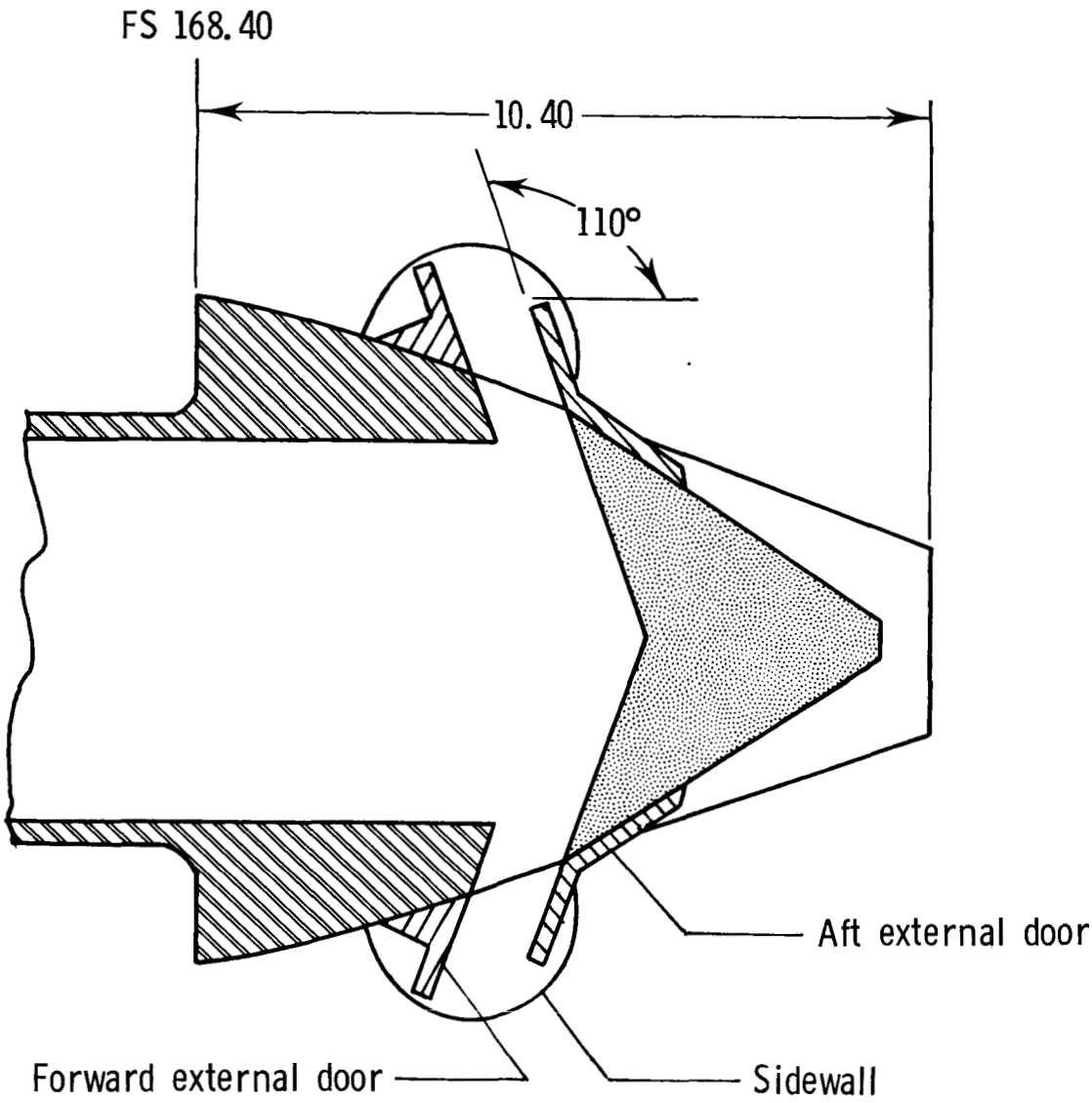

Doors and sidewalls	v	s	w_v	h_b	v/w_v	s/w_v
None	0.09	0.92	1.13	2.67	0.03	0.82
All	1.61	1.05	1.13	2.67	1.42	.93

Figure 15.- Reverser with short internal passage length and with external doors and sidewalls installed. θ = 110°. All linear dimensions in centimeters.

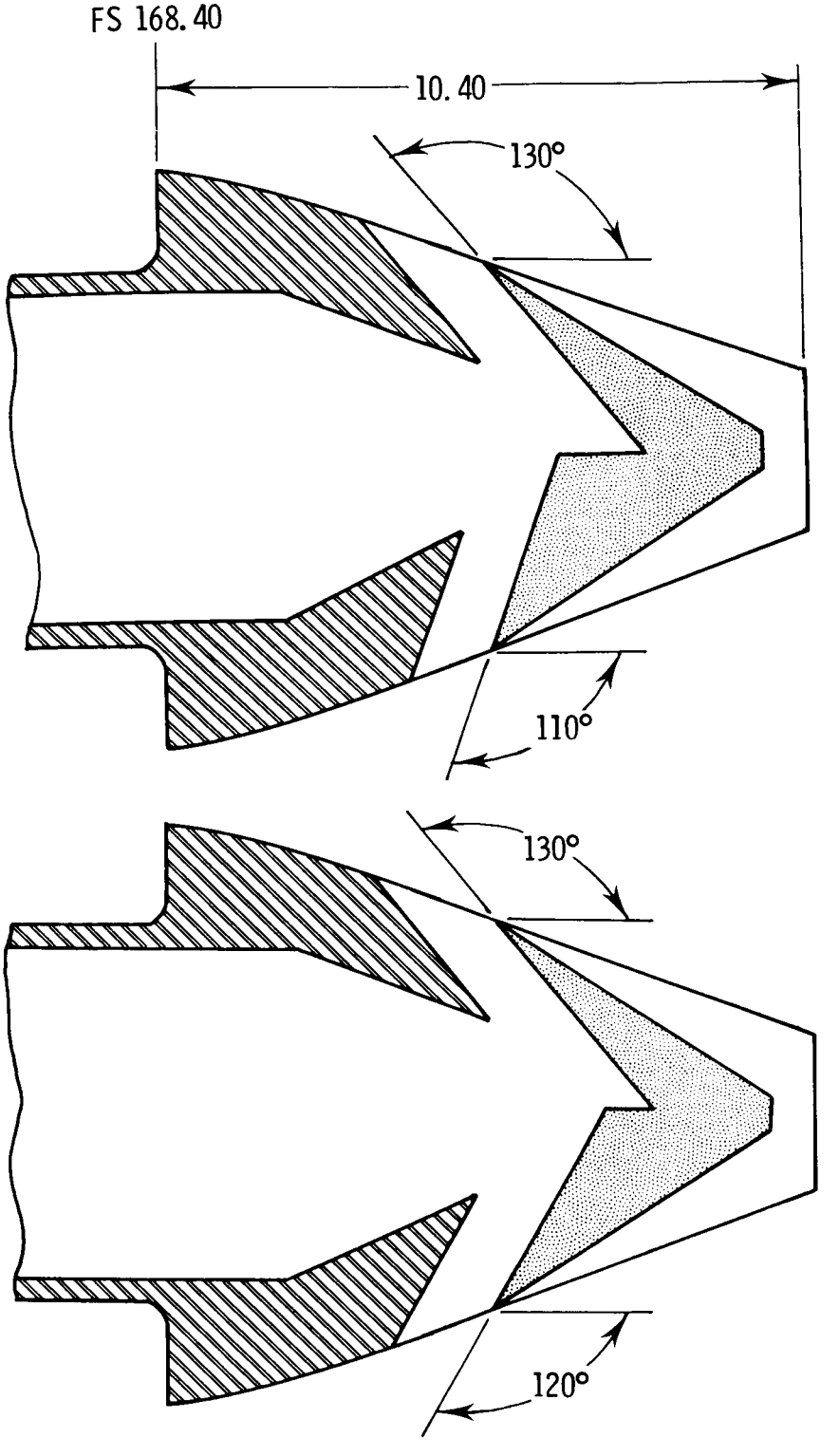

Figure 16.- Reversers with differential port angles. All linear dimensions in centimeters.

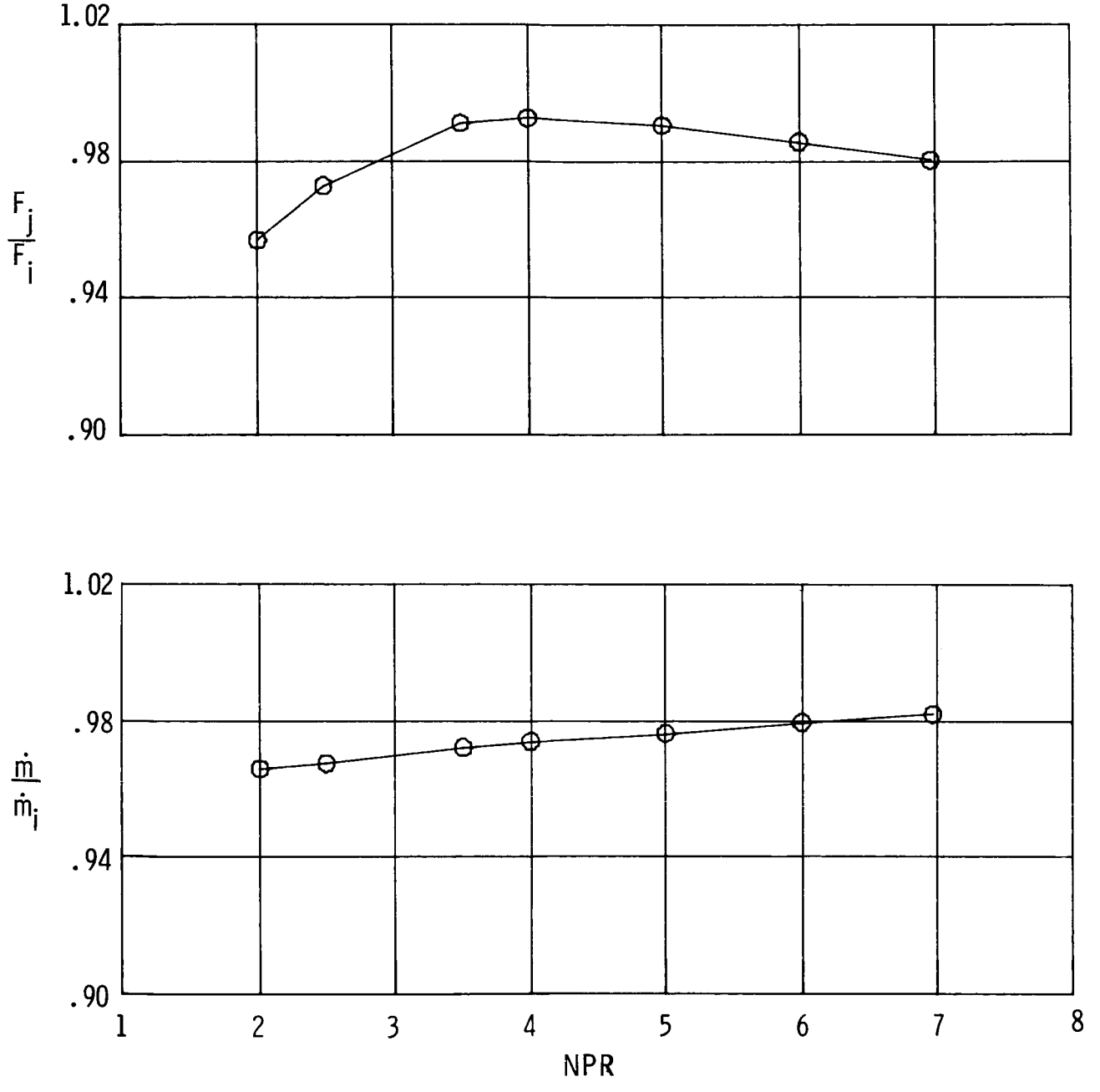

Figure 17.- Static performance and discharge coefficient of base-line (forward-thrust) nozzle.

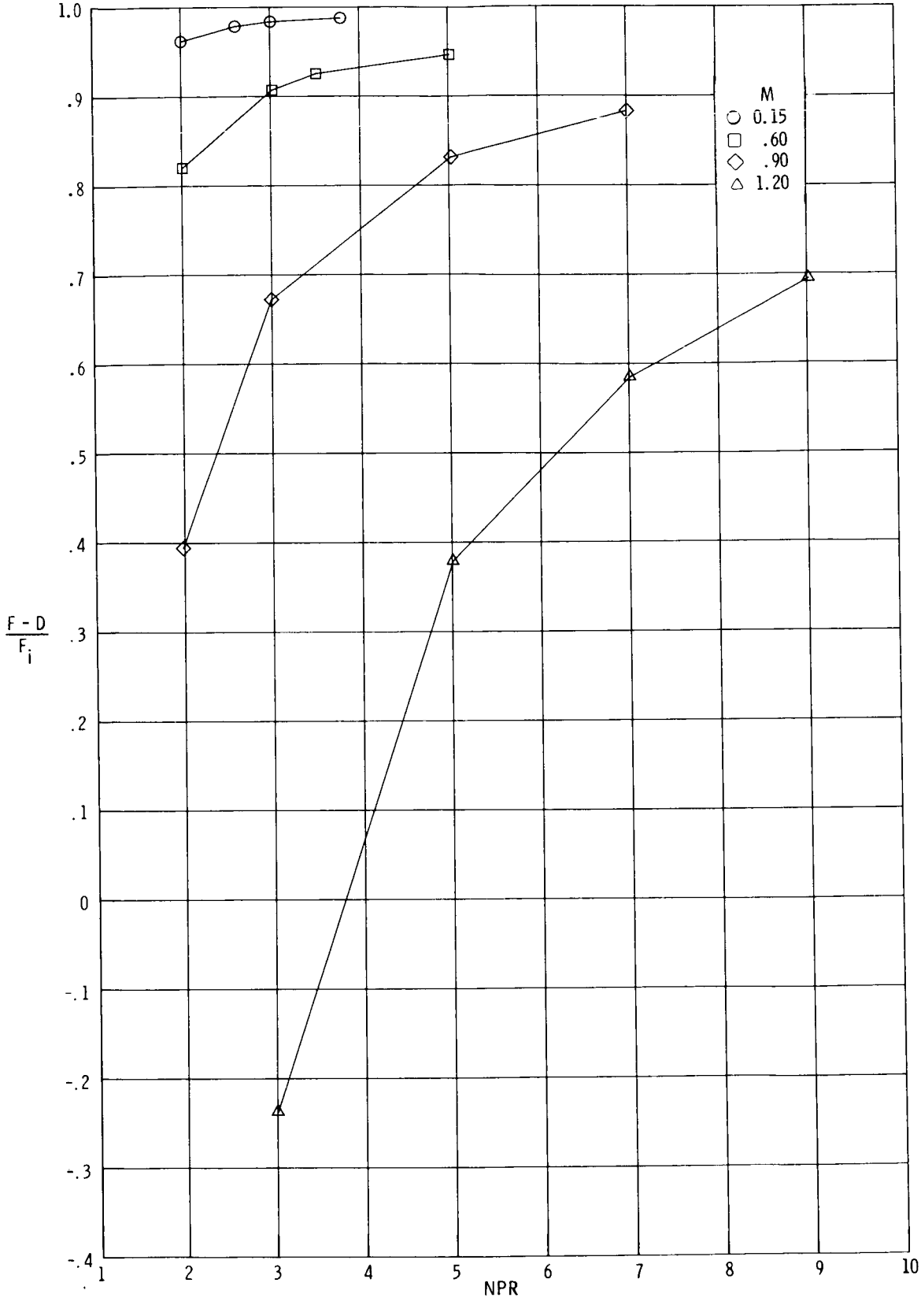

Figure 18.- Aeropropulsive performance of base-line (forward-thrust) nozzle.

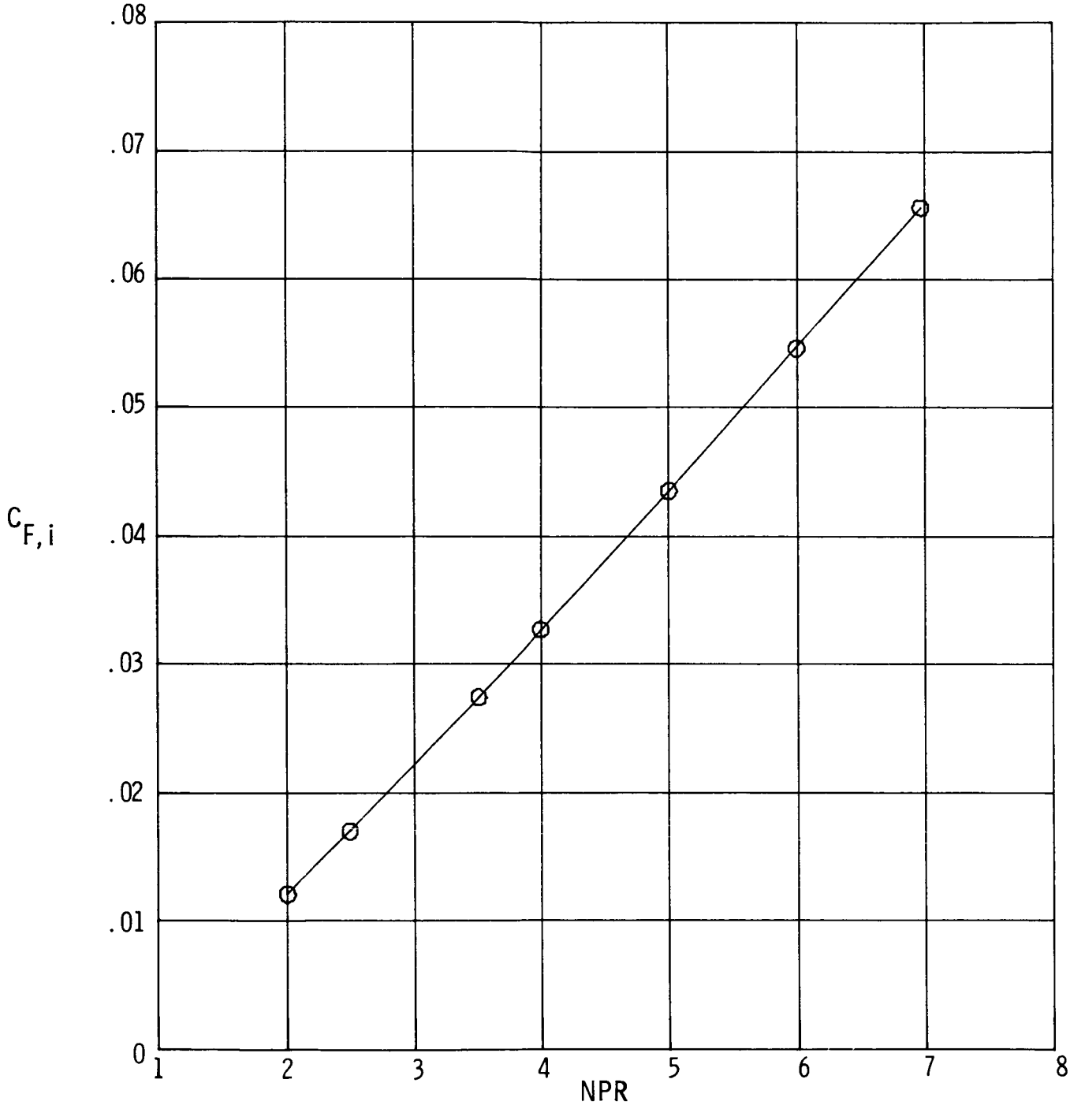

(a) Static (wind-off) conditions.

Figure 19.- Variation of ideal thrust coefficient with nozzle pressure ratio for base-line (forward-thrust) nozzle.

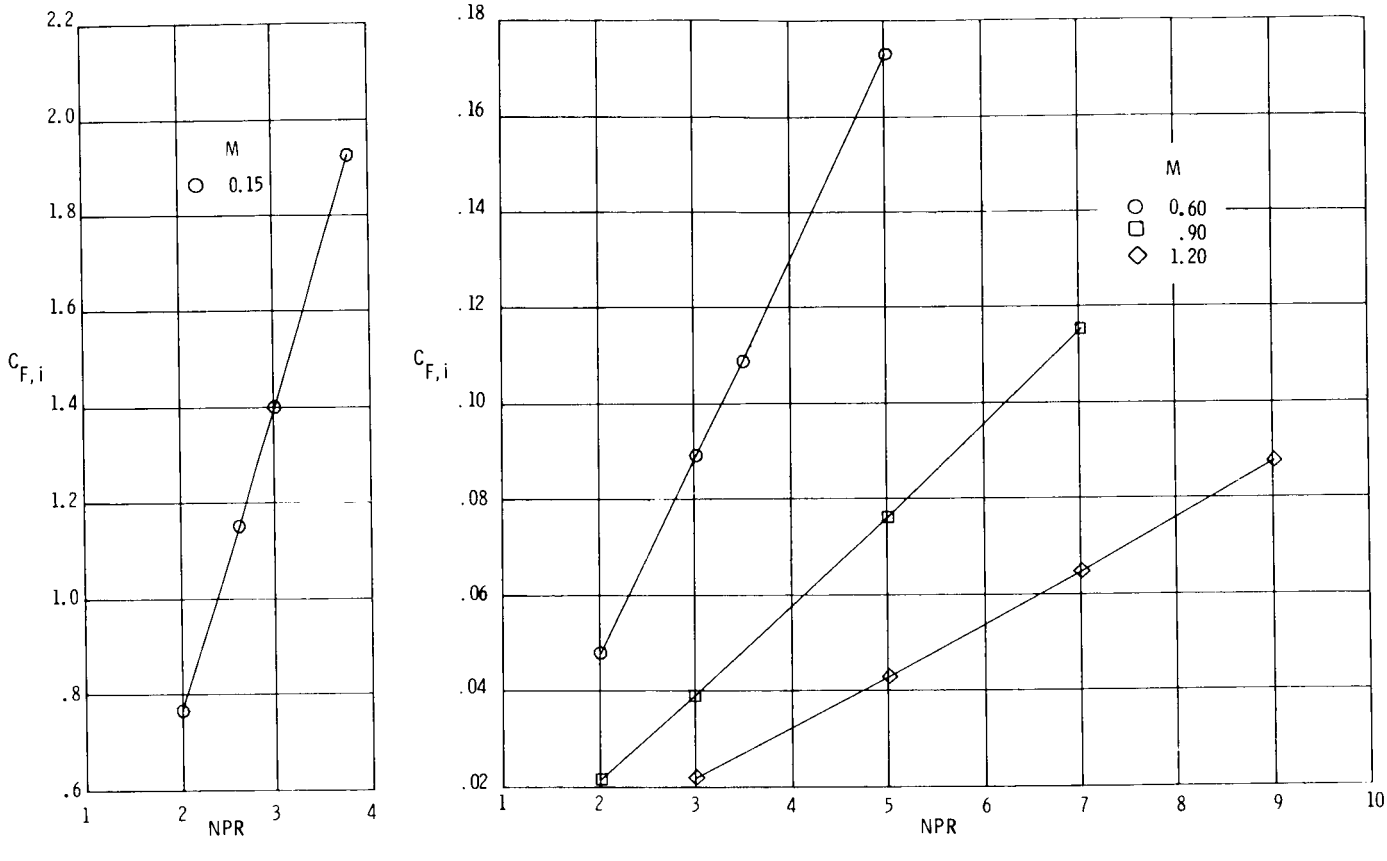

(b) Wind-on conditions.

Figure 19.- Concluded.

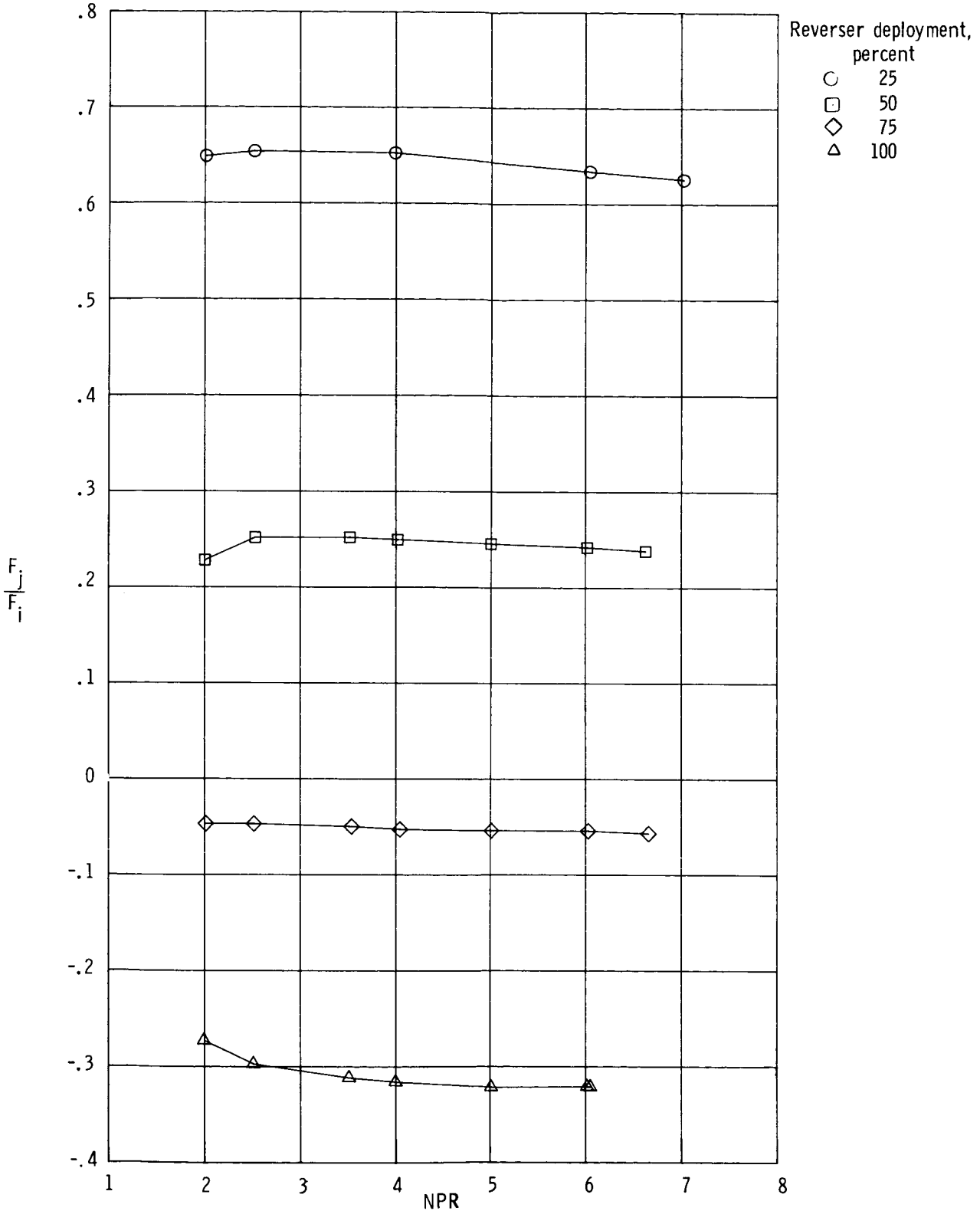

(a) Static performance.

Figure 20.- Static performance and discharge coefficient of reverse-thrust nozzles at various percentages of deployment.

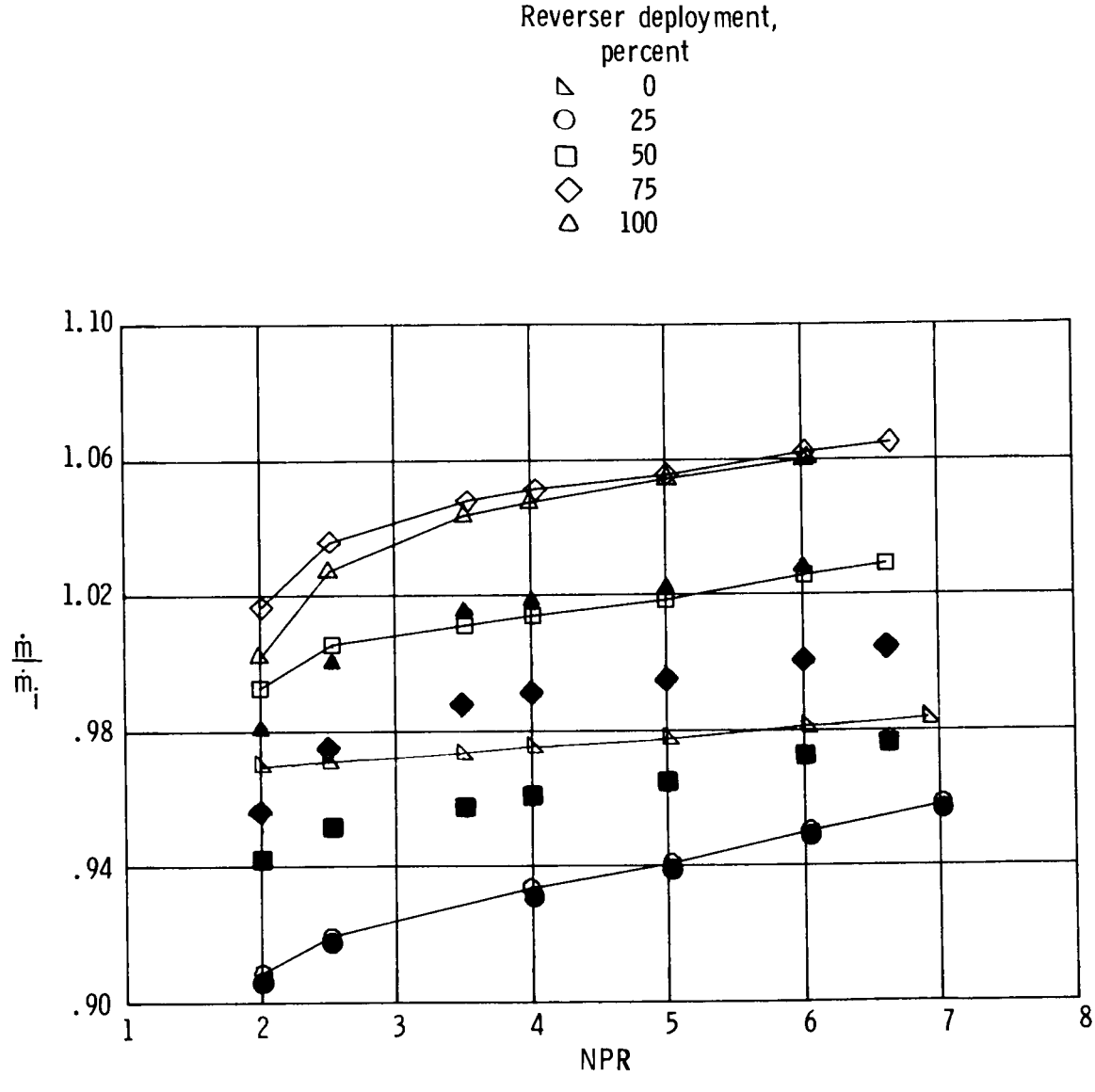

(b) Static discharge coefficient; solid symbols corrected to reverser area for $\dot{m}_i$.

Figure 20.- Concluded.

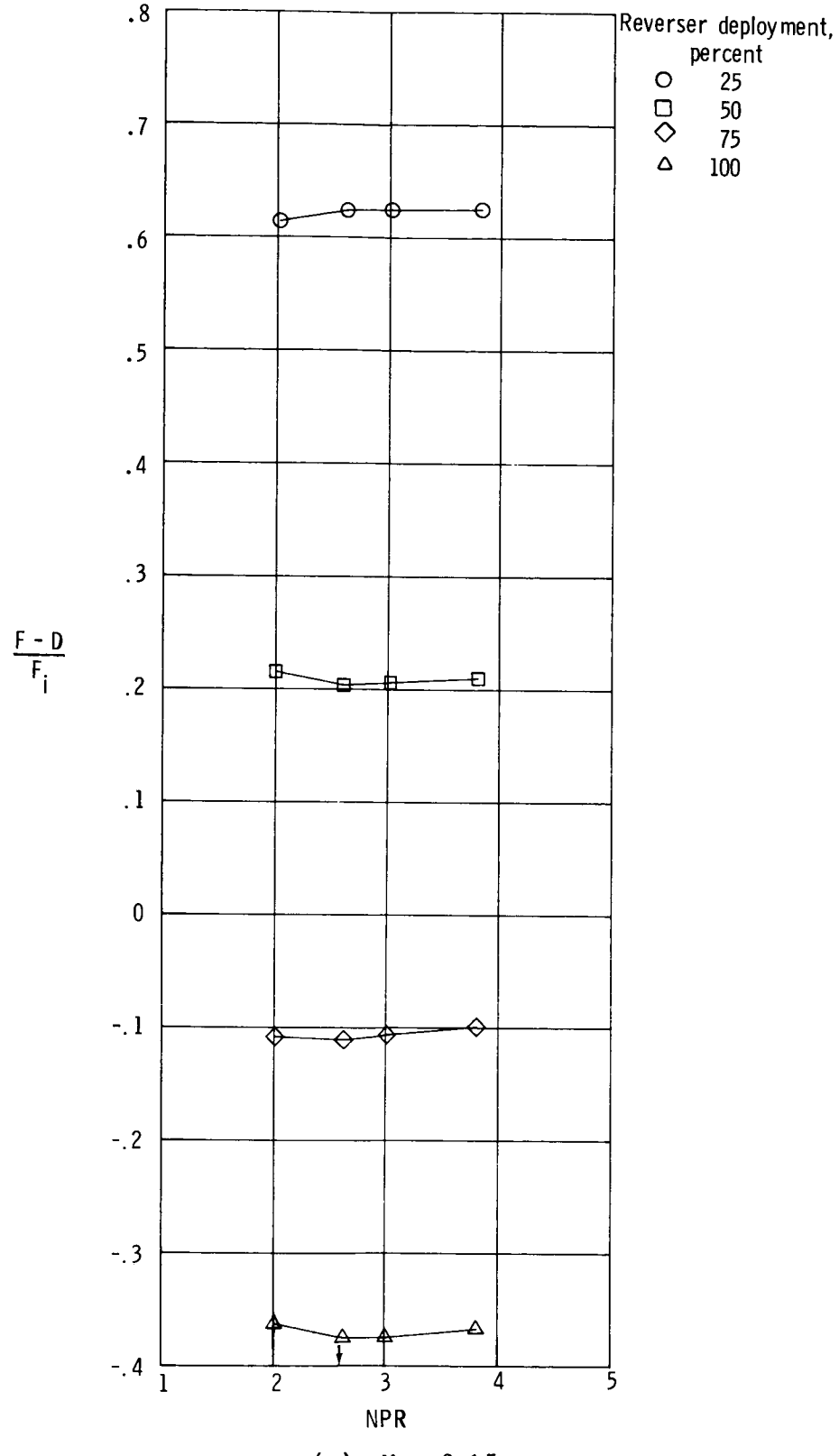

(a) M = 0.15.

Figure 21.- Aeropropulsive performance of reverse-thrust nozzles at various percentages of deployment. Arrow denotes typical operating NPR.

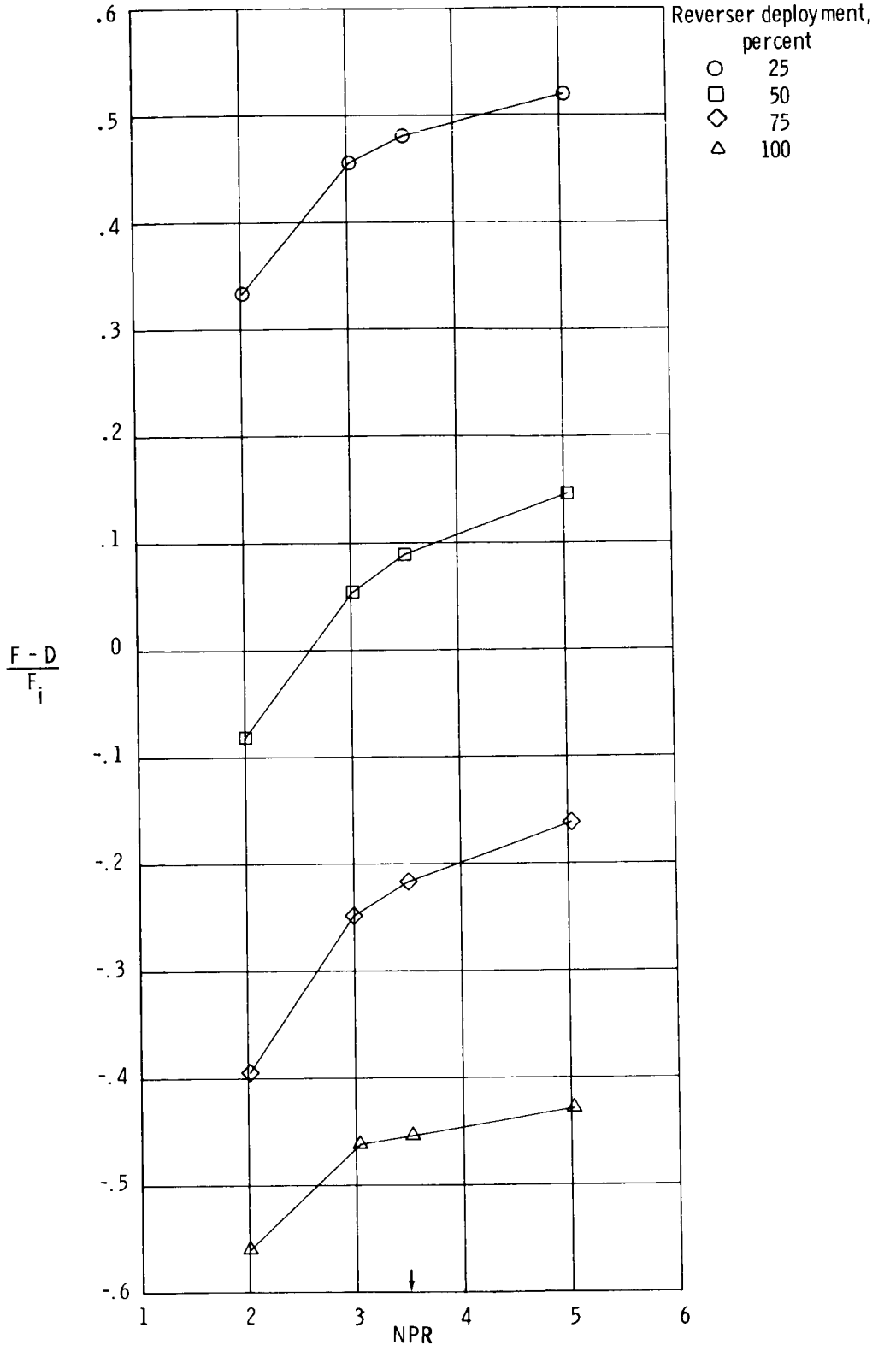

(b) M = 0.60.

Figure 21.- Continued.

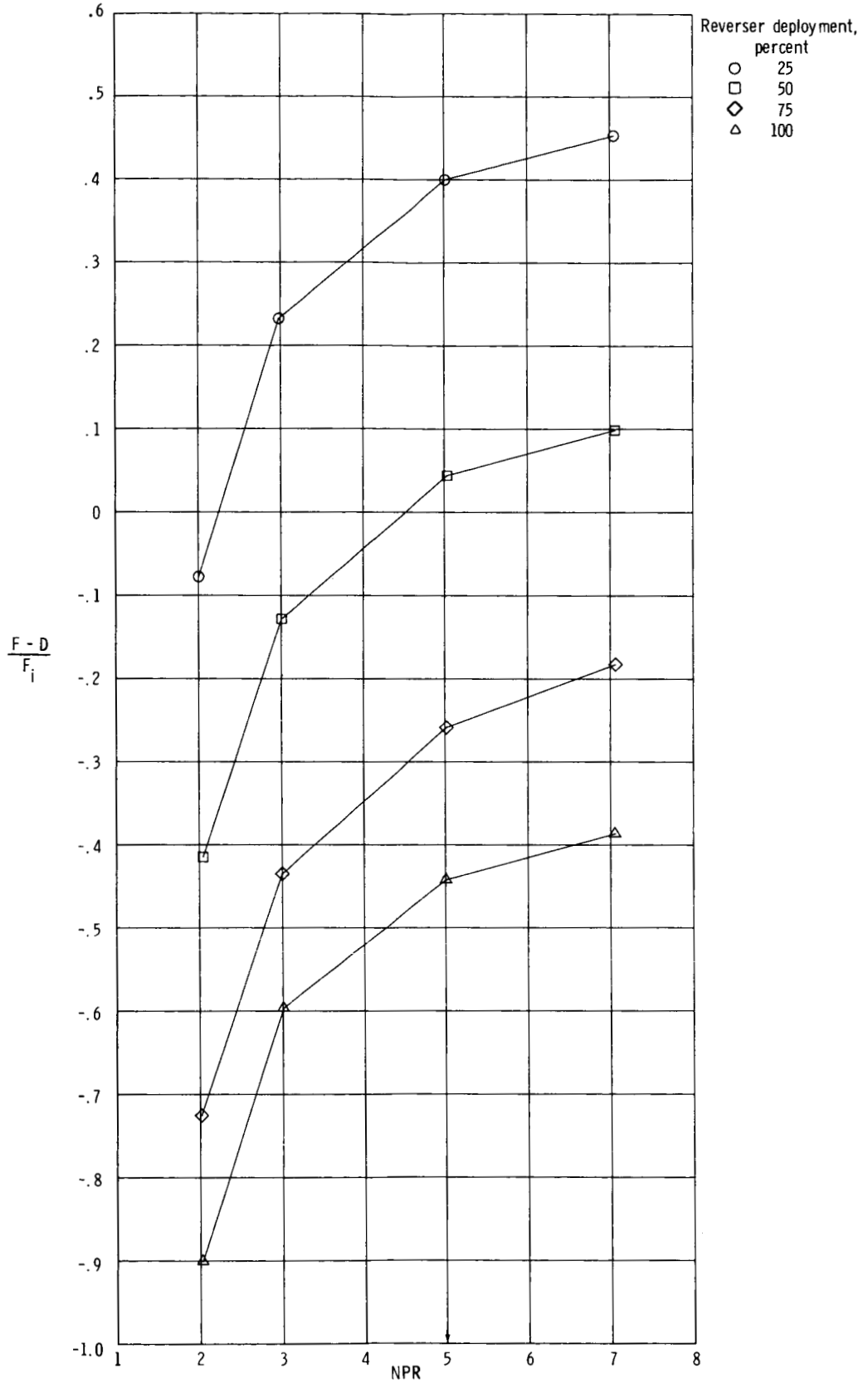

(c) M = 0.90.

Figure 21.- Continued.

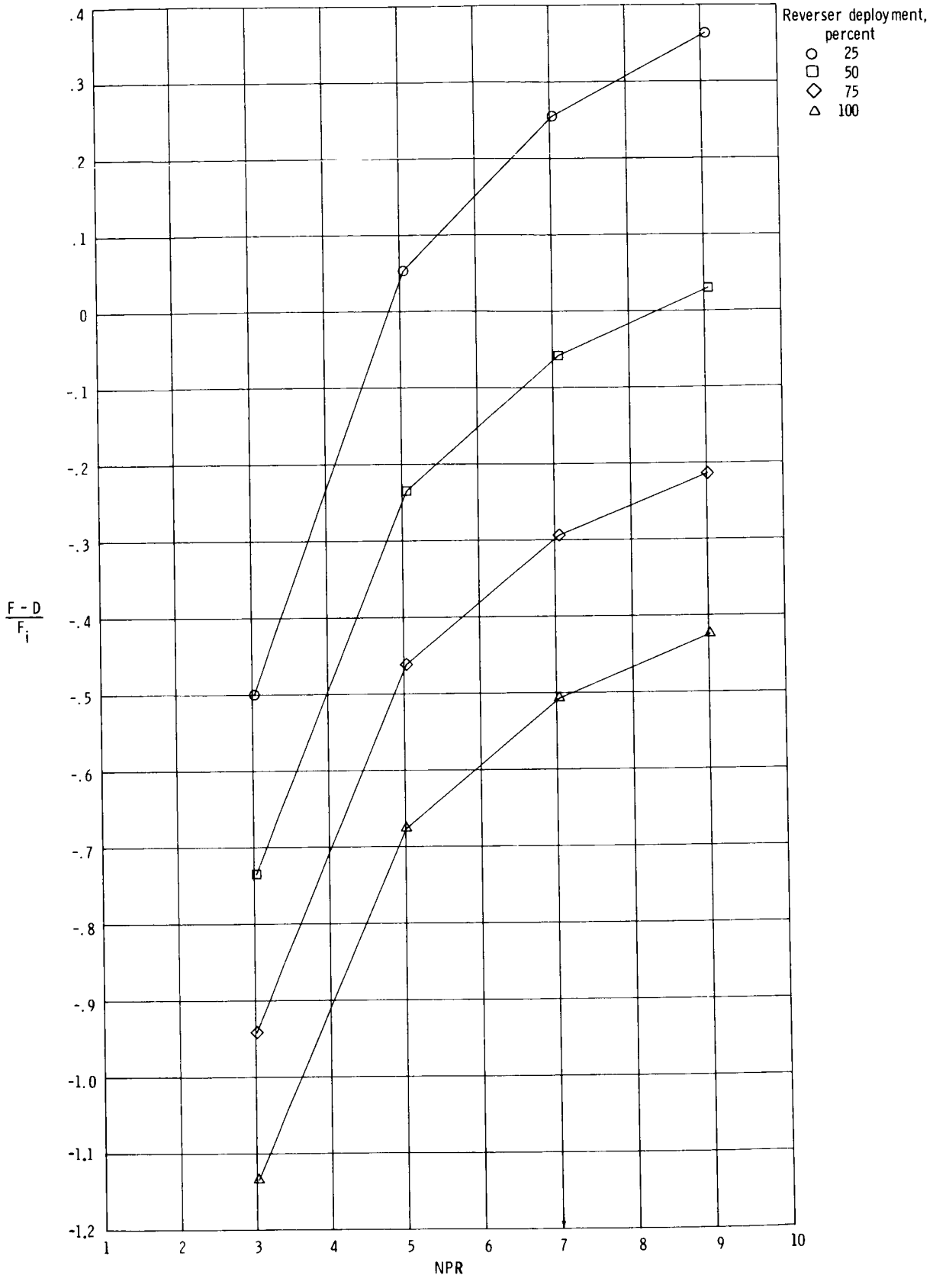

(d) M = 1.20.

Figure 21.- Continued.

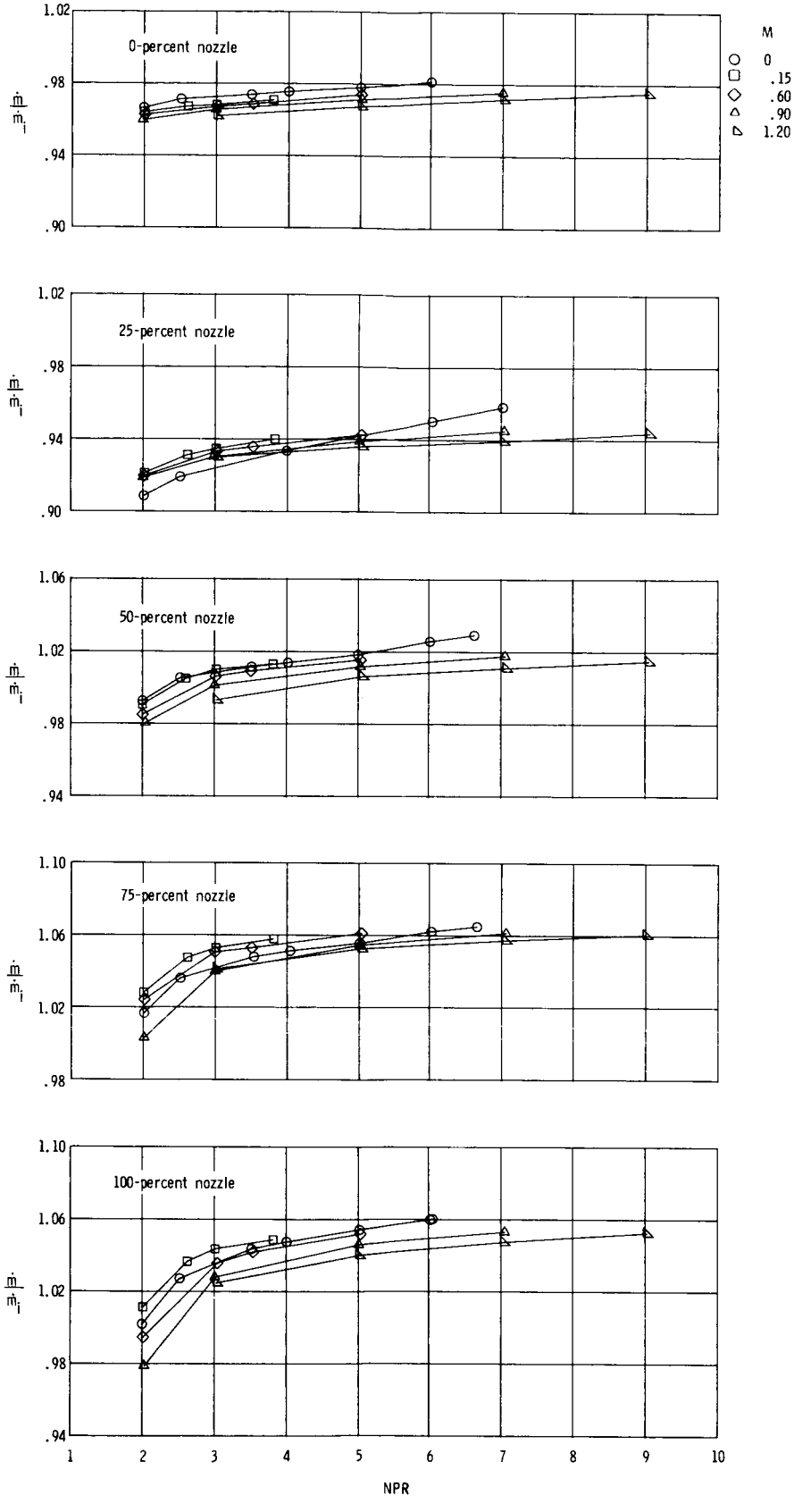

(e) Discharge coefficient.

Figure 21.- Concluded.

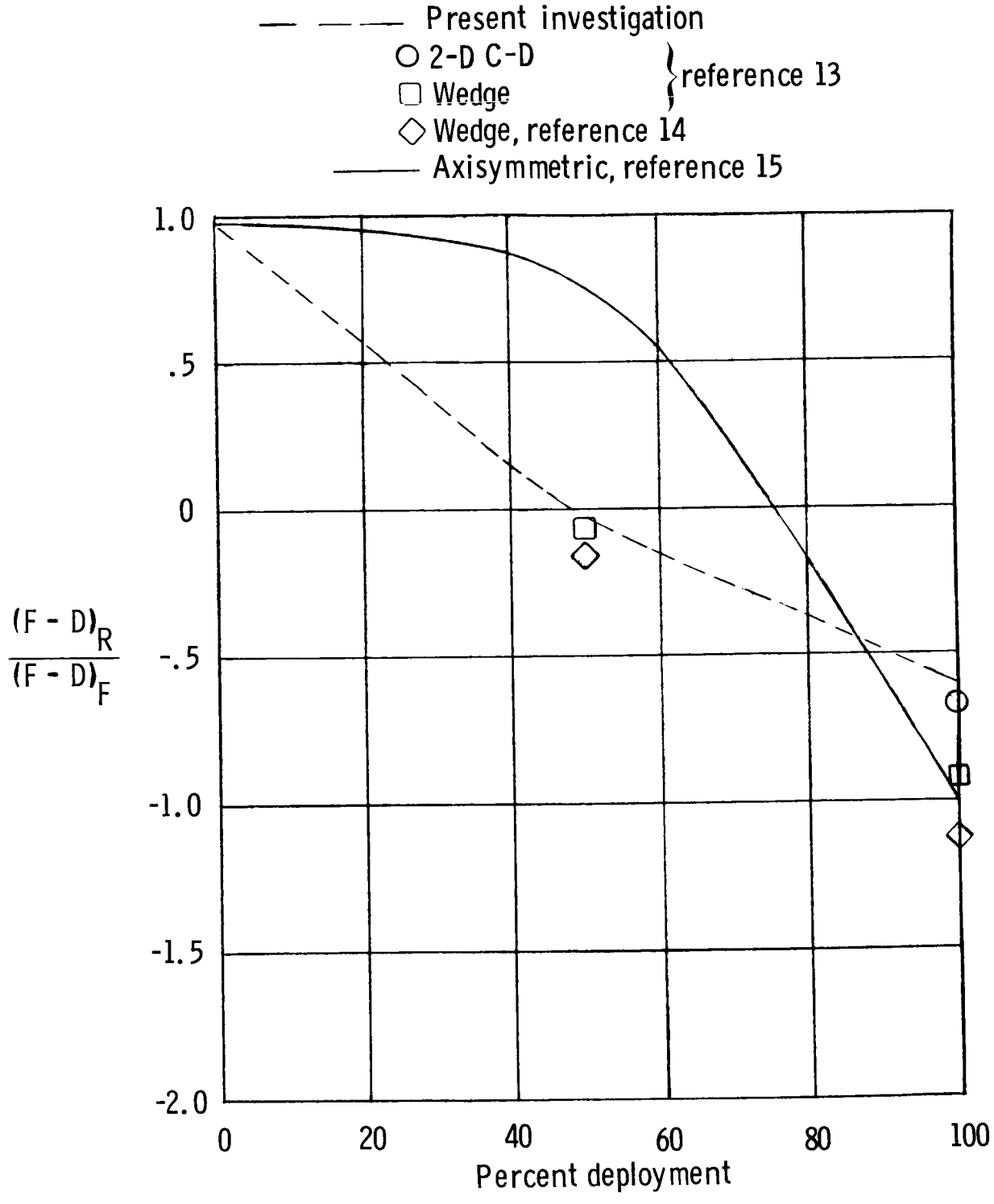

(a) M = 0.60; NPR = 2.65.

Figure 22.- Comparison of effectiveness of reverser nozzles.

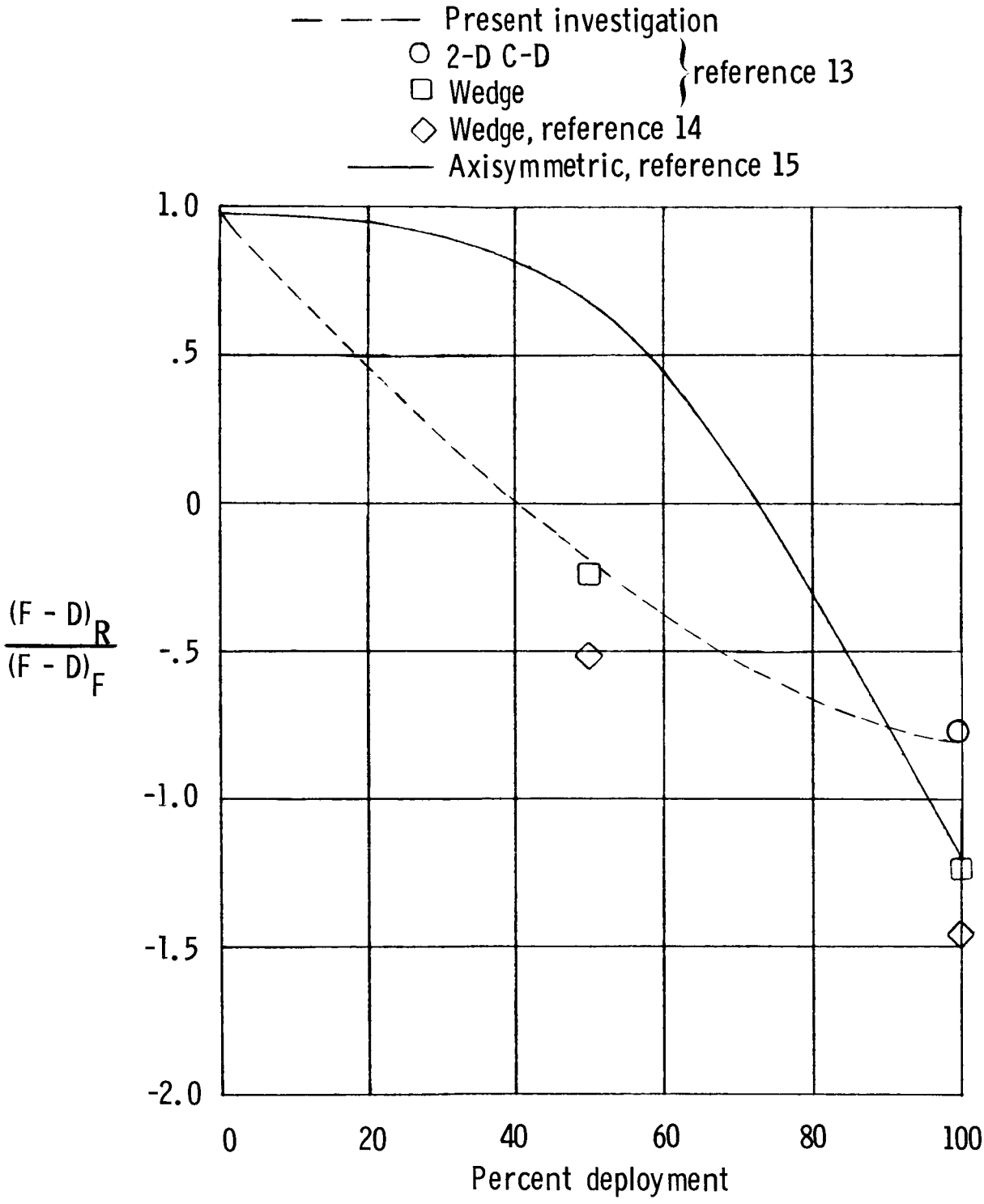

(b) M = 0.90; NPR = 3.3.

Figure 22.- Concluded.

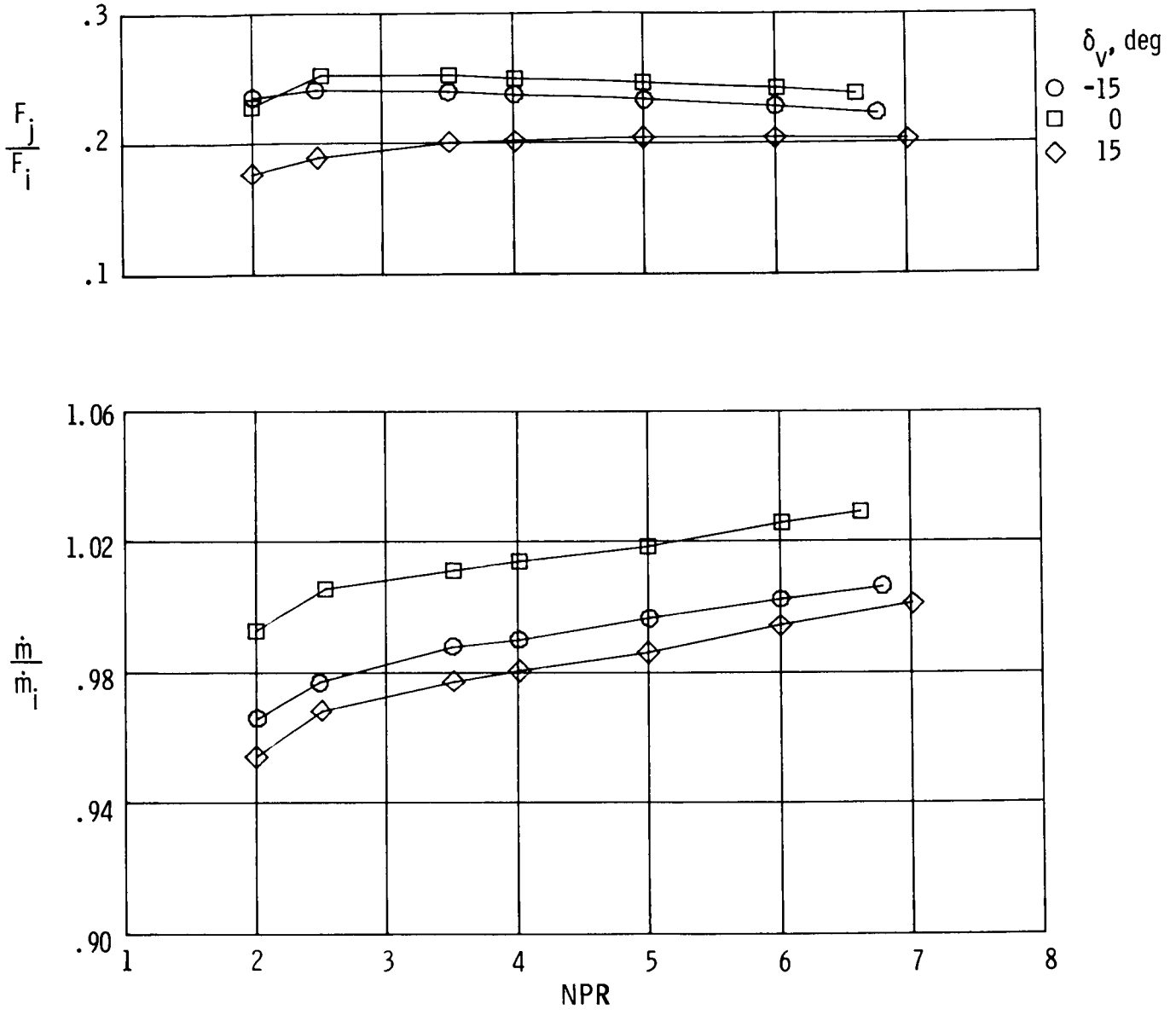

(a) Static performance and discharge coefficient.

Figure 23.- Effects on basic static performance parameters for 15° vectoring on nozzle at 50-percent thrust-reverser deployment.

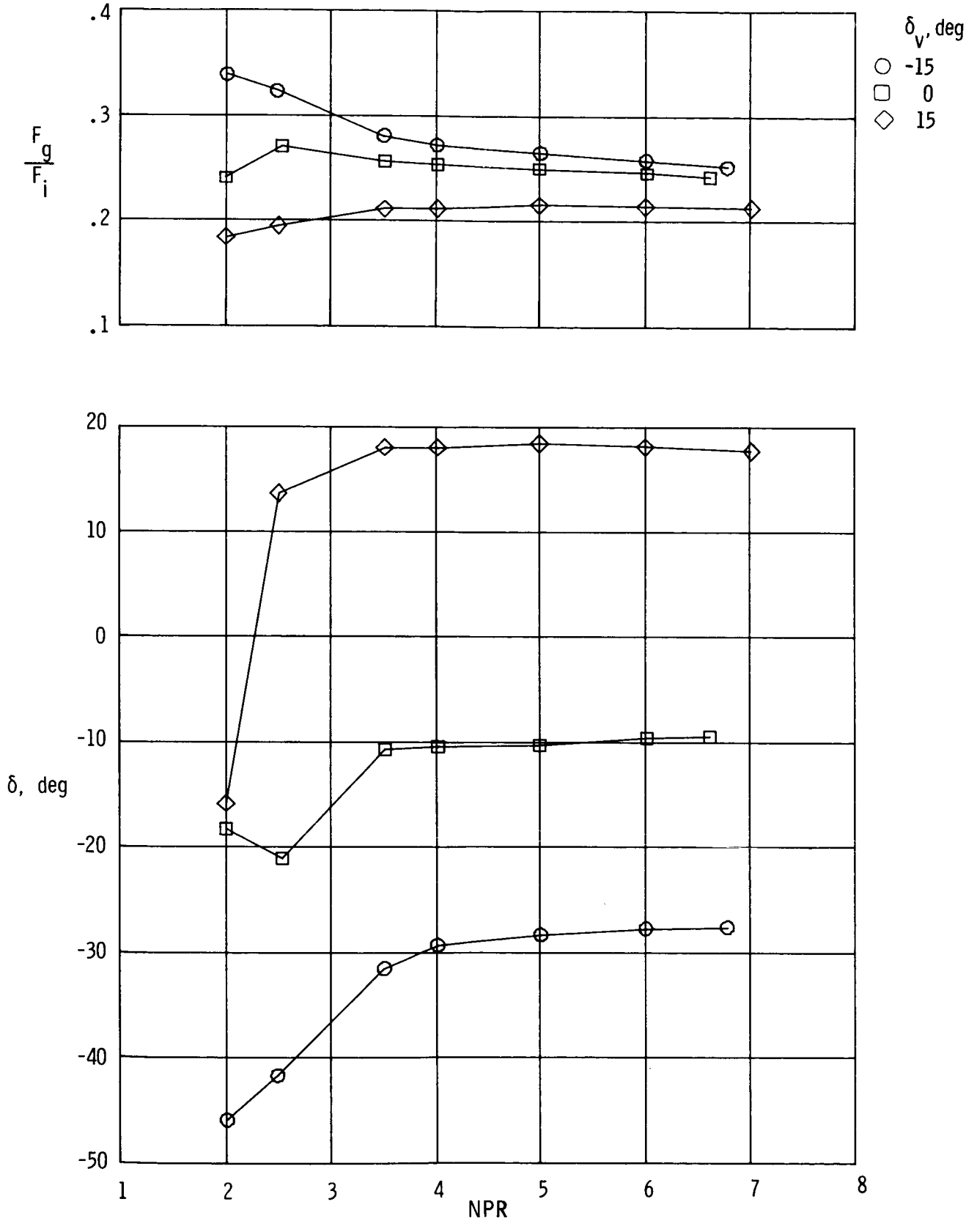

(b) Static gross-thrust performance and effective jet-turning angle.

Figure 23.- Concluded.

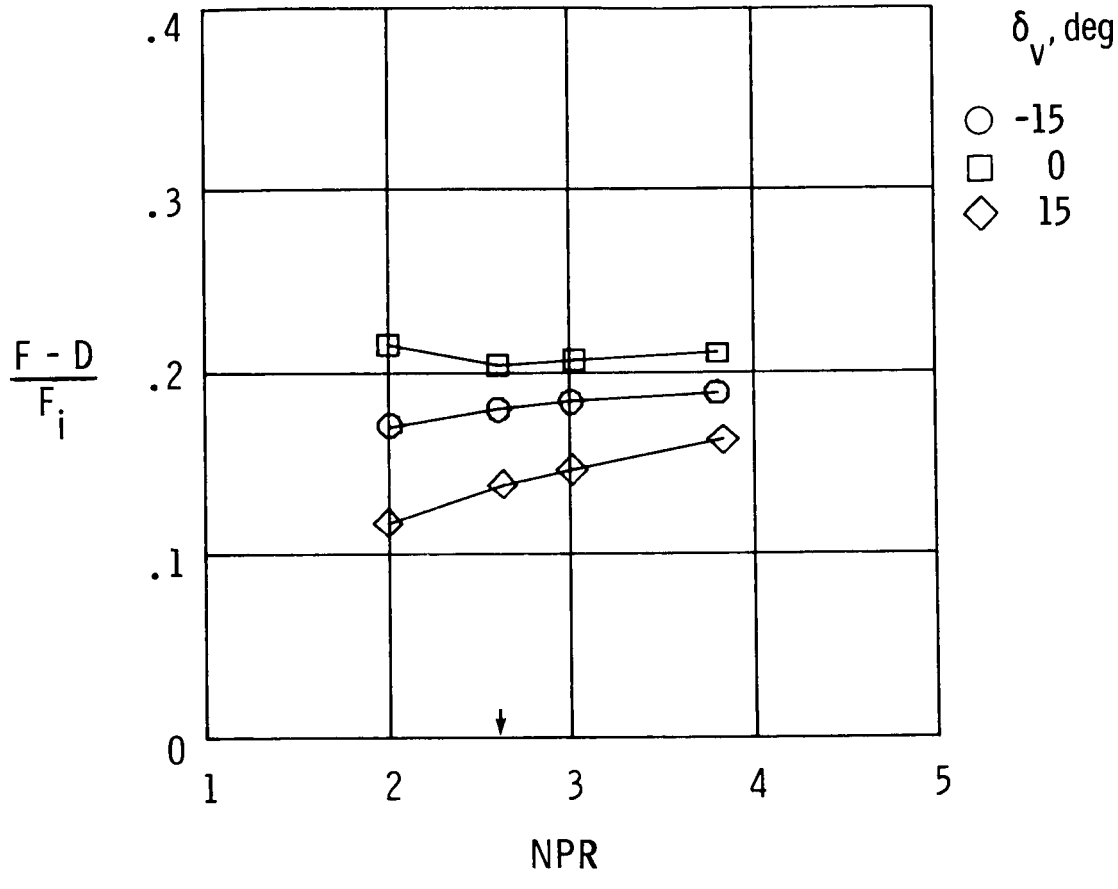

Figure 24.- Aeropropulsive characteristics of reverse-thrust nozzles with 15° vectoring at 50-percent thrust-reverser deployment for M = 0.15. Arrow denotes typical operating NPR.

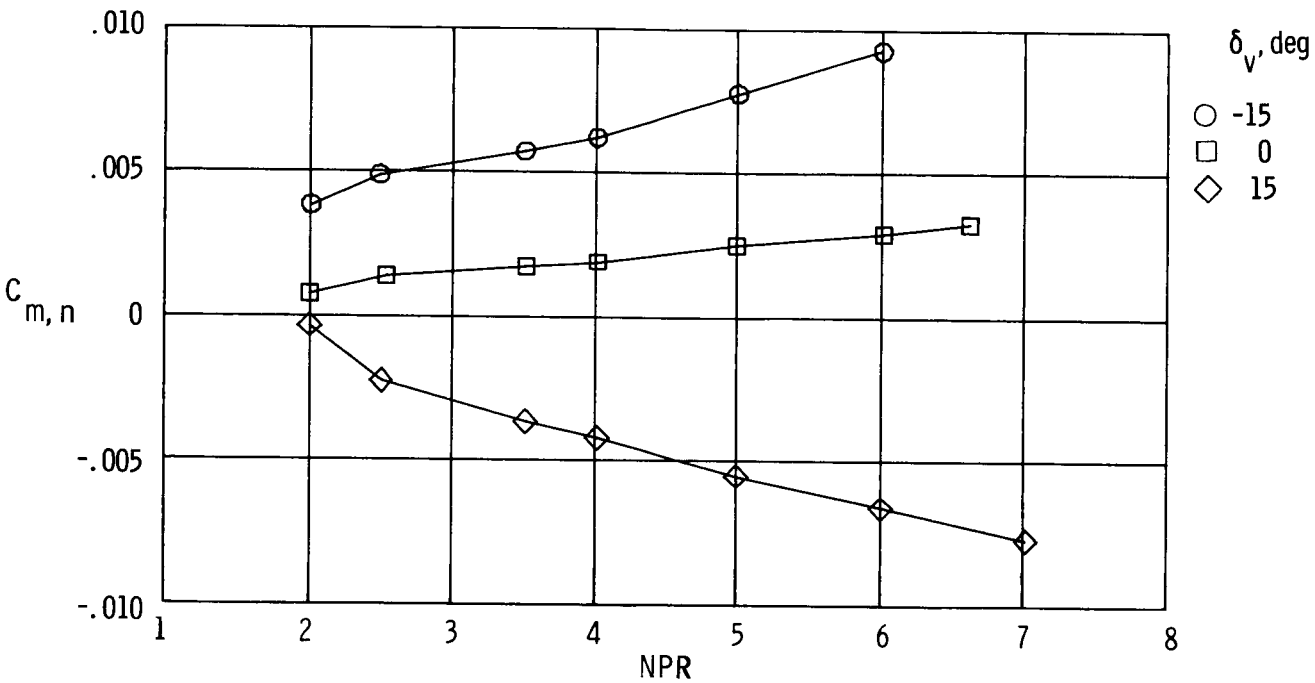

(a) M = 0.

Figure 25.- Nozzle pitching-moment coefficient for 15° vectoring at 50-percent thrust-reverser deployment.

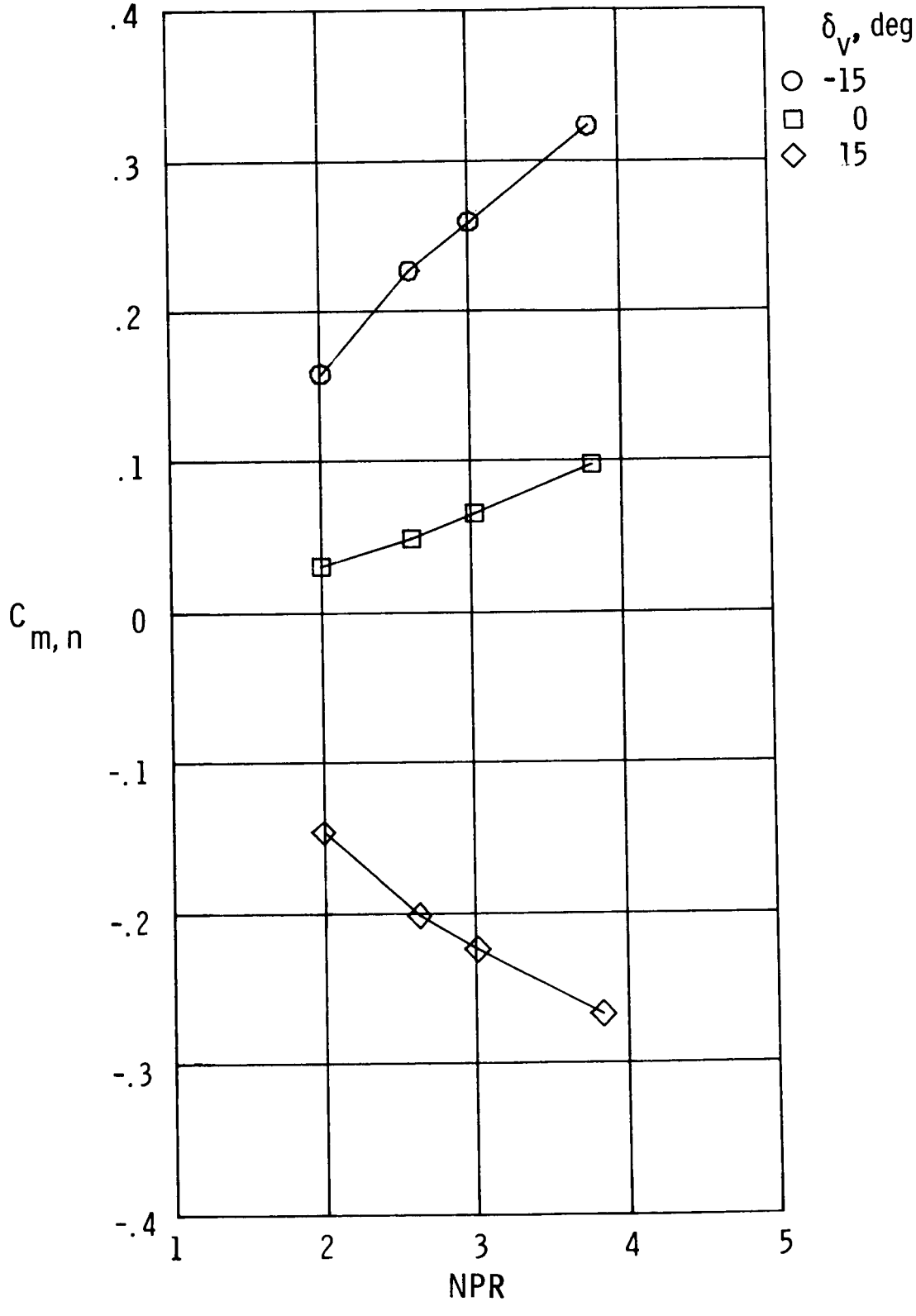

(b) M = 0.15.

Figure 25.- Concluded.

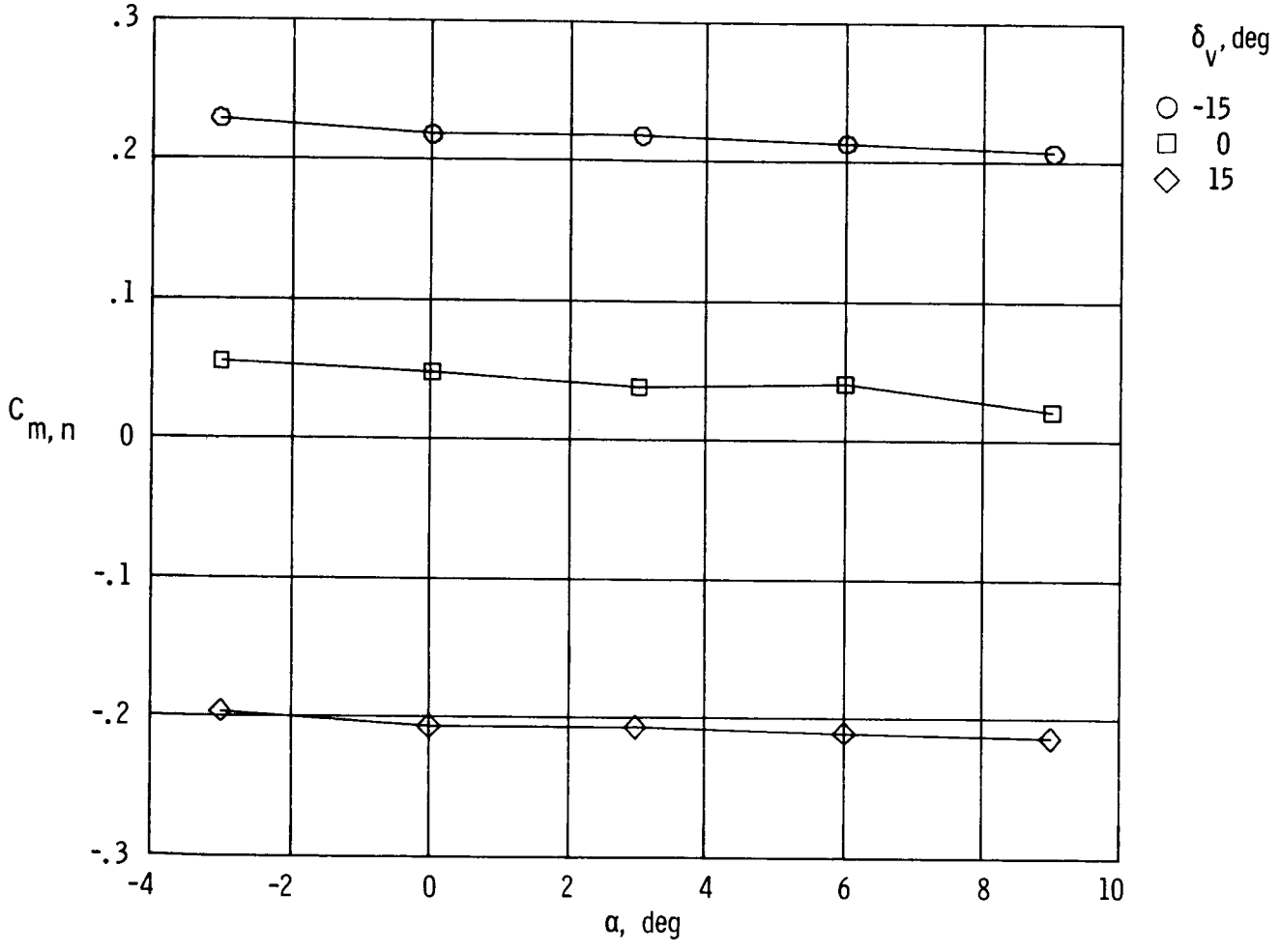

Figure 26.- Variation of nozzle pitching-moment coefficient with angle of attack showing effect of 15° vectoring on nozzles at 50-percent thrust-reverser deployment for M = 0.15 and NPR = 2.6.

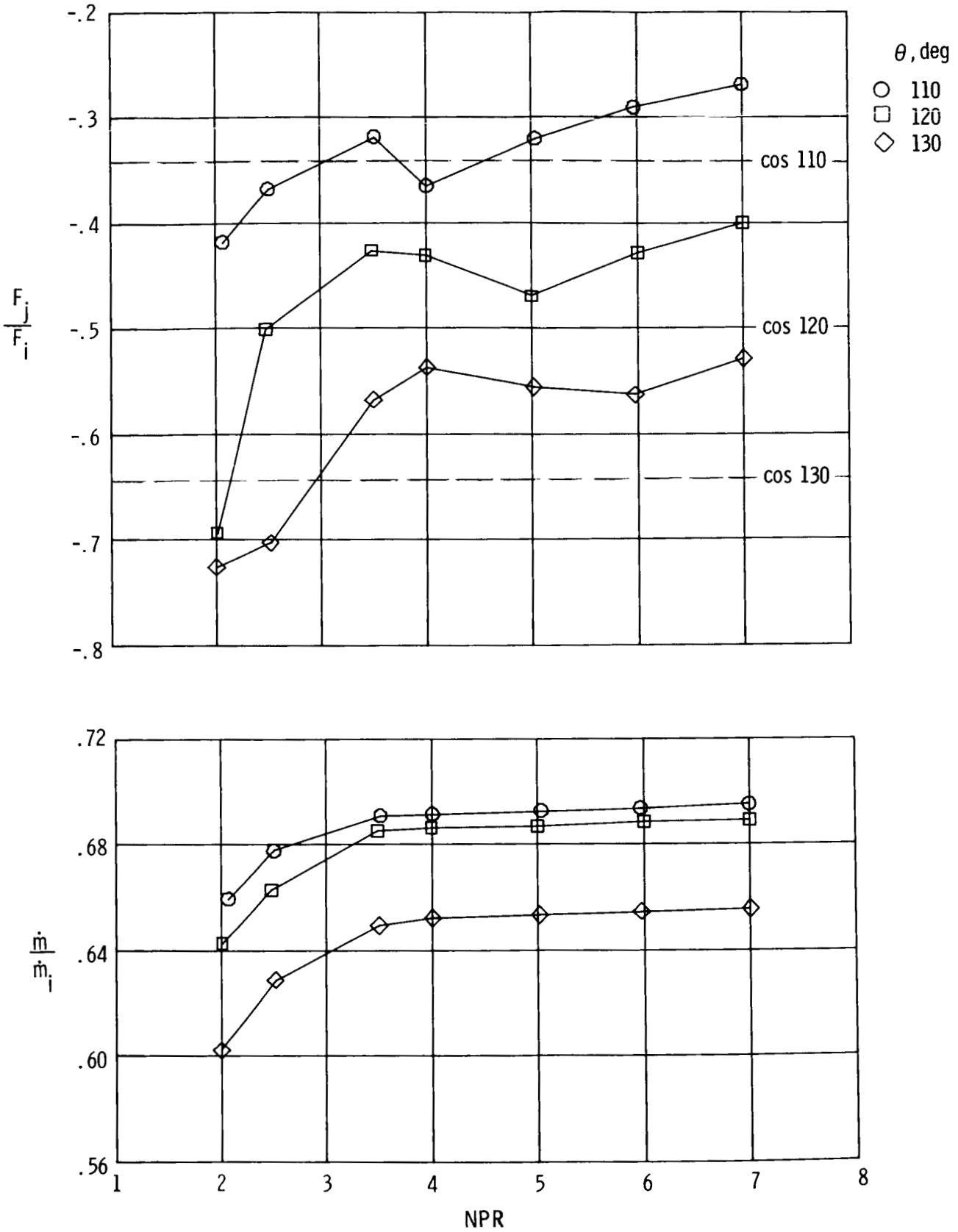

Figure 27.- Static performance and discharge coefficient of reverse-thrust nozzles at various reverser-port angles.

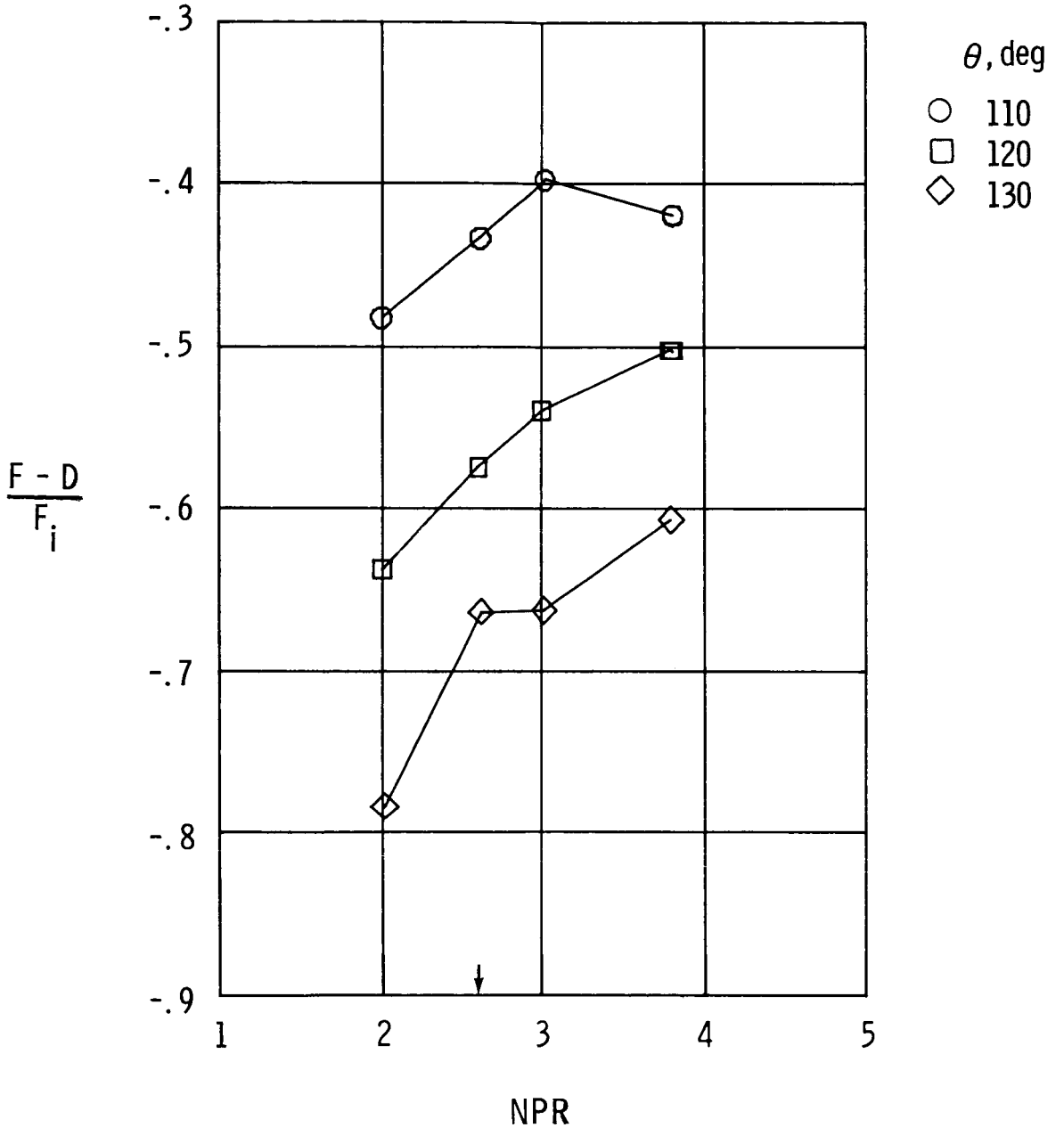

(a) M = 0.15.

Figure 28.- Aeropropulsive performance of reverse-thrust nozzles for various reverser-port angles. Arrow denotes typical NPR.

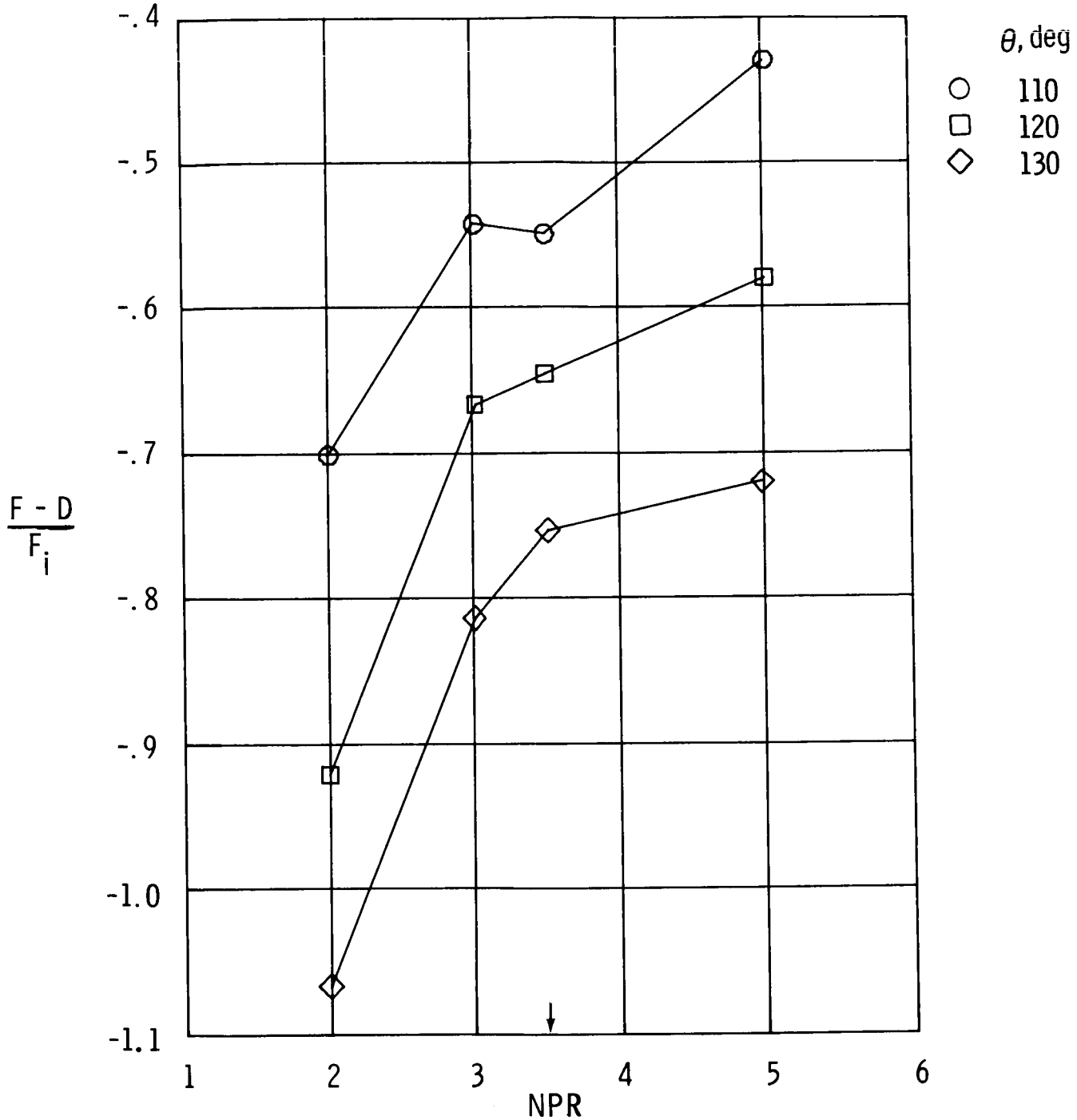

(b) M = 0.60.

Figure 28.- Continued.

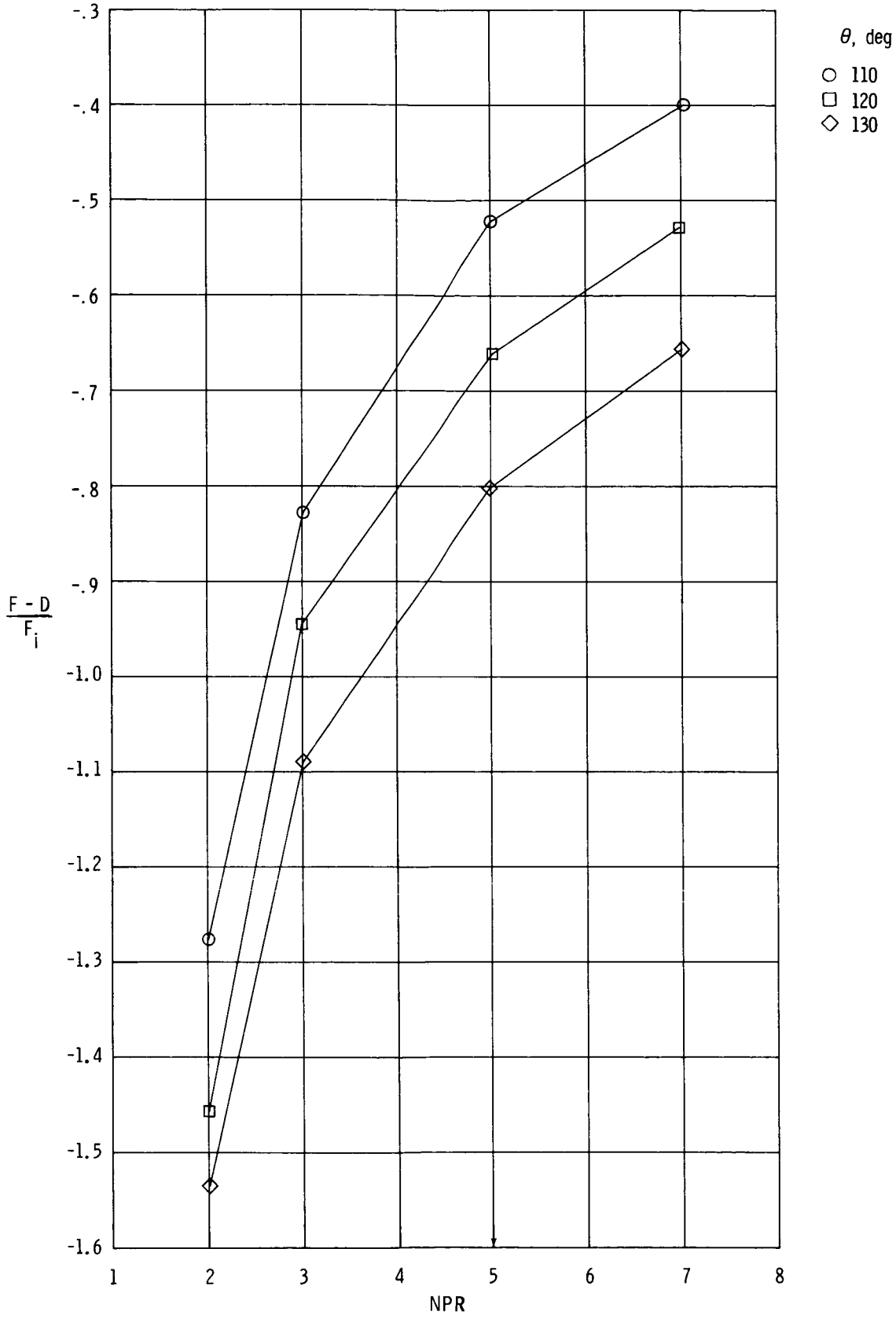

(c) M = 0.90.

Figure 28.- Continued.

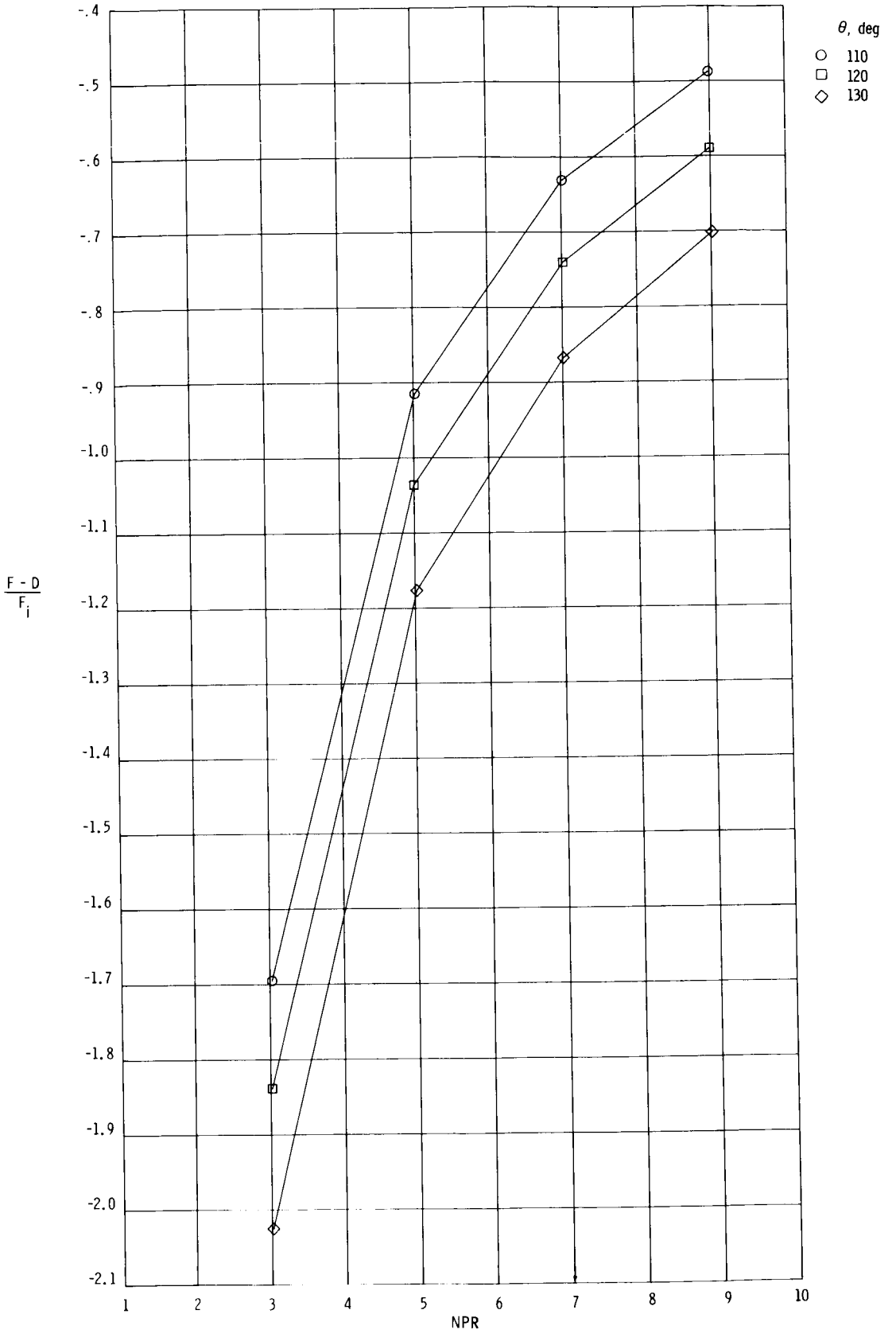

(d) M = 1.20.

Figure 28.- Concluded.

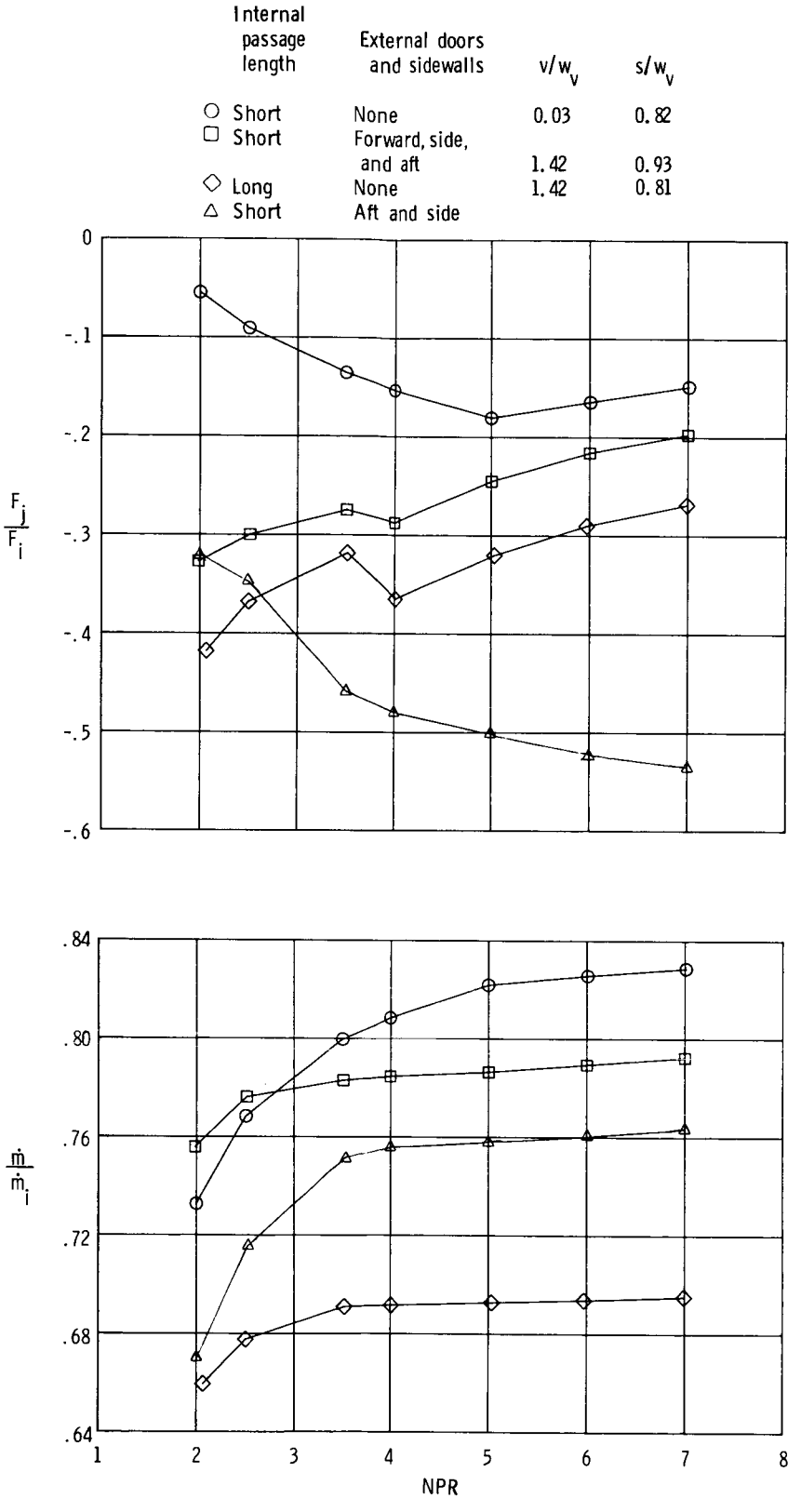

Figure 29.- Static performance and discharge coefficient of reverse-thrust nozzles at reverser-port angle of 110° having two different internal passage lengths and various external door and sidewall combinations.

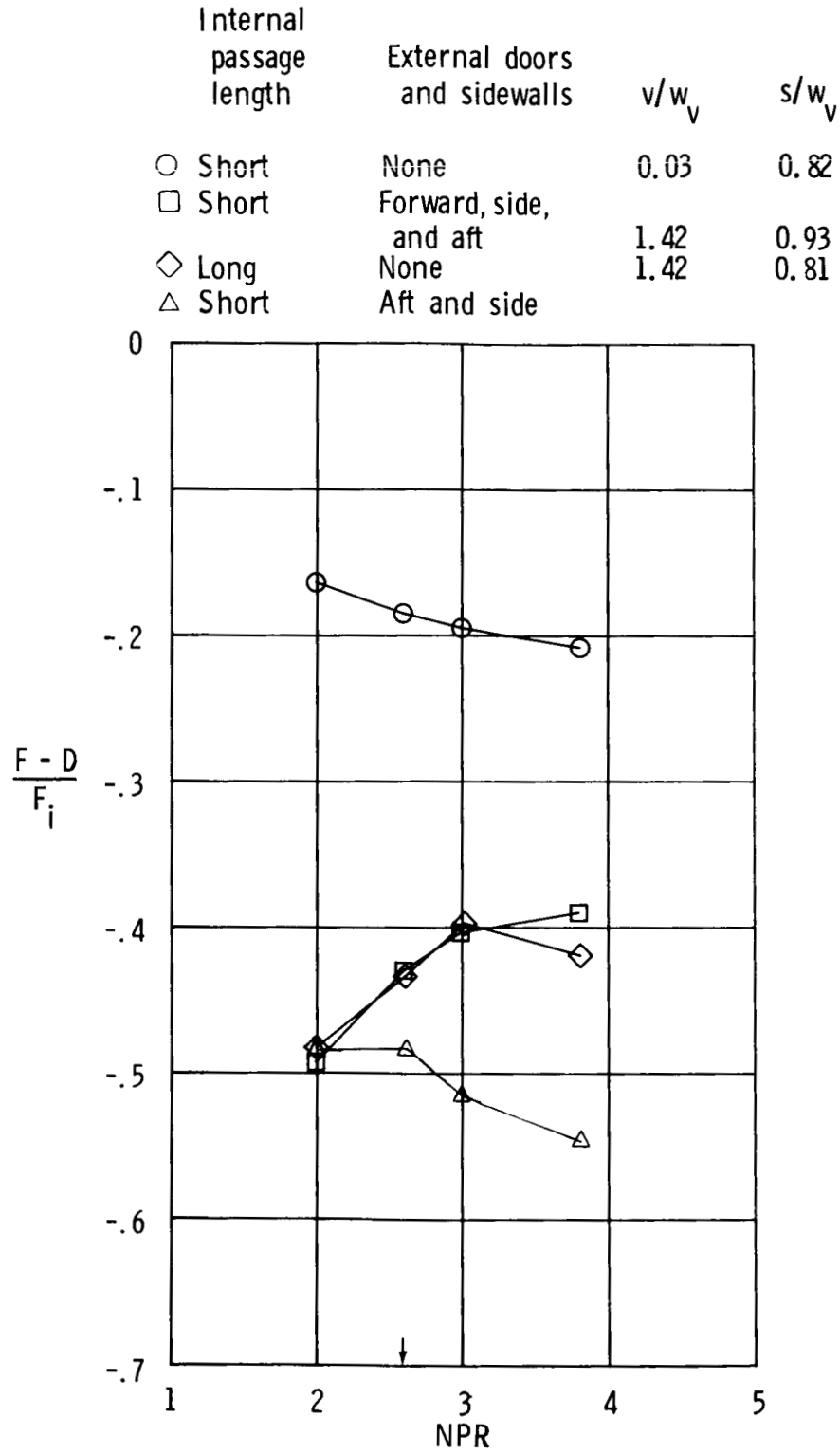

(a) M = 0.15.

Figure 30.- Aeropropulsive performance of reverse-thrust nozzles at reverser-port angle of 110° having two different internal passage lengths and various external door and sidewall combinations. Arrow denotes typical operating NPR.

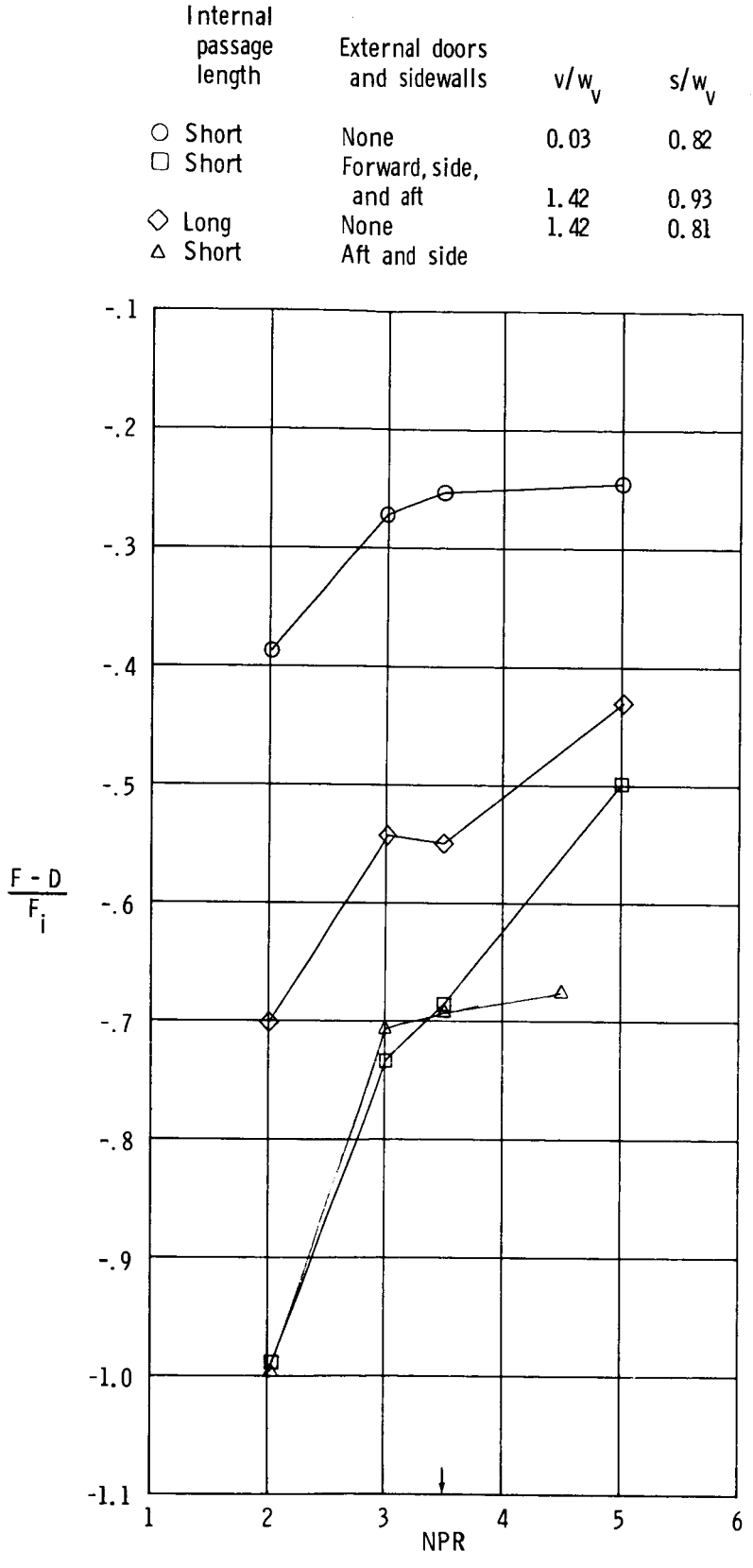

(b) M = 0.60.

Figure 30.- Continued.

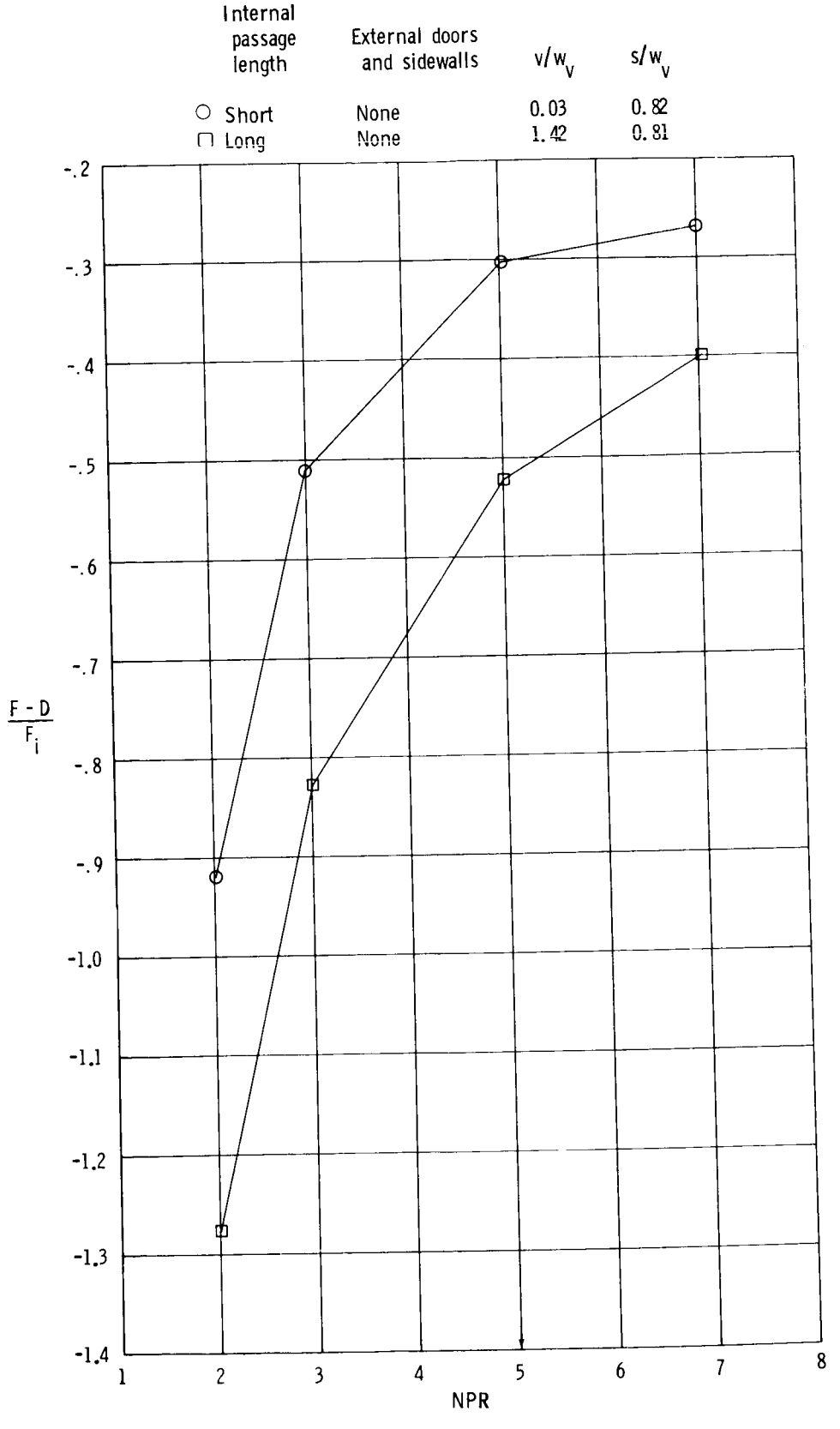

(c) M = 0.90.

Figure 30.- Continued.

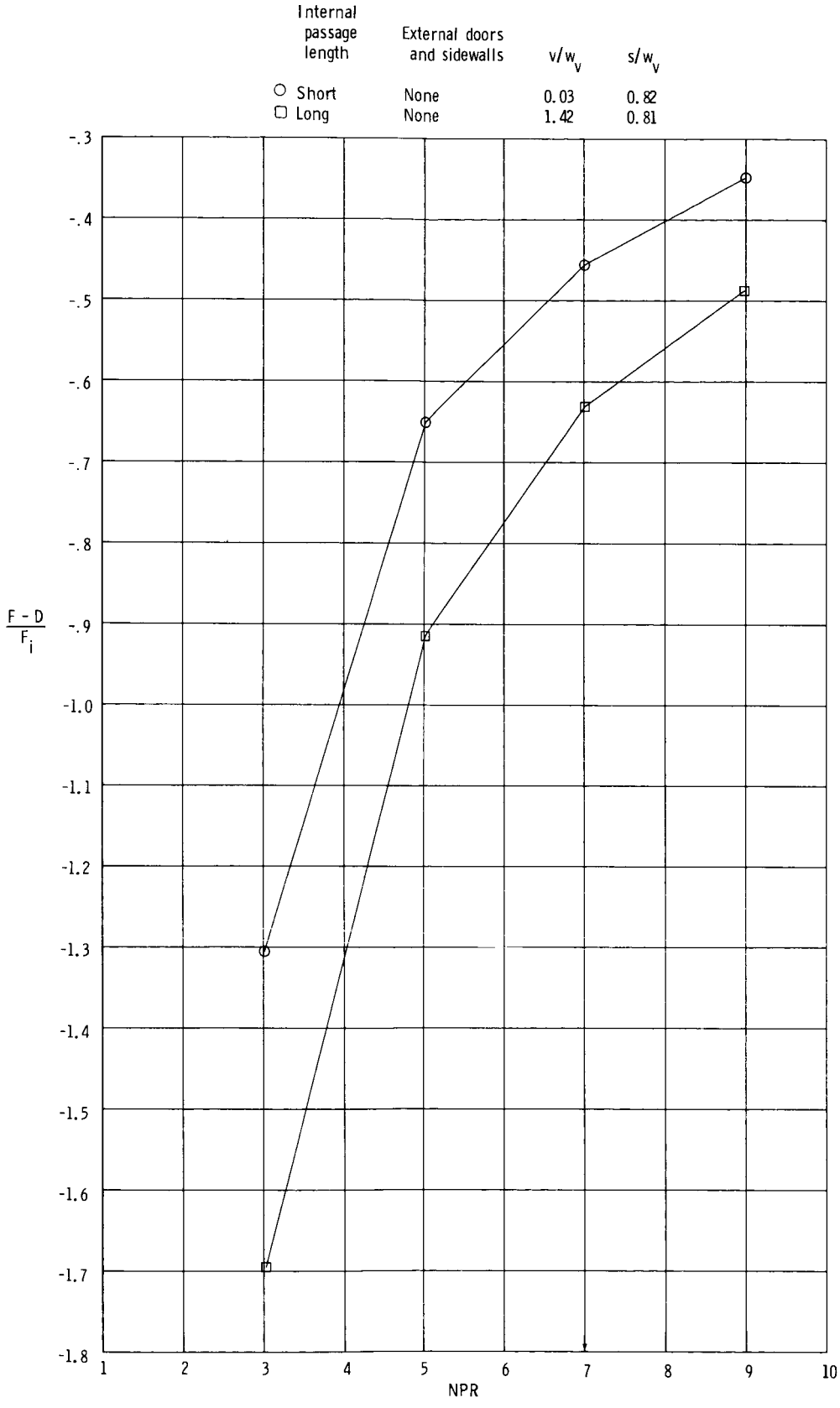

(d) M = 1.20.

Figure 30.- Concluded.

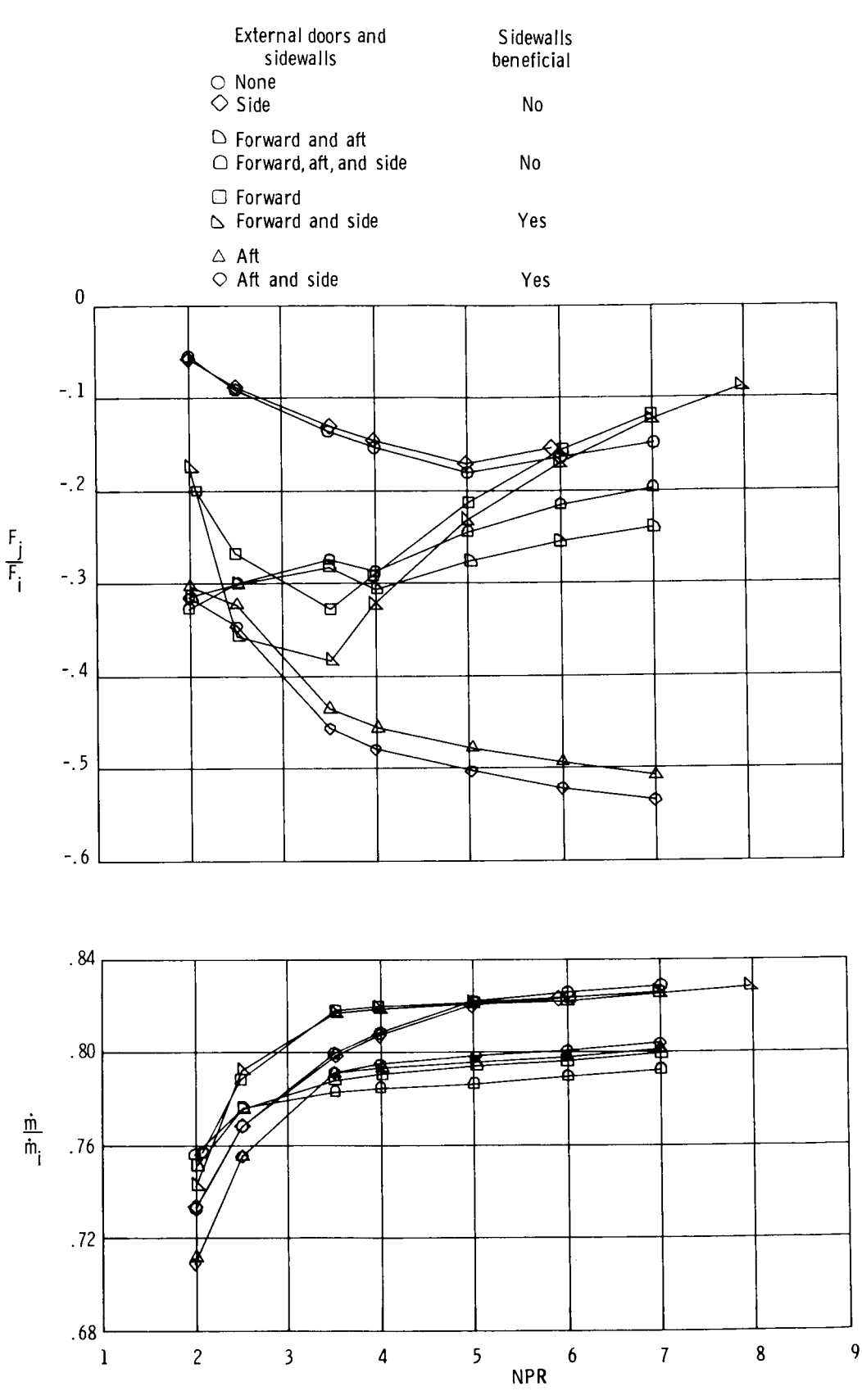

Figure 31.- Static performance and discharge coefficient of short internal passage length reverse-thrust nozzle at reverser-port angle of 110° with various external door and sidewall combinations.

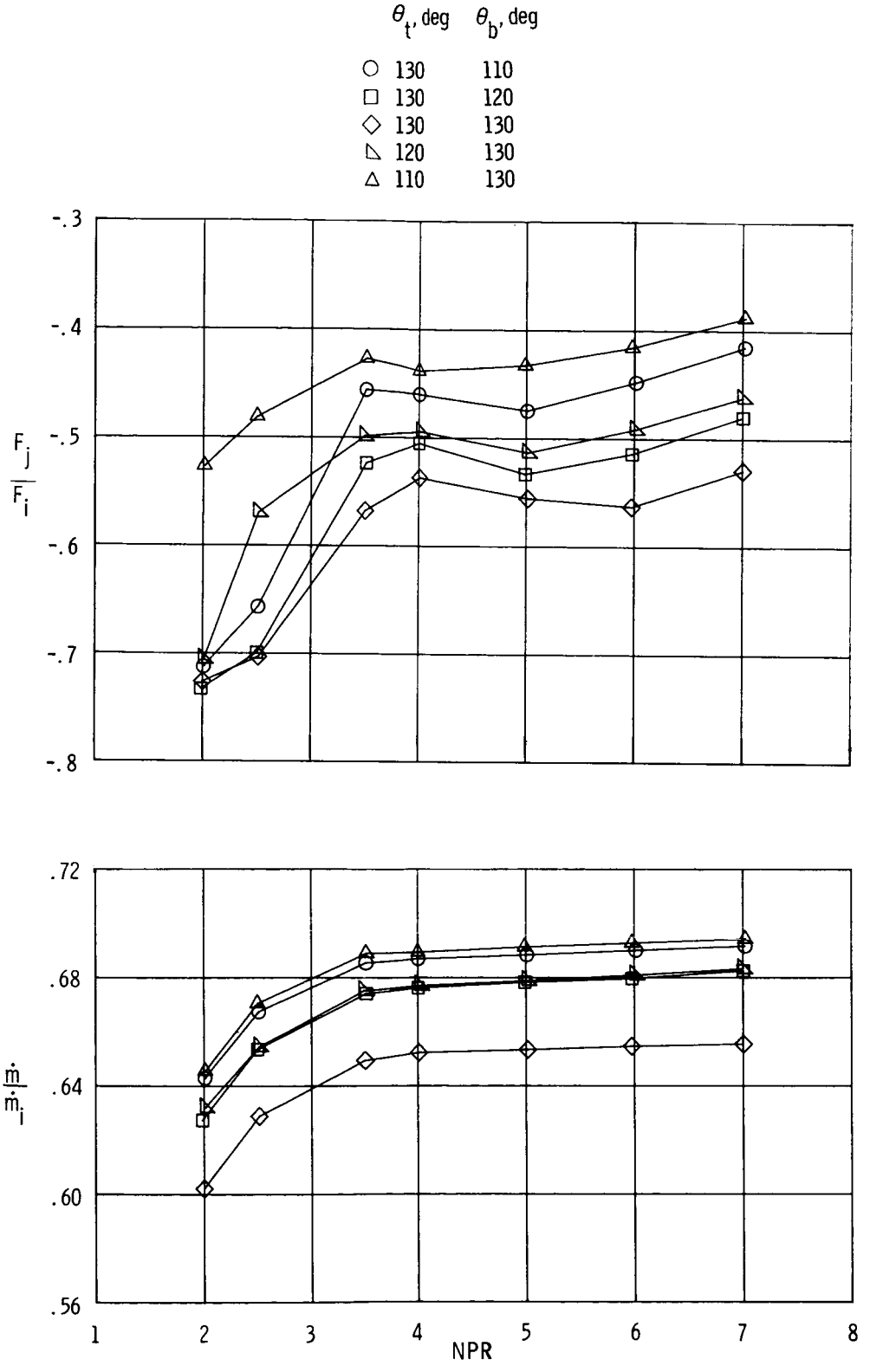

Figure 32.- Static performance and discharge coefficient of reverse-thrust nozzles with different top and bottom reverser-port angles.

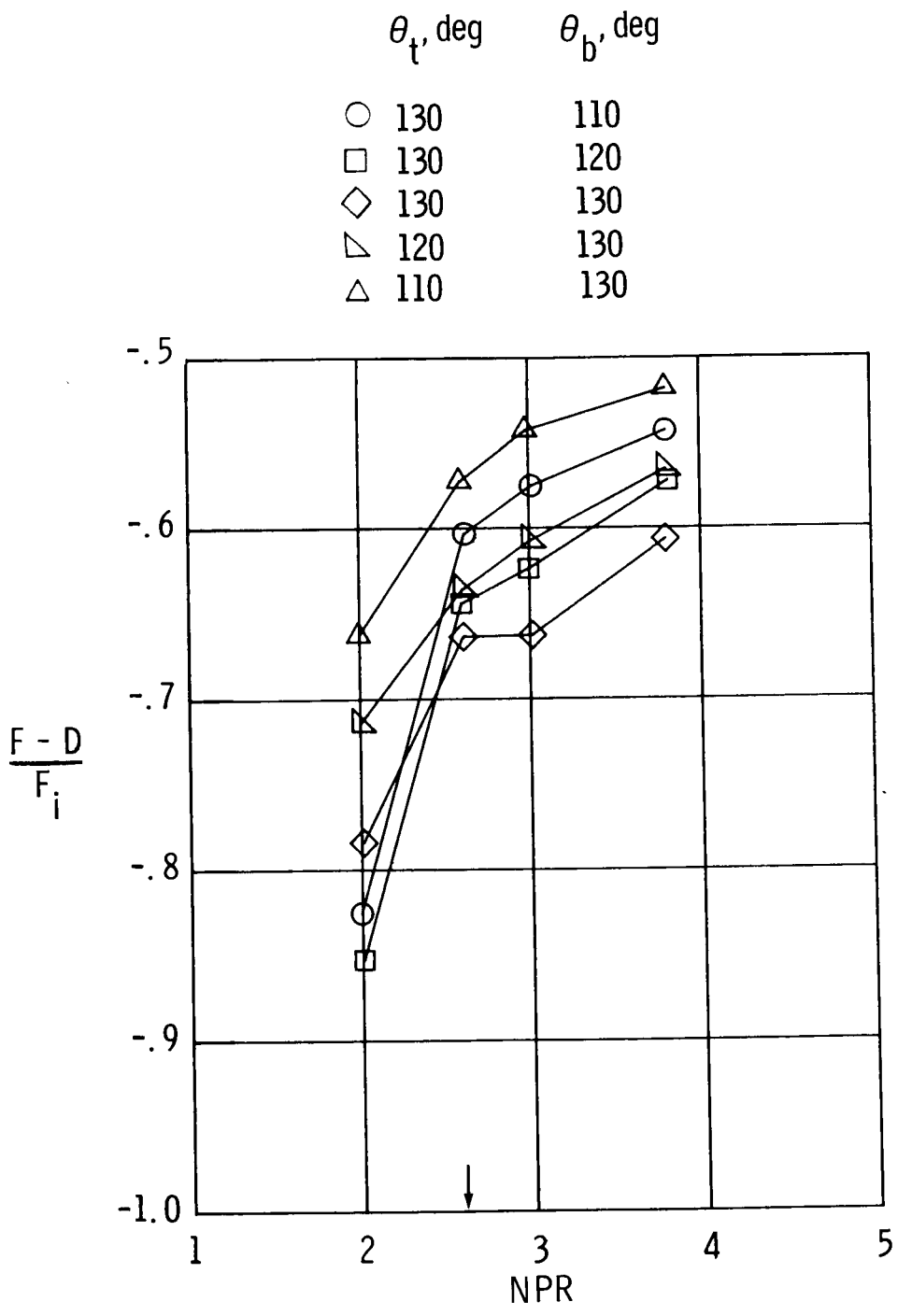

Figure 33.- Aeropropulsive performance of reverse-thrust nozzles with different top and bottom reverser-port angles at M = 0.15. Arrow denotes typical operating NPR.

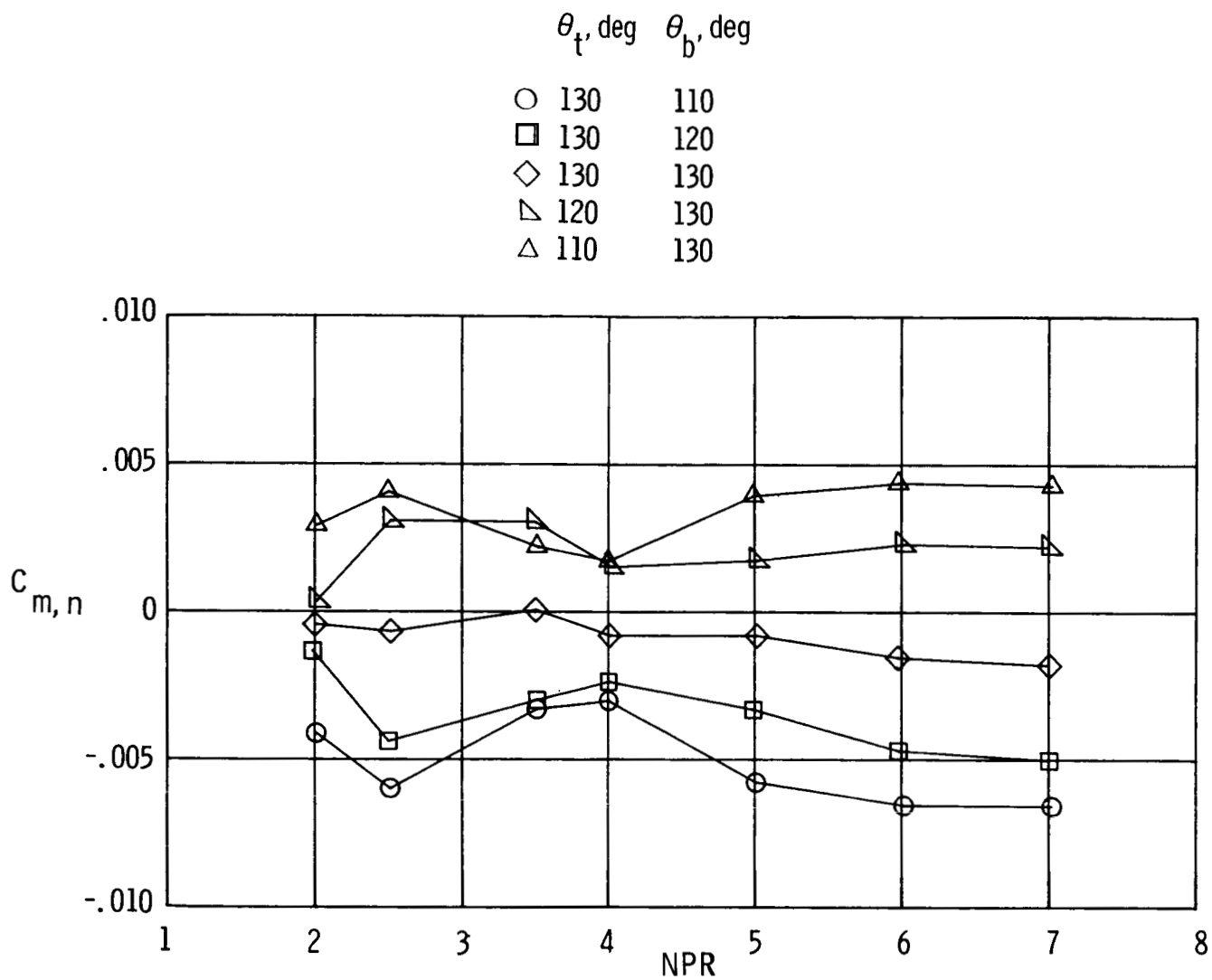

(a) M = 0.

Figure 34.- Nozzle pitching-moment coefficient of reverse-thrust nozzles with different top and bottom reverser-port angles.

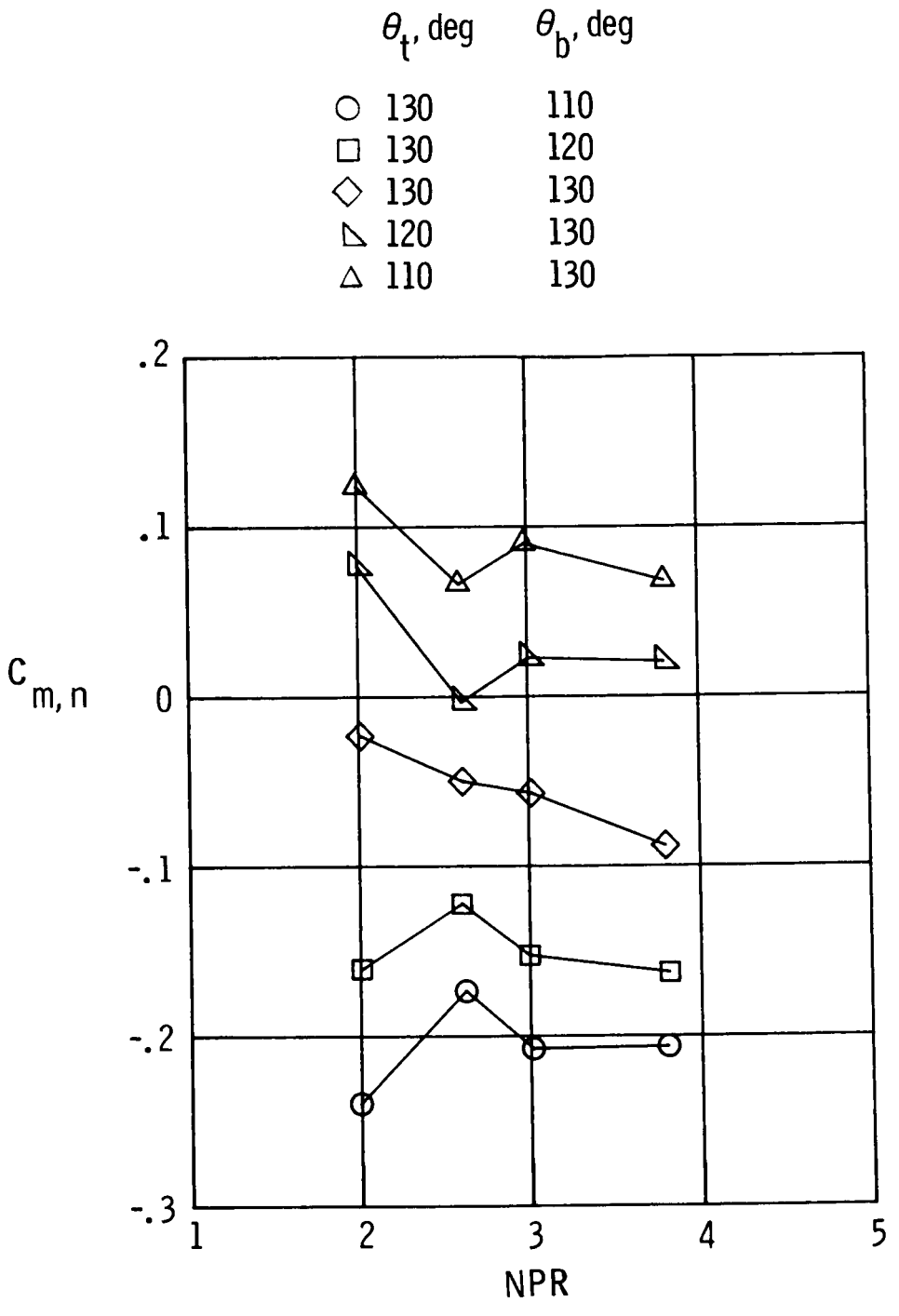

(b) M = 0.15.

Figure 34.- Concluded.

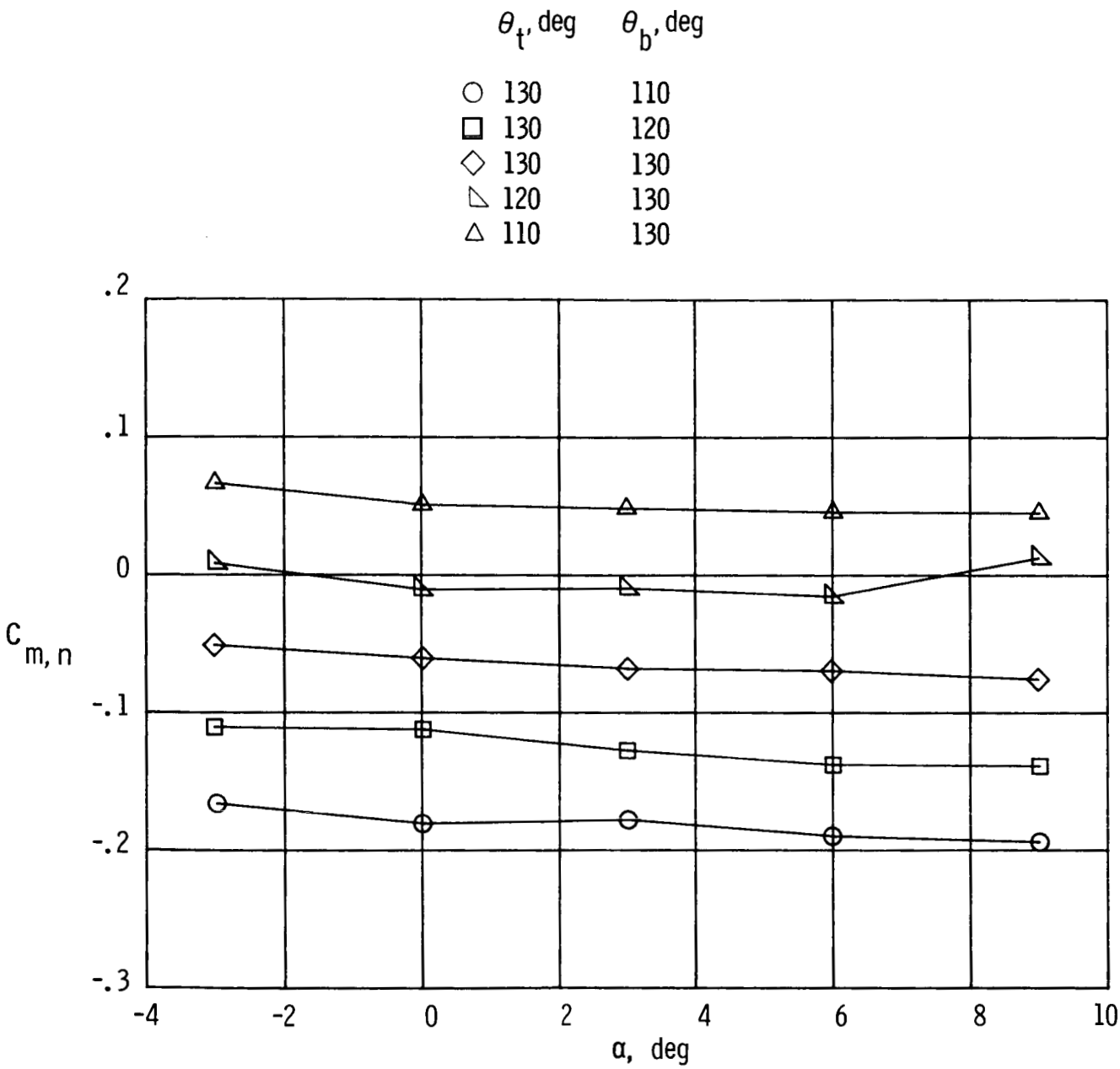

Figure 35.- Nozzle pitching-moment coefficient variation with angle of attack for reverse-thrust nozzles with different top and bottom reverser-port angles at M = 0.15 and NPR = 2.6.

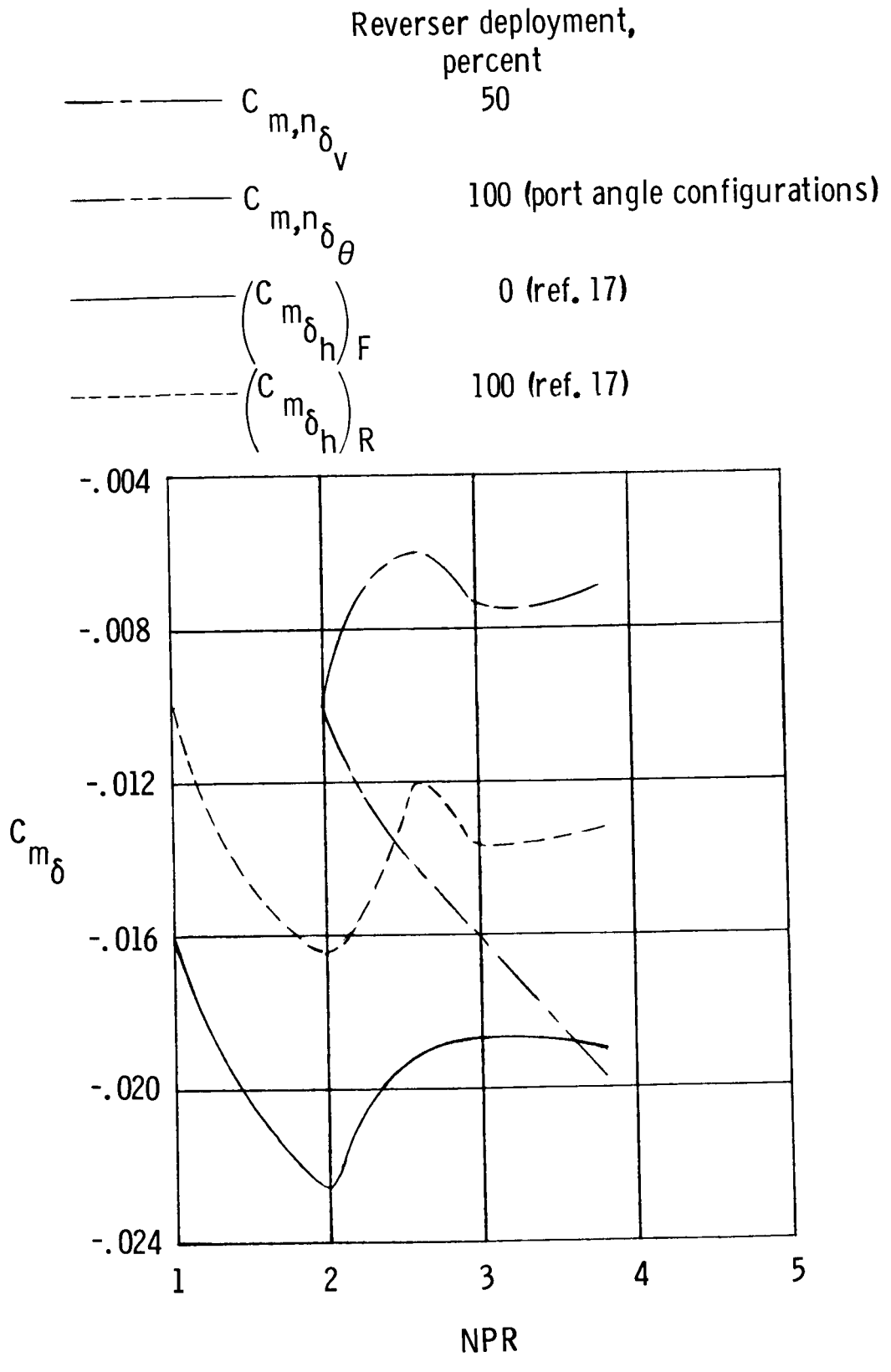

(a) Variation with NPR for $\alpha = 0°$.

Figure 36.- Effectiveness of trim devices at $M = 0.15$.

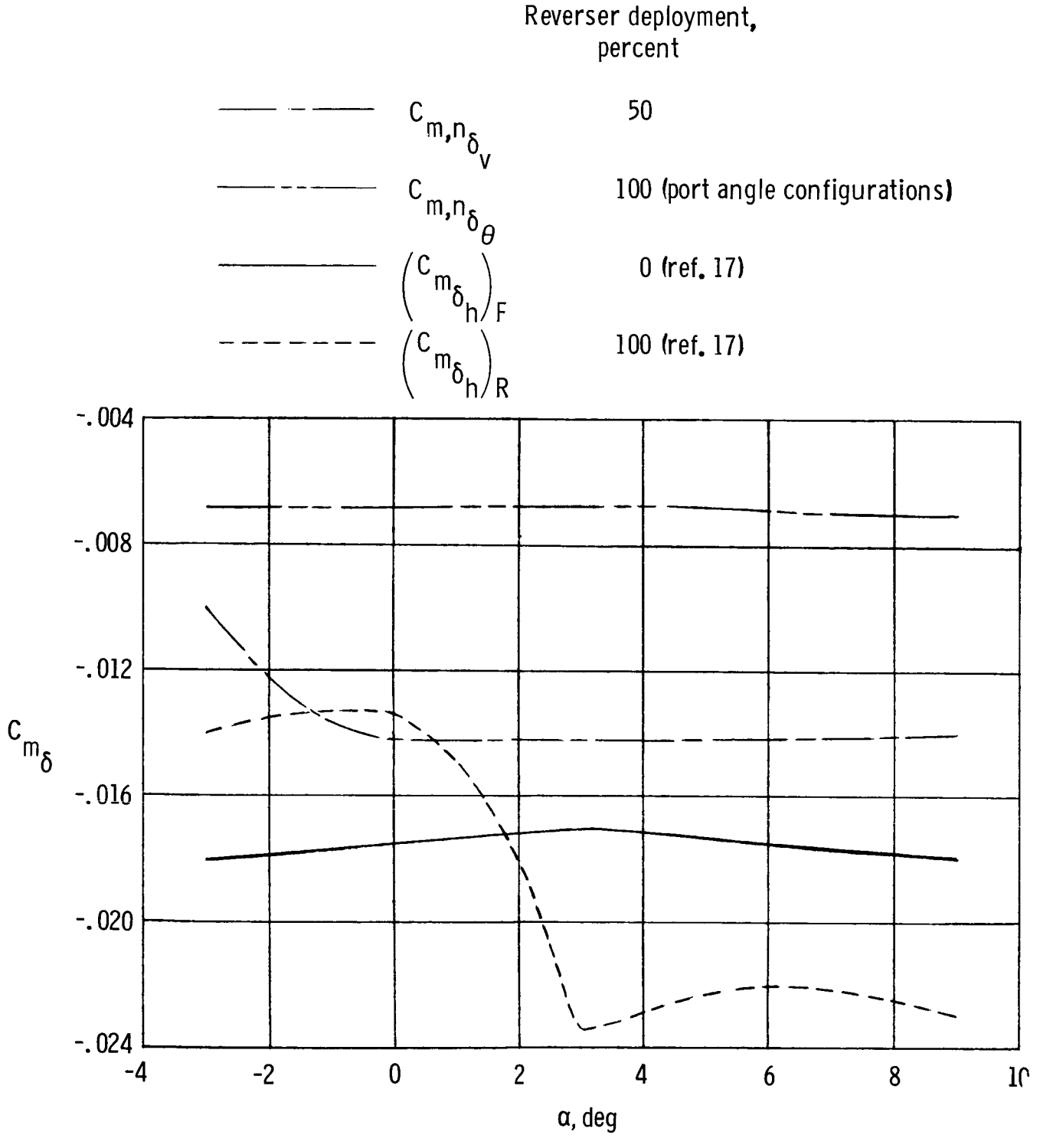

(b) Variation with α for NPR = 2.6.

Figure 36.- Concluded.

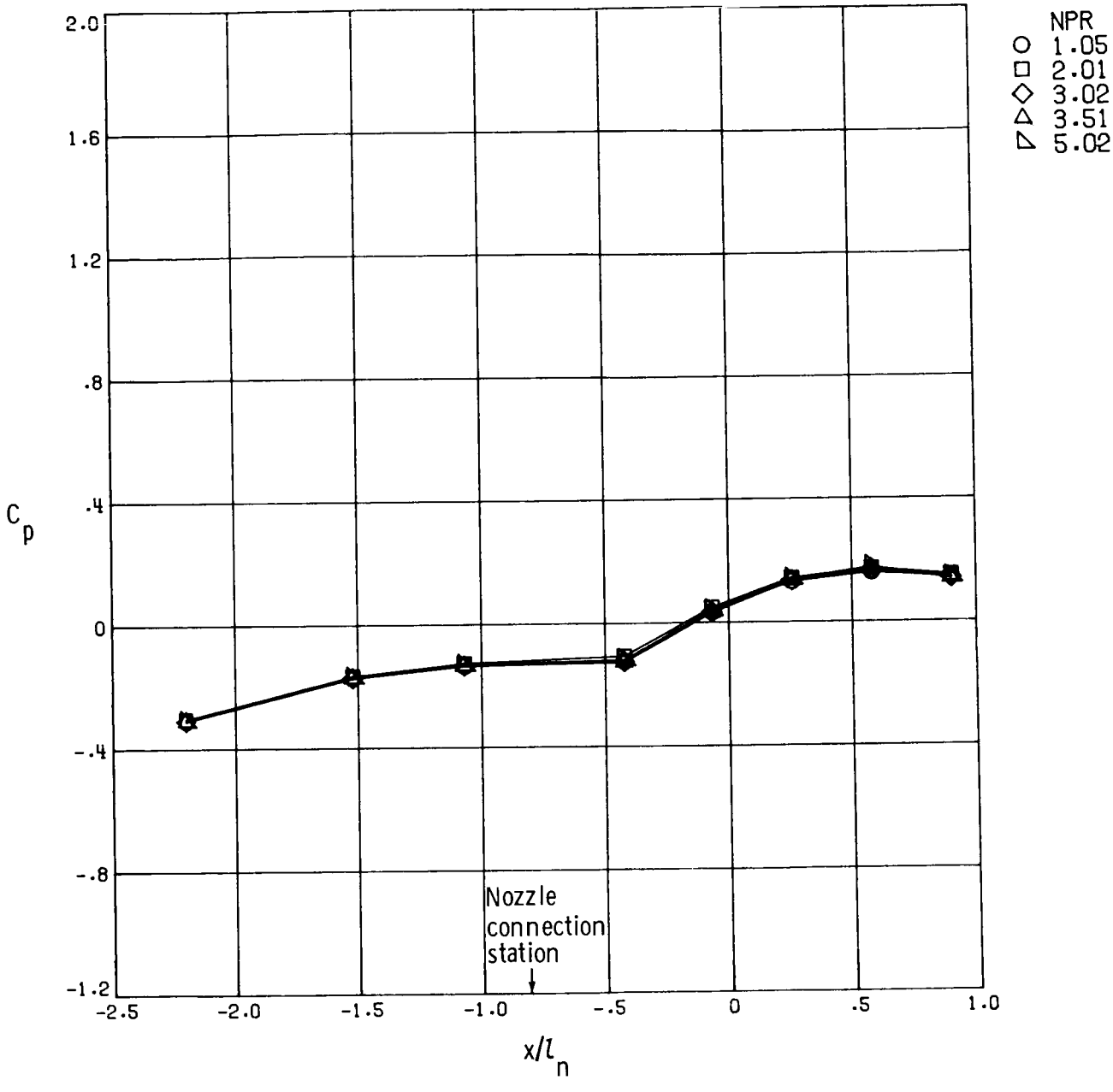

(a) M = 0.60.

Figure 37.- External pressure distribution of base-line (forward-thrust) nozzle.

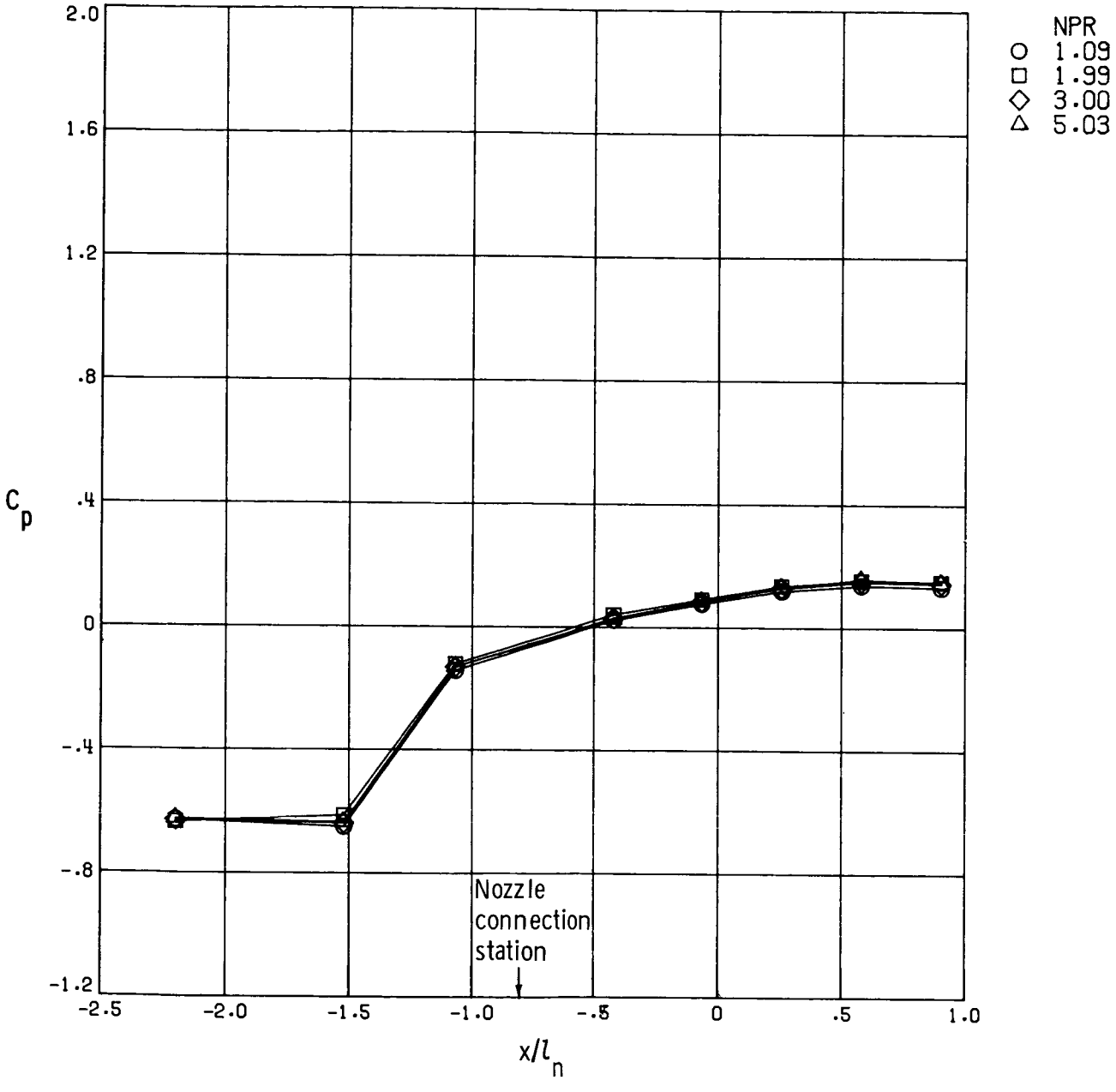

(b) M = 0.90.

Figure 37.- Continued.

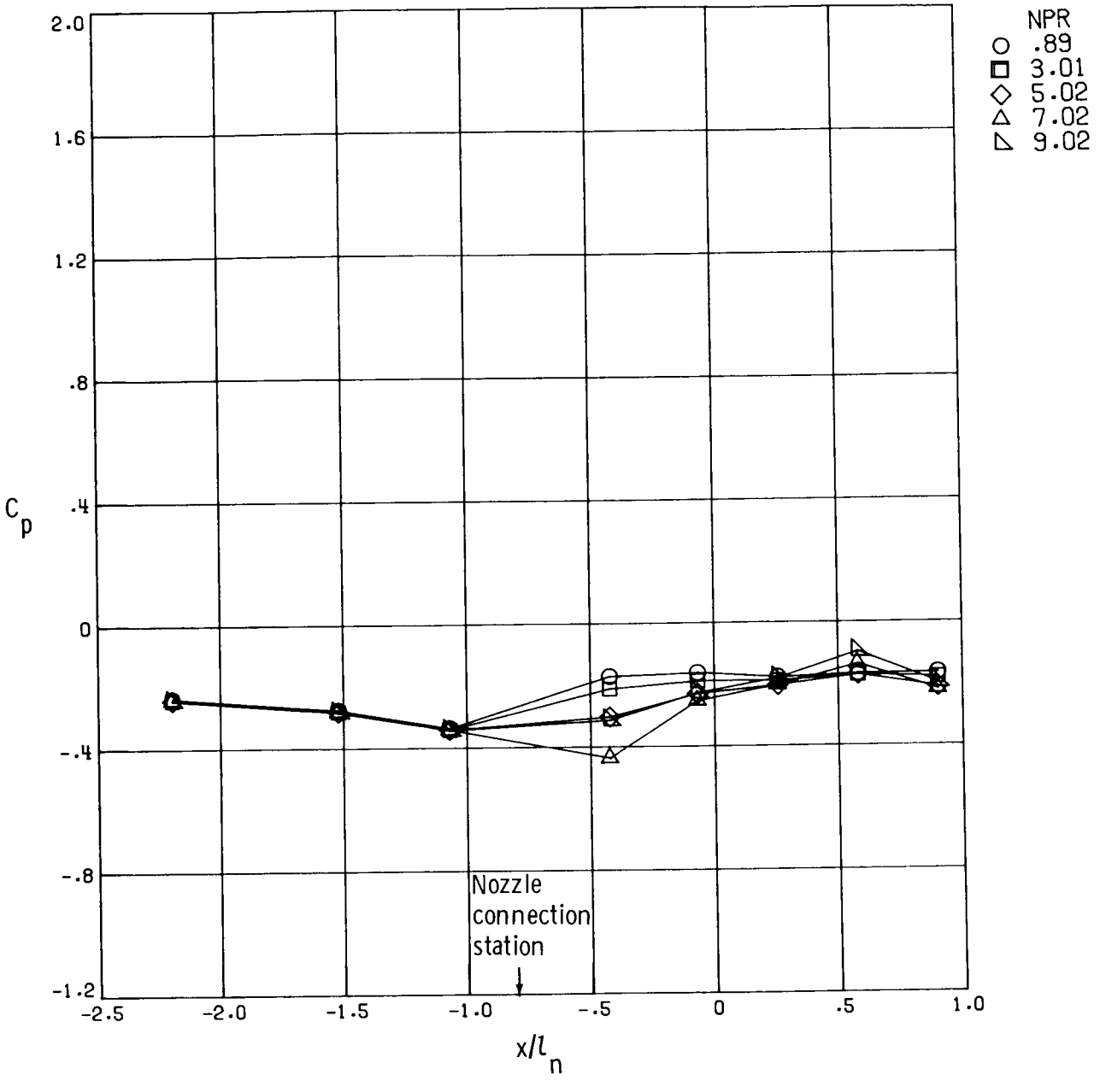

(c) M = 1.20.

Figure 37.- Concluded.

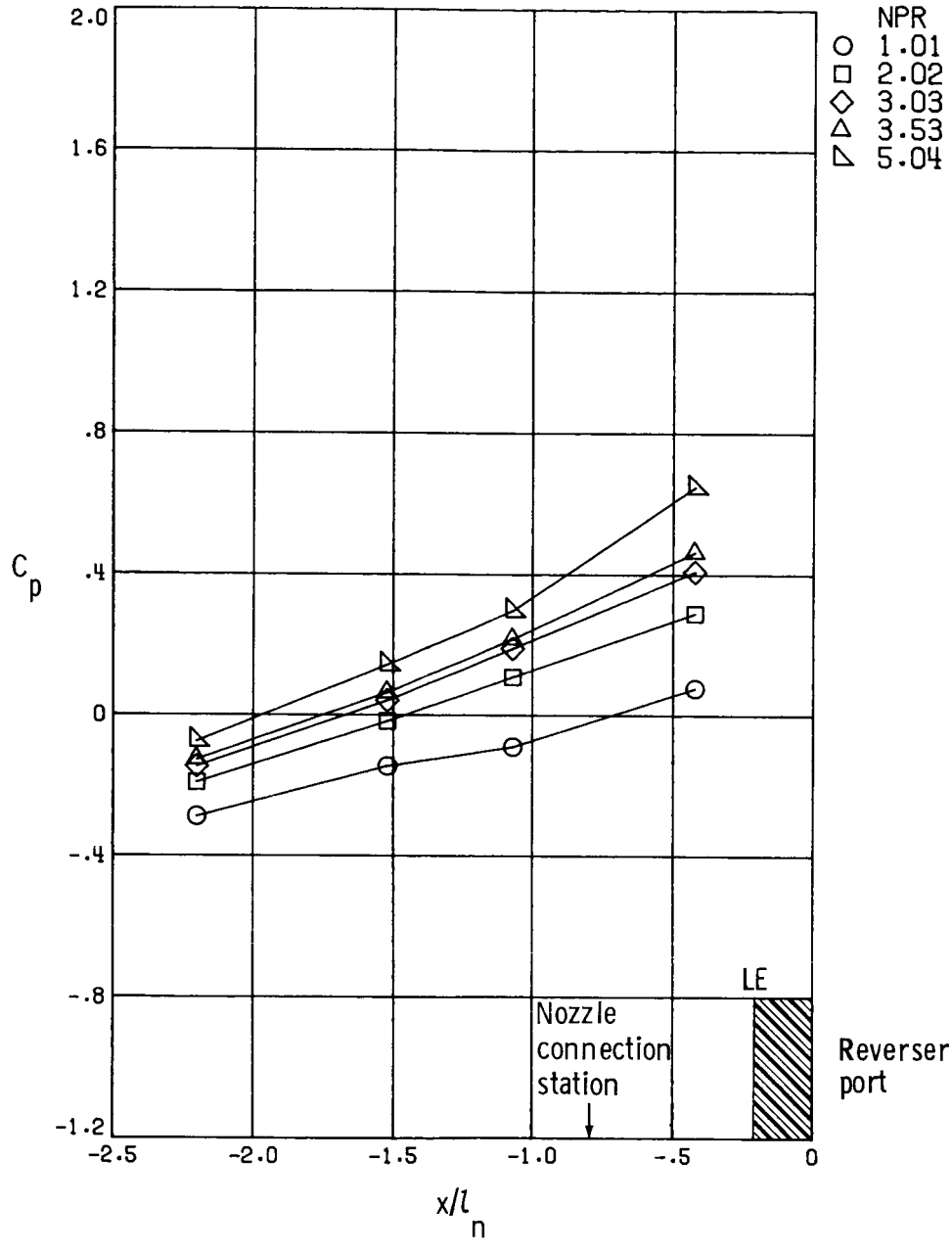

(a) M = 0.60.

Figure 38.- External pressure distribution of 25-percent reverser deployment nozzle.

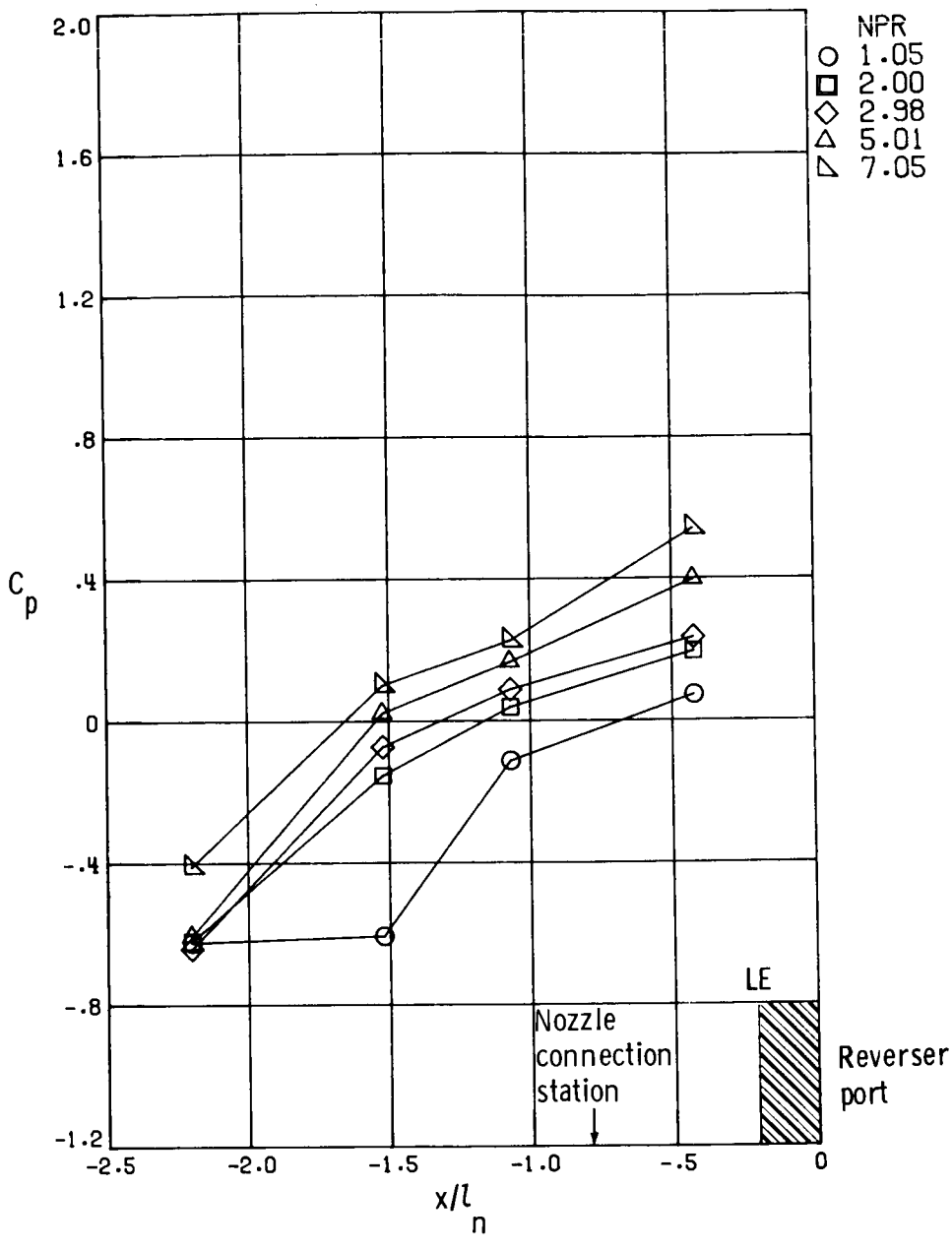

(b) M = 0.90.

Figure 38.- Continued.

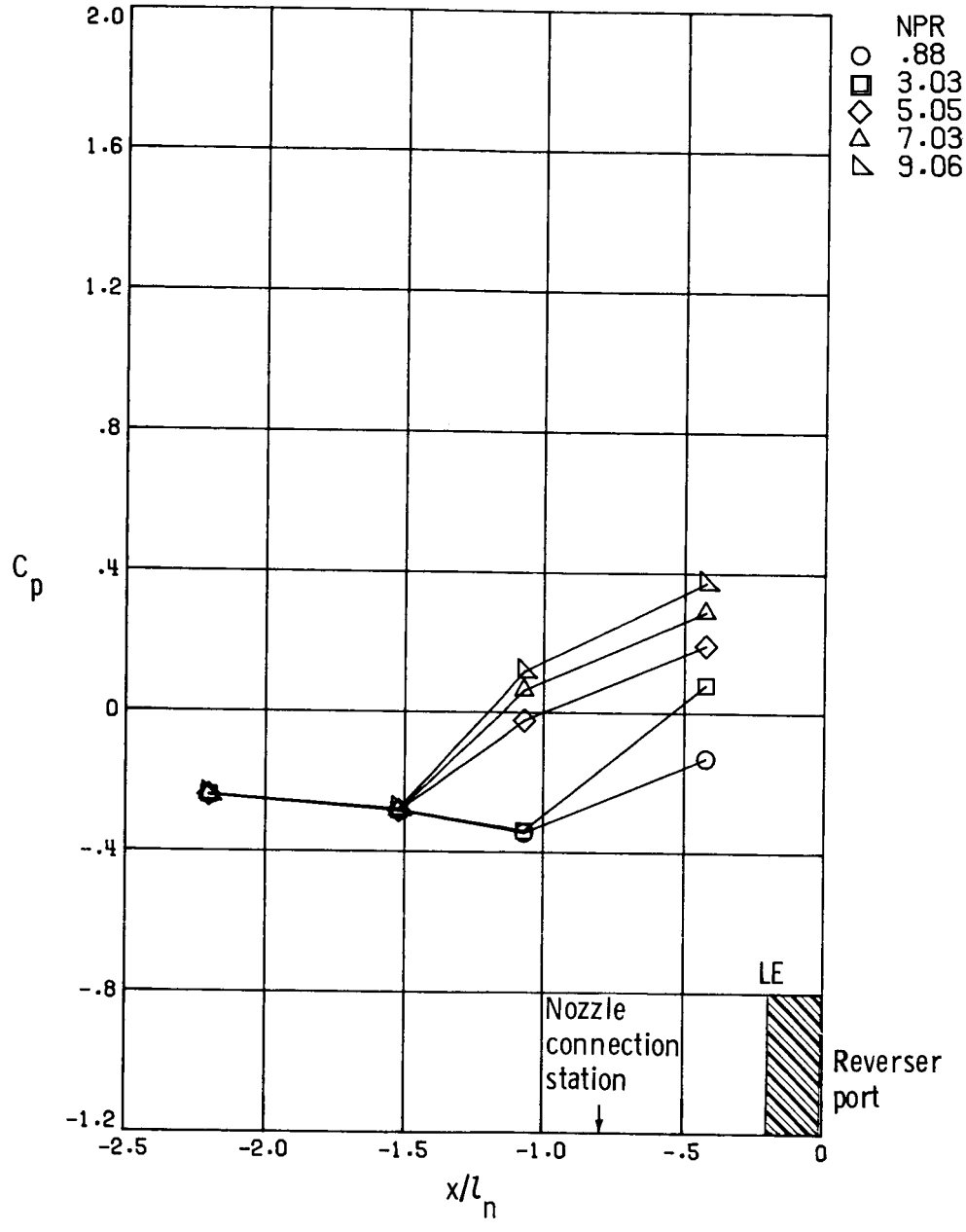

(c) M = 1.20.

Figure 38.- Concluded.

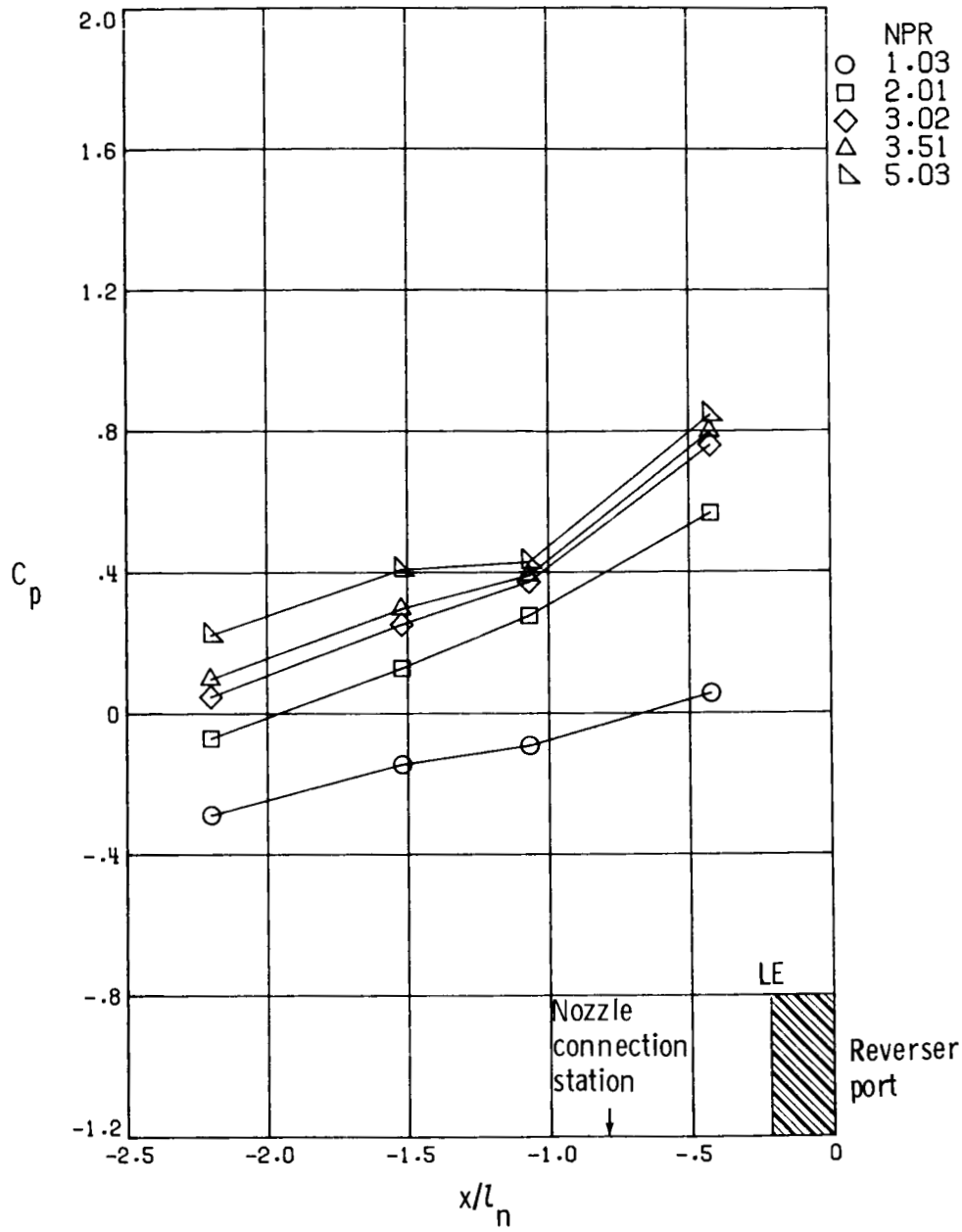

(a) M = 0.60.

Figure 39.- External pressure distribution of 50-percent reverser deployment nozzle.

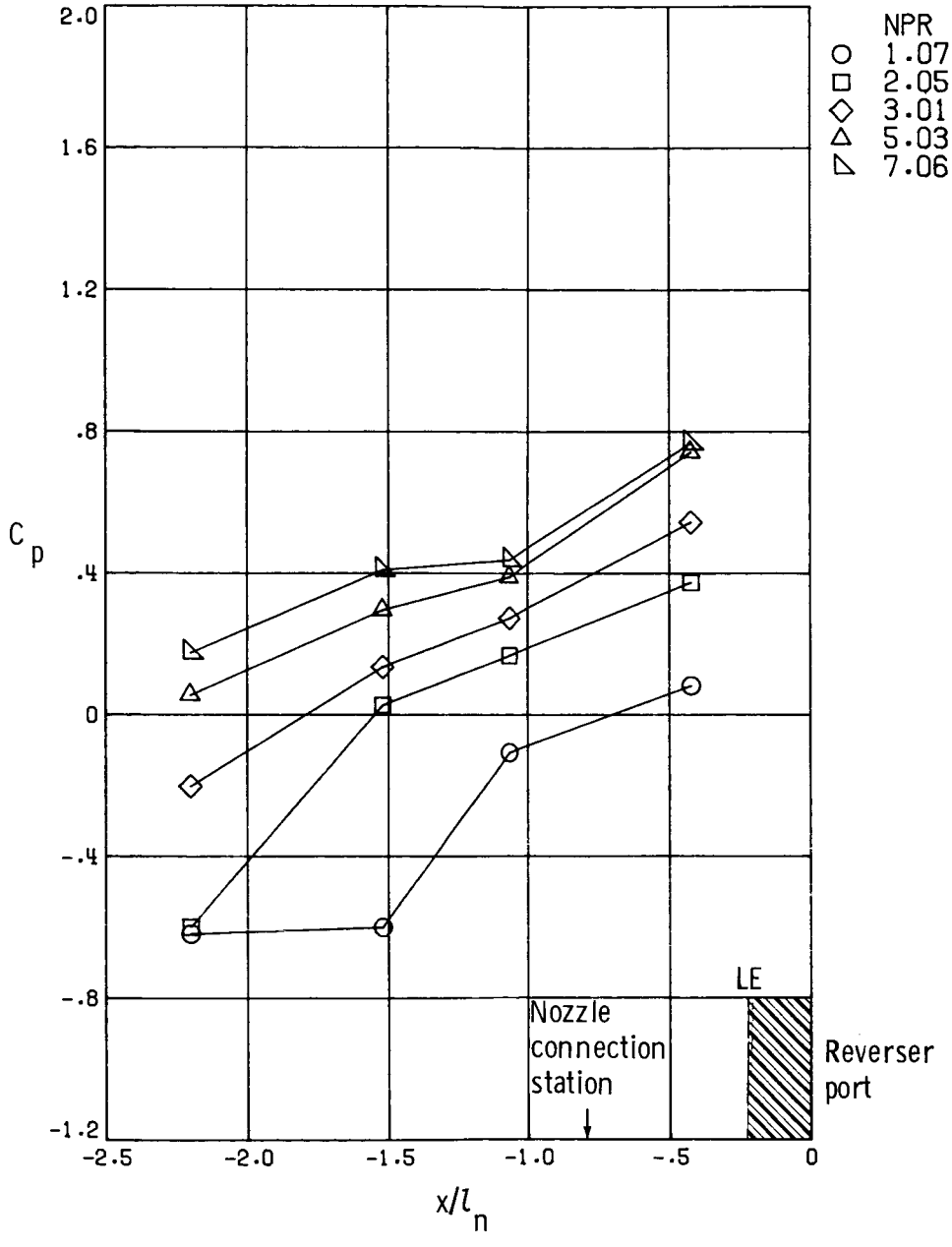

(b) M = 0.90.

Figure 39.- Continued.

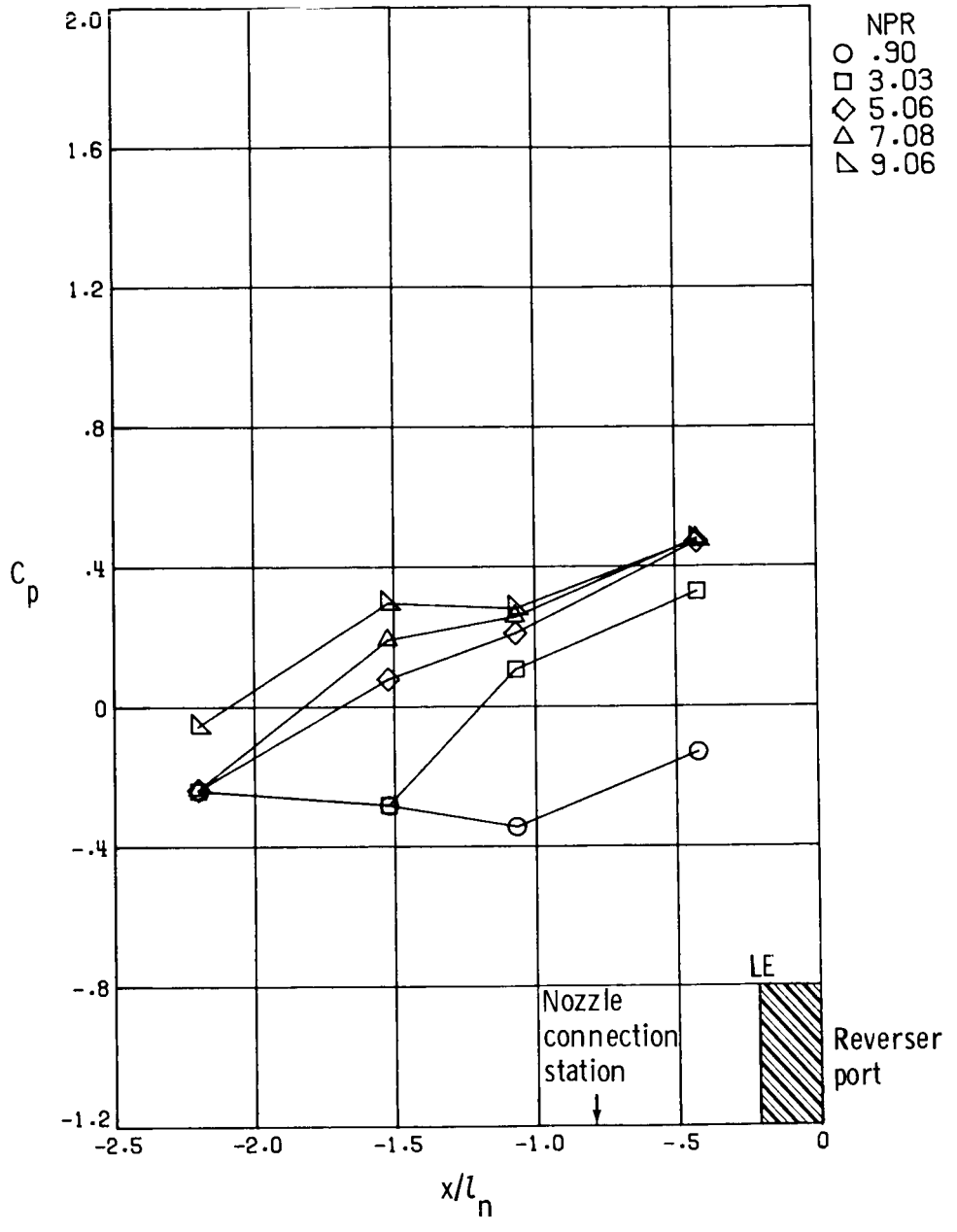

(c) M = 1.20.

Figure 39.- Concluded.

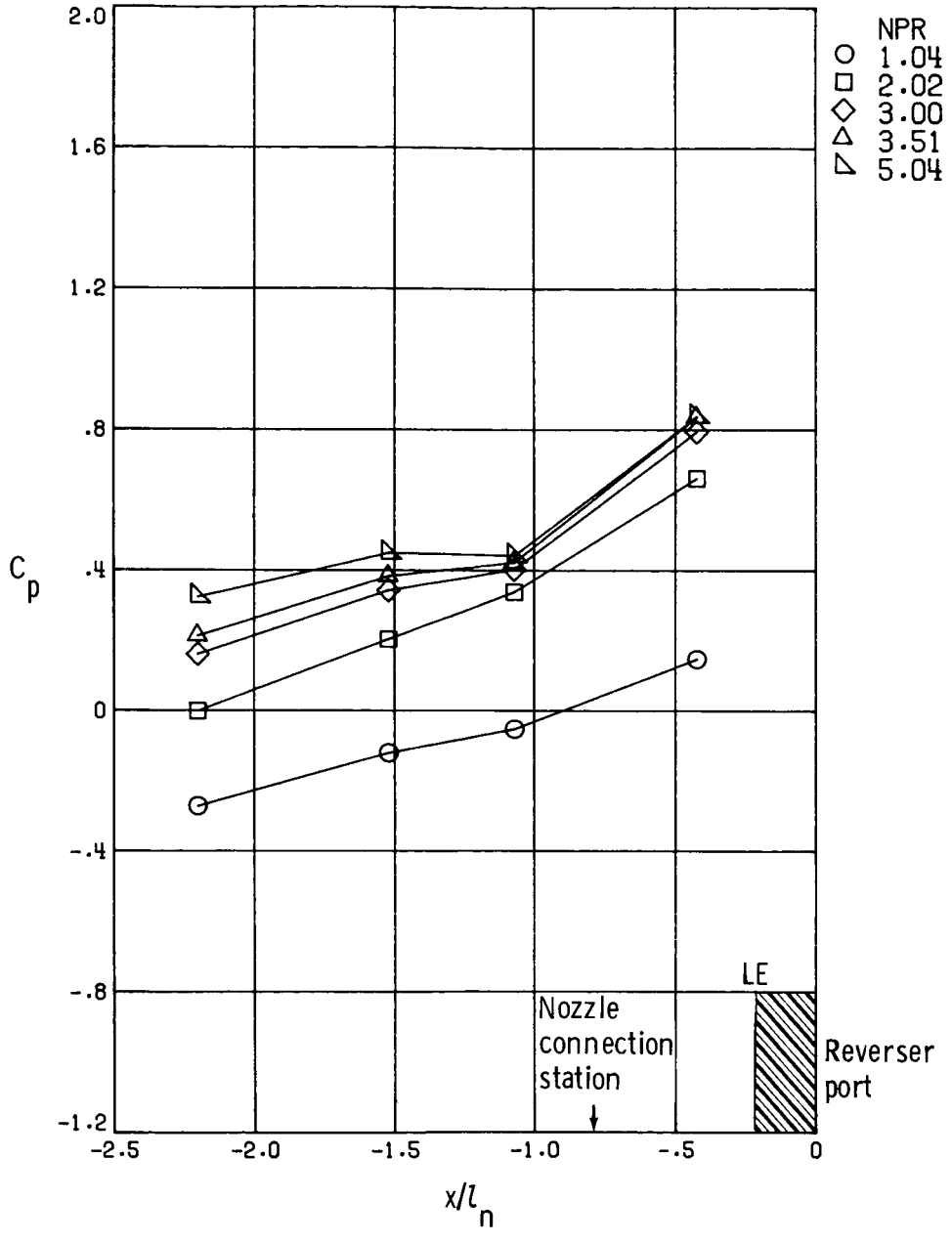

(a) M = 0.60.

Figure 40.- External pressure distribution of 75-percent reverser deployment nozzle.

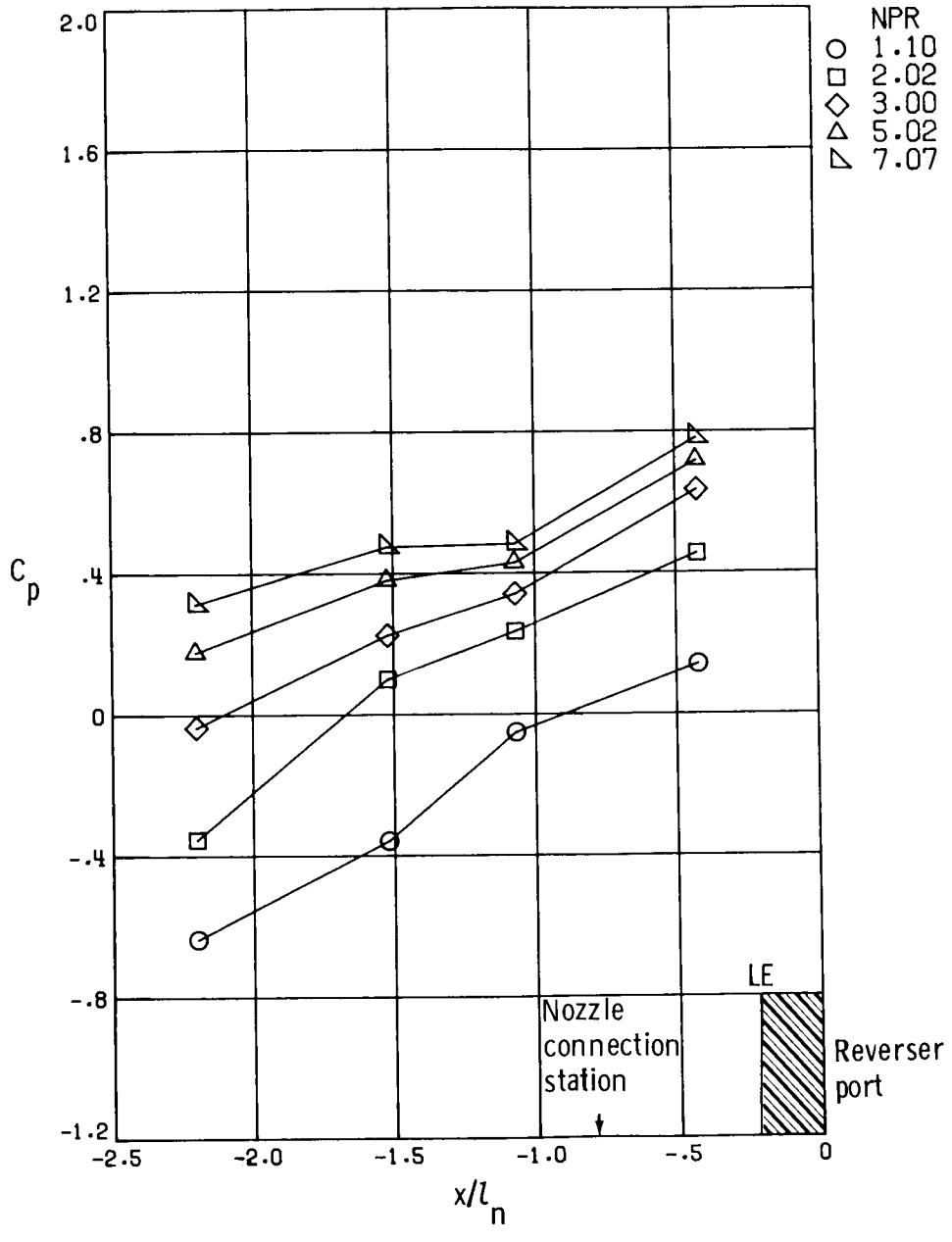

(b) M = 0.90.

Figure 40.- Continued.

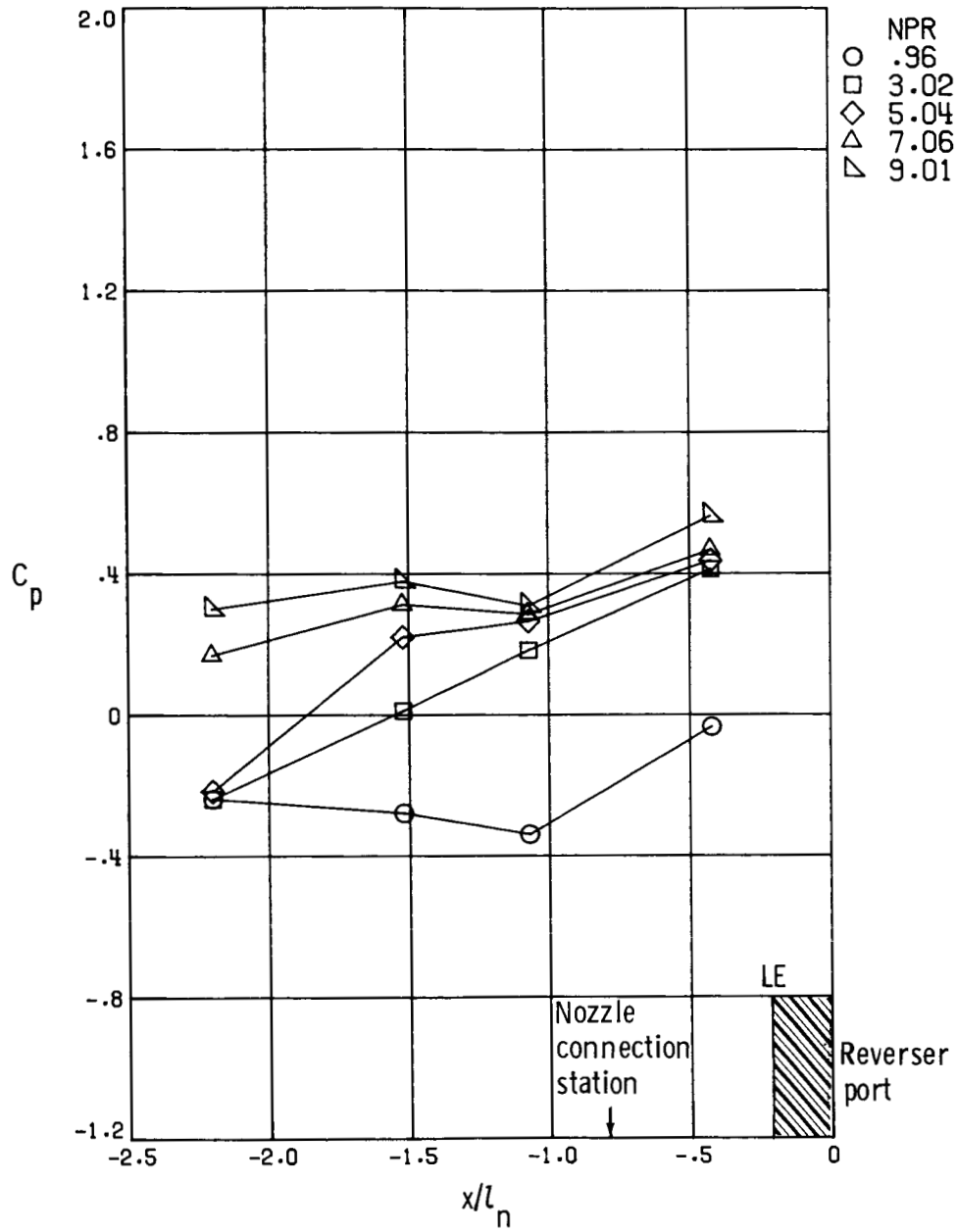

(c) M = 1.20.

Figure 40.- Concluded.

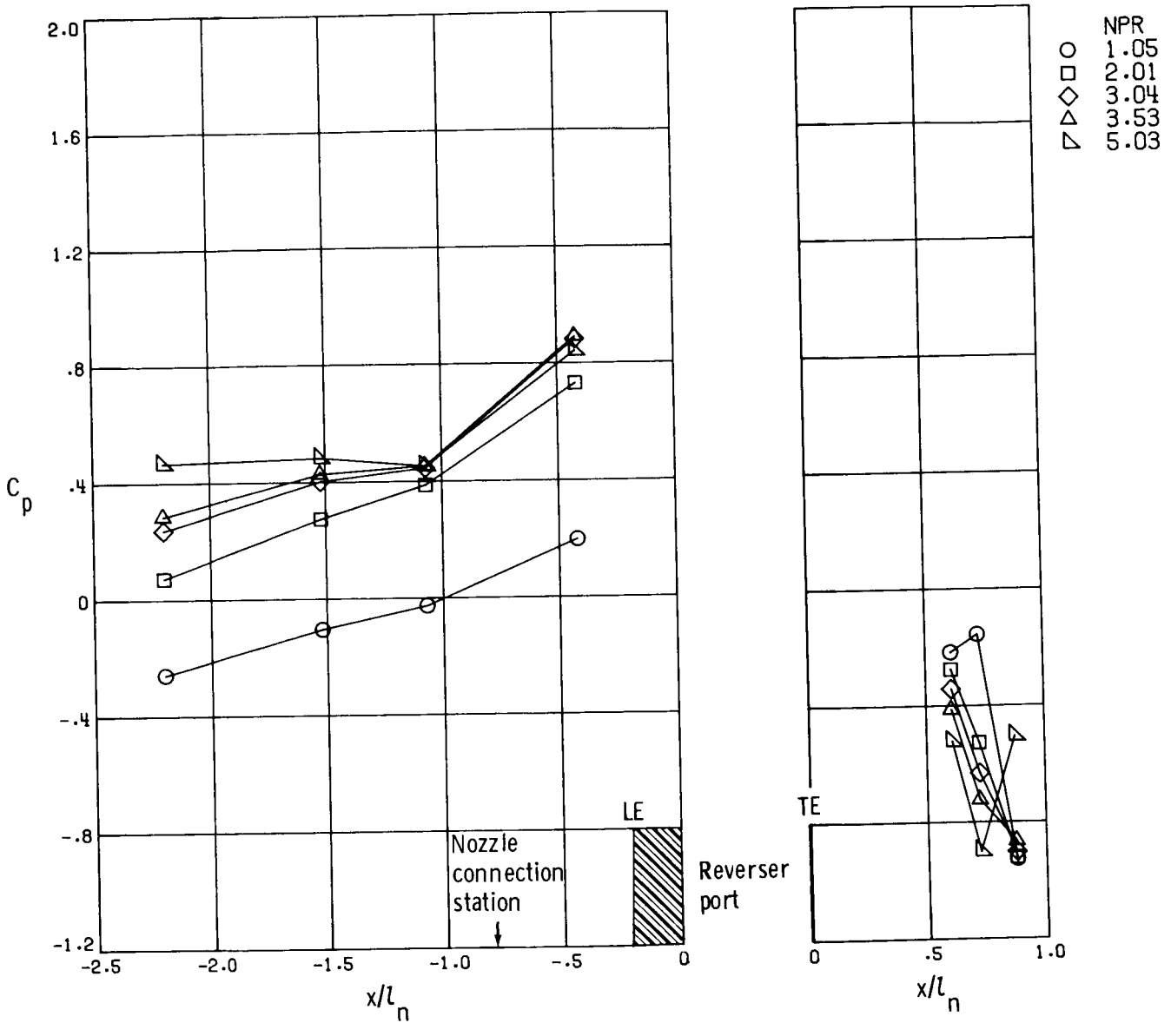

(a) M = 0.60.

Figure 41.- External pressure distribution of 100-percent reverser deployment nozzle.

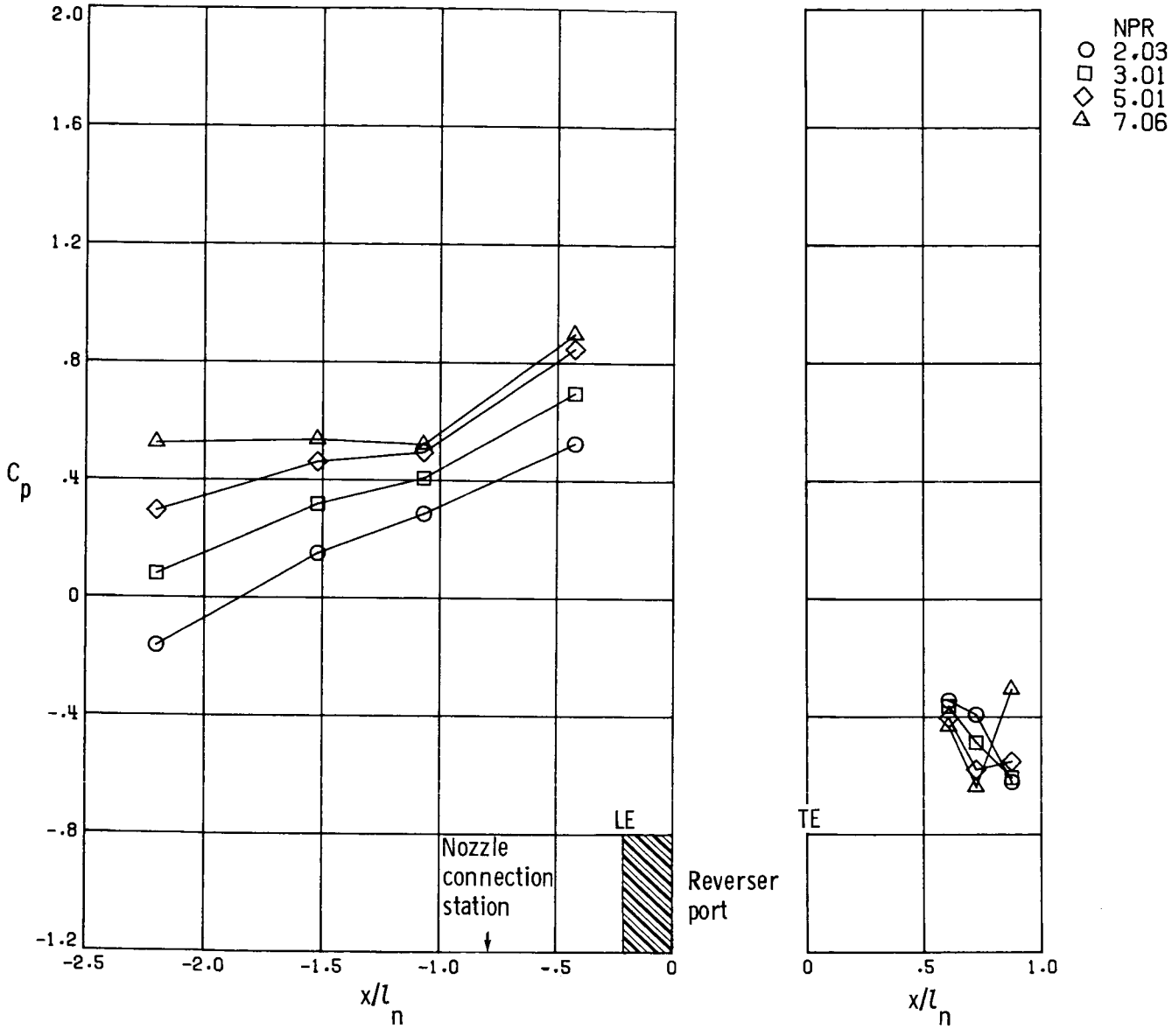

(b) M = 0.90.

Figure 41.- Continued.

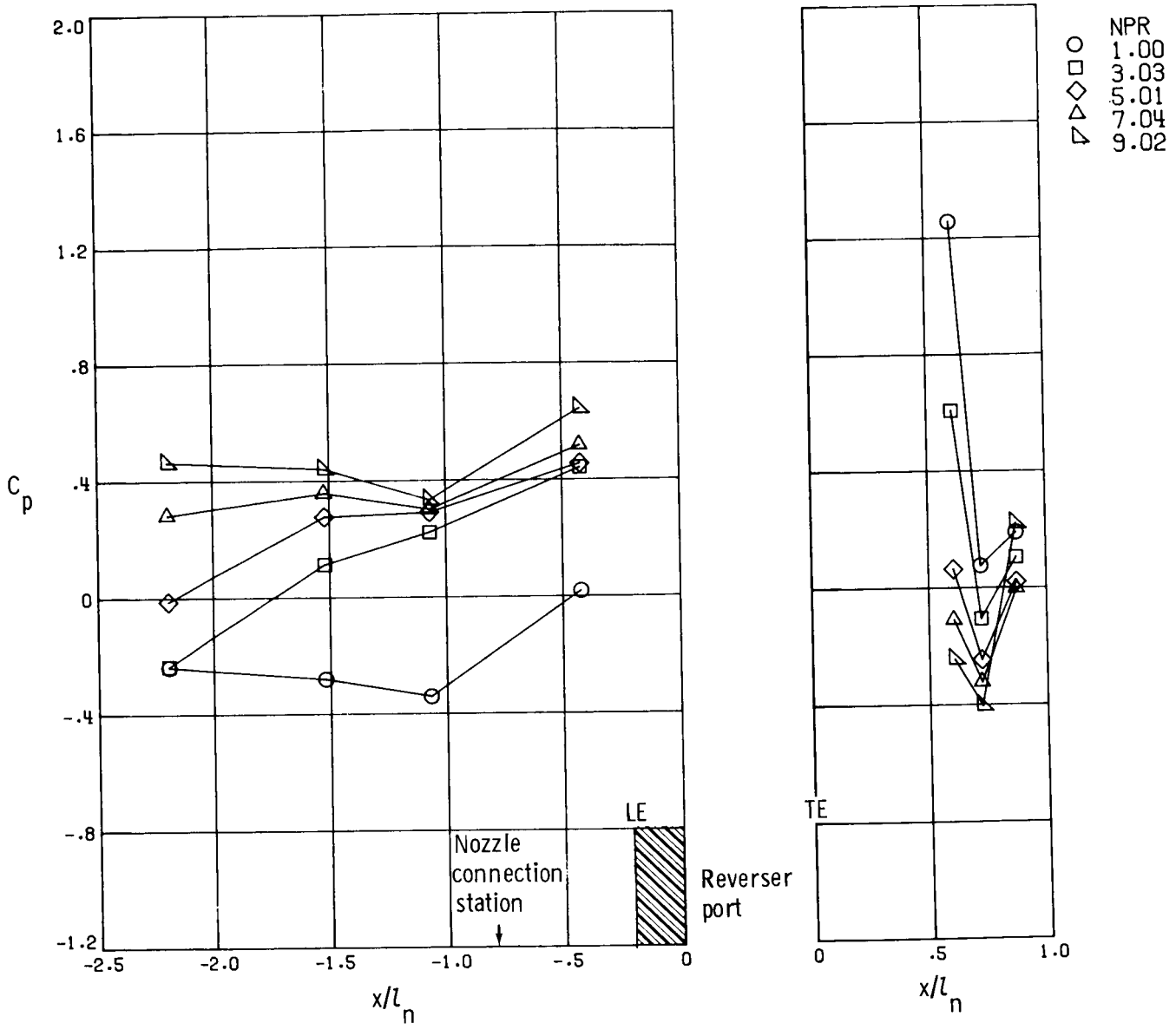

(c) M = 1.20.

Figure 41.- Concluded.

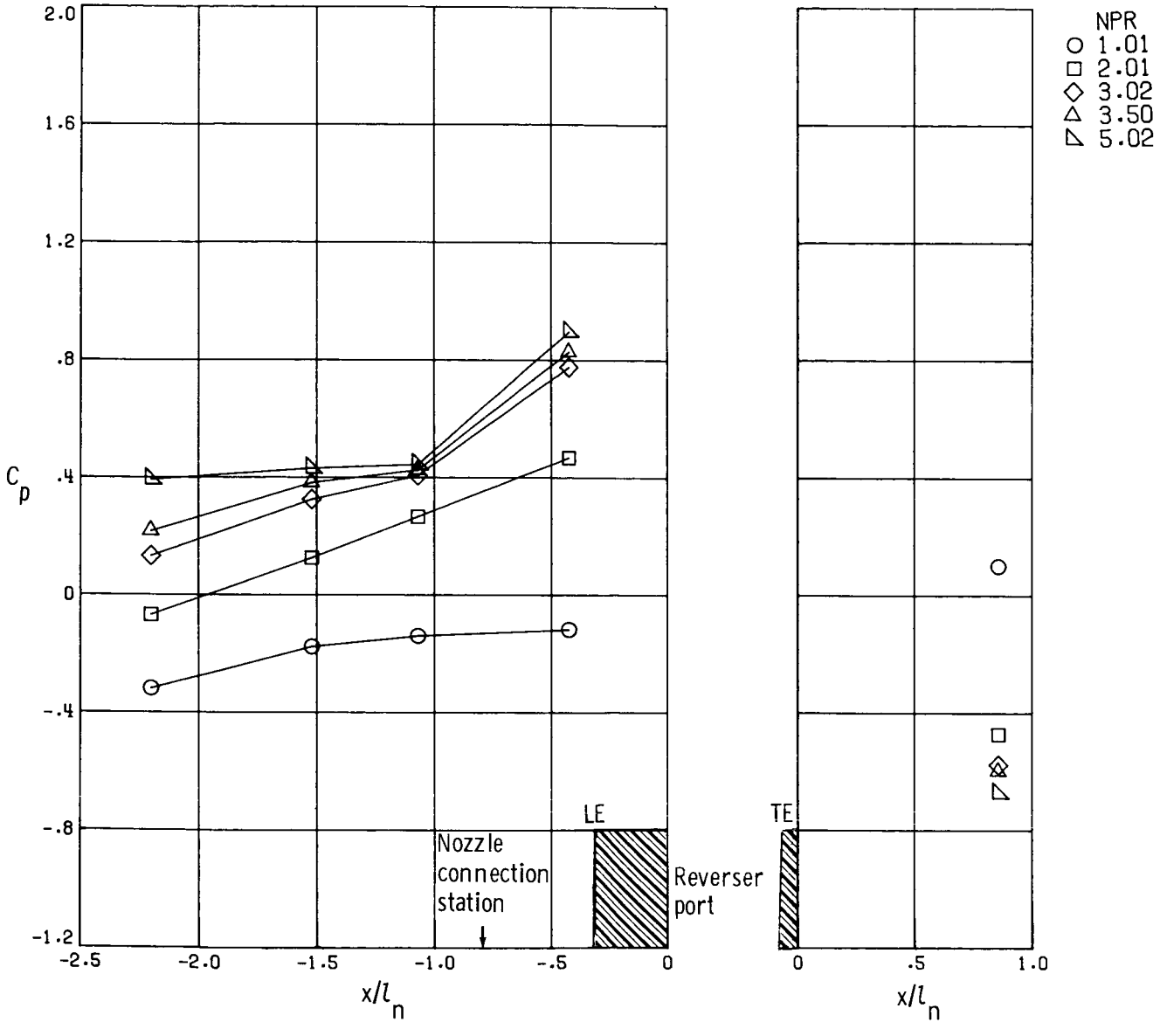

(a) M = 0.60.

Figure 42.- External pressure distribution of 110° reverser-port angle nozzle.

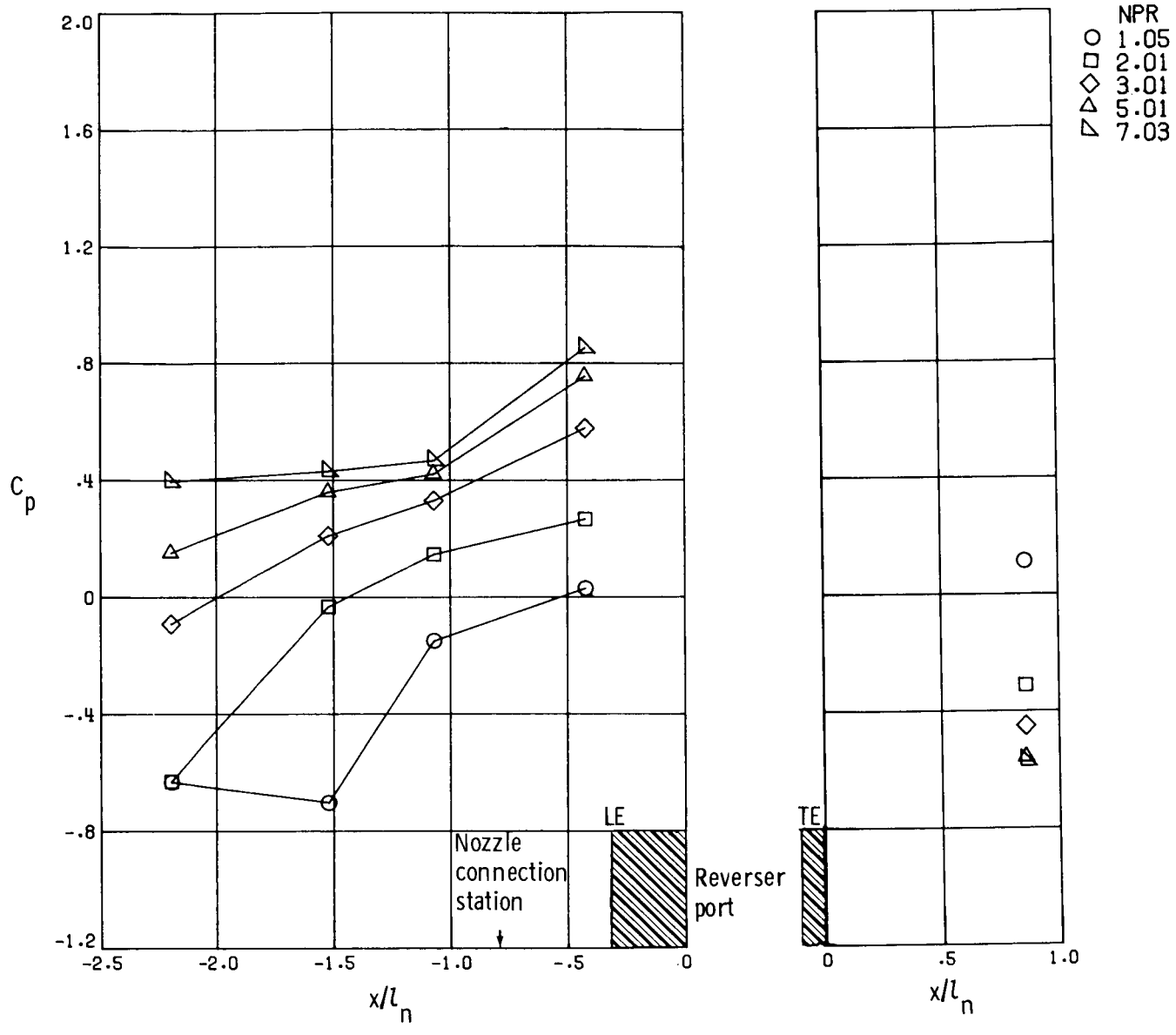

(b) M = 0.90.

Figure 42.- Continued.

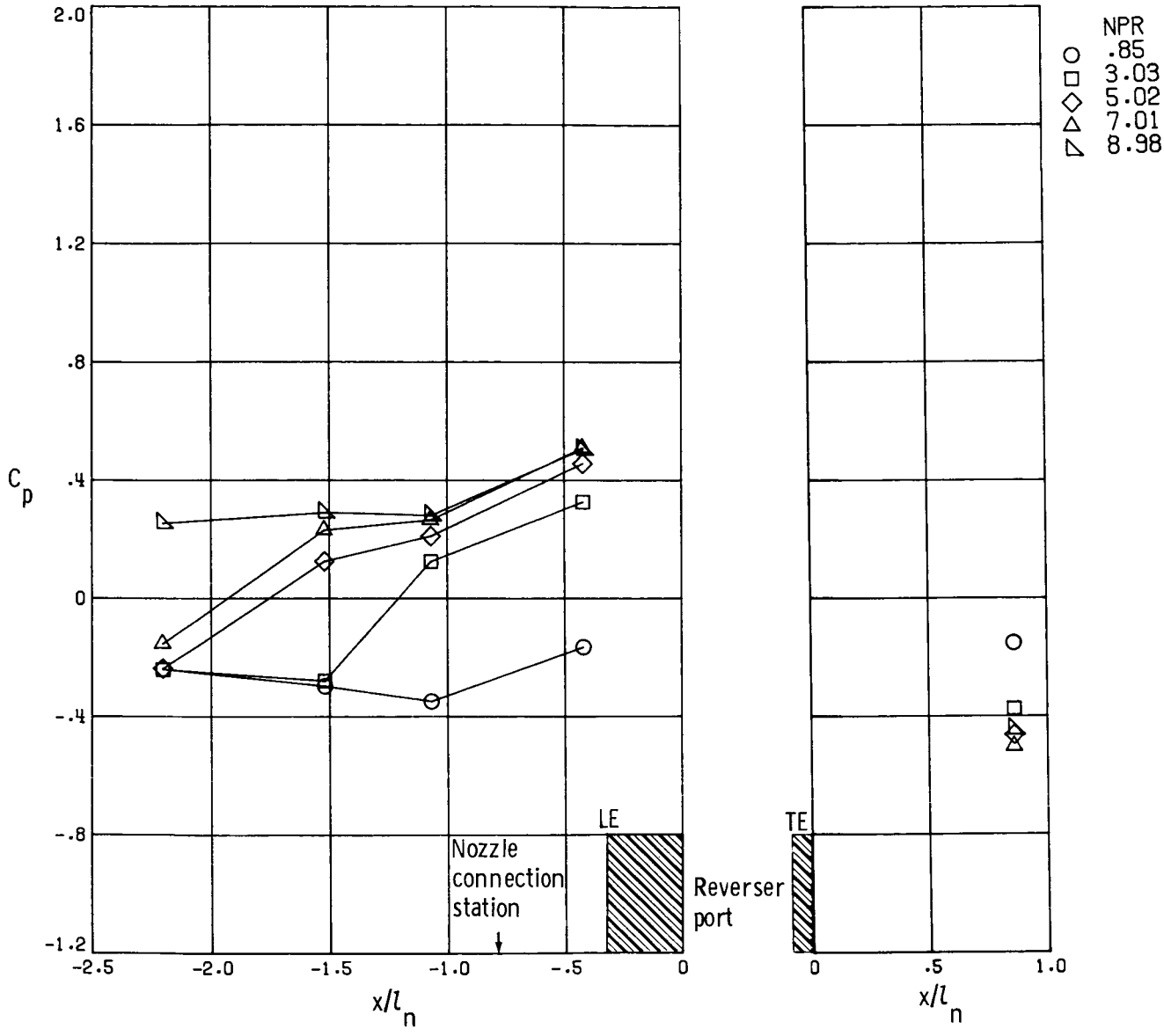

(c) M = 1.20.

Figure 42.- Concluded.

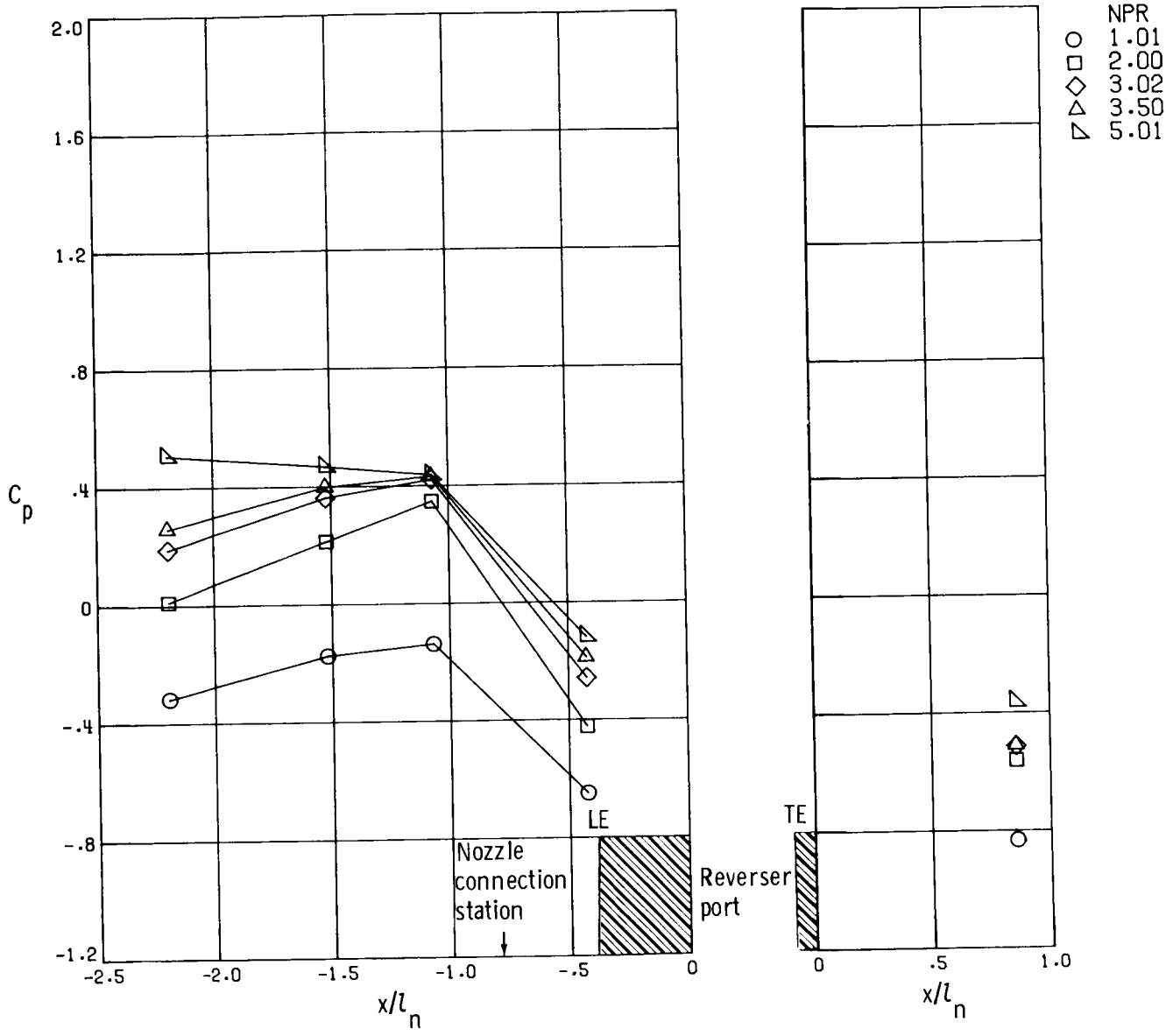

(a) M = 0.60.

Figure 43.- External pressure distribution of 120° reverser-port angle nozzle.

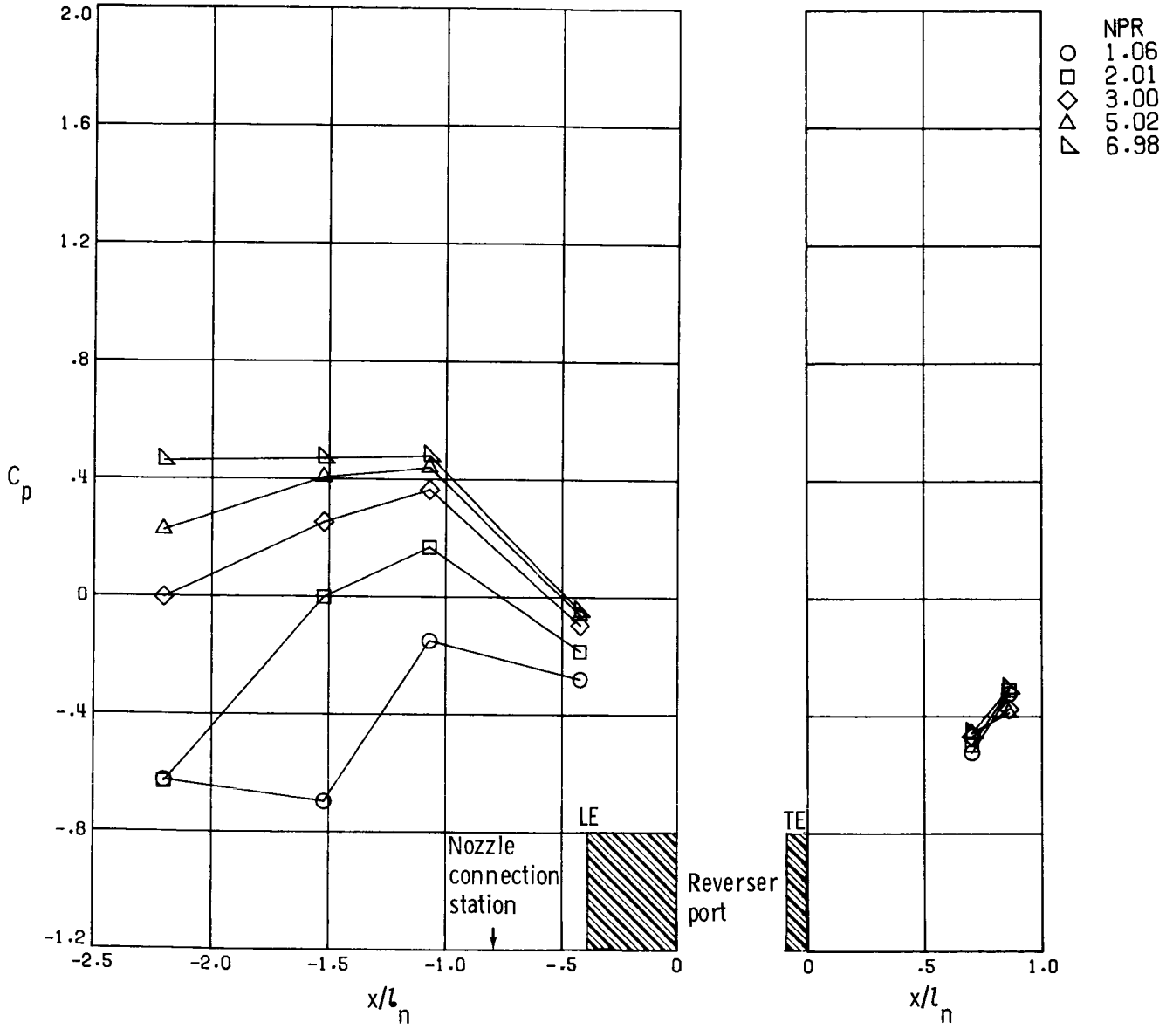

(b) M = 0.90.

Figure 43.- Continued.

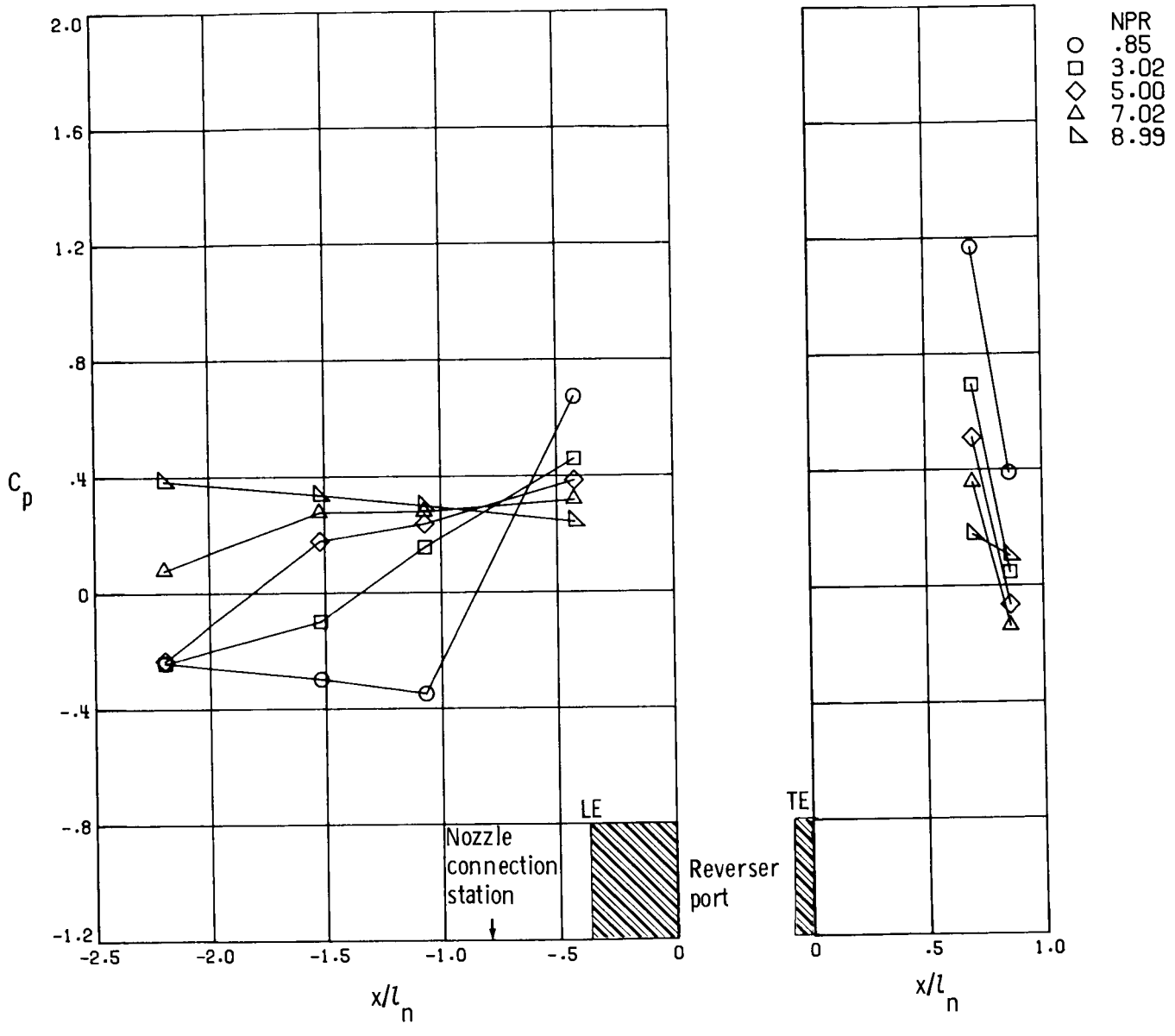

(c) M = 1.20.

Figure 43.- Concluded.

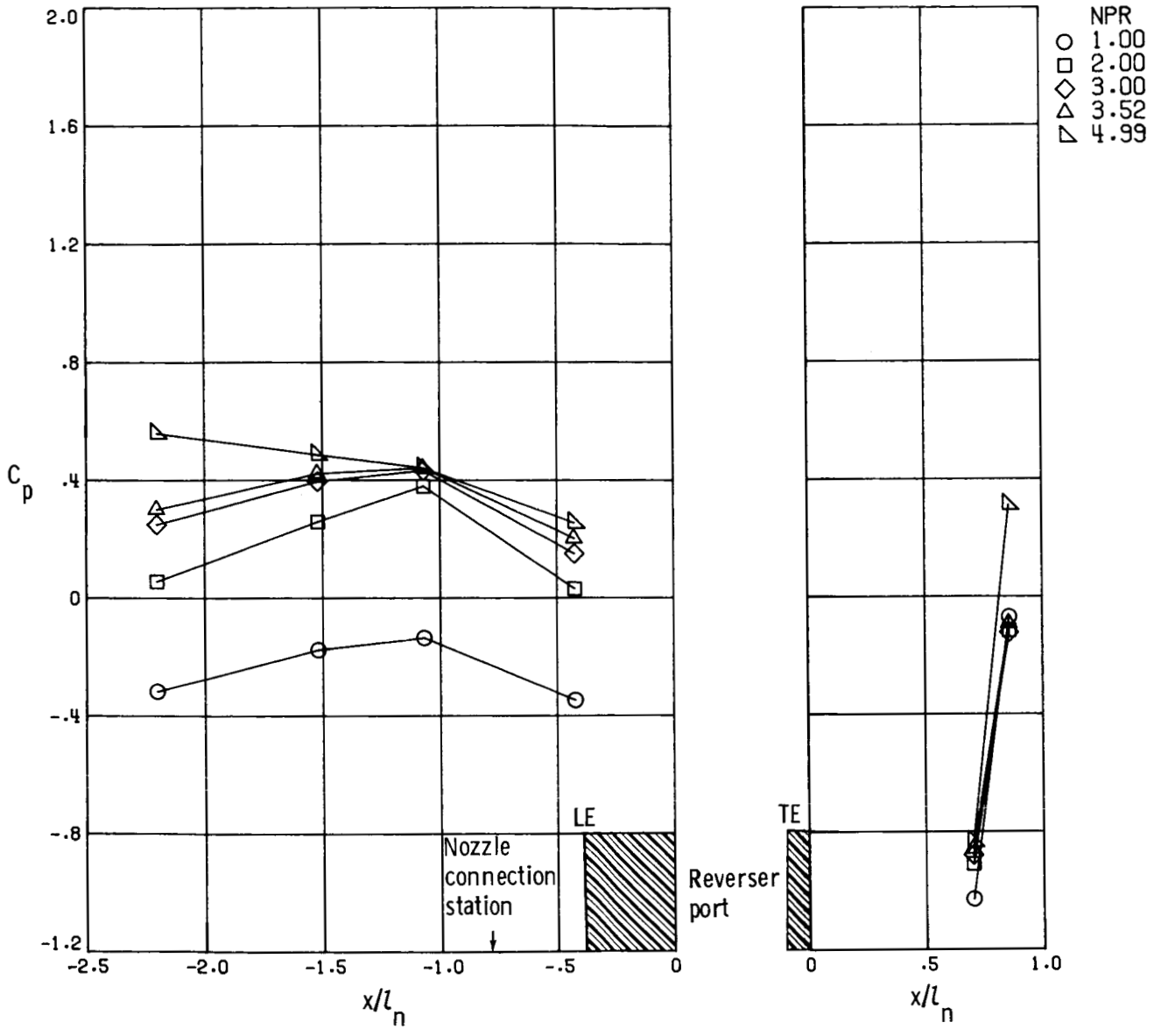

(a) M = 0.60.

Figure 44.- External pressure distribution of 130° reverser-port angle nozzle.

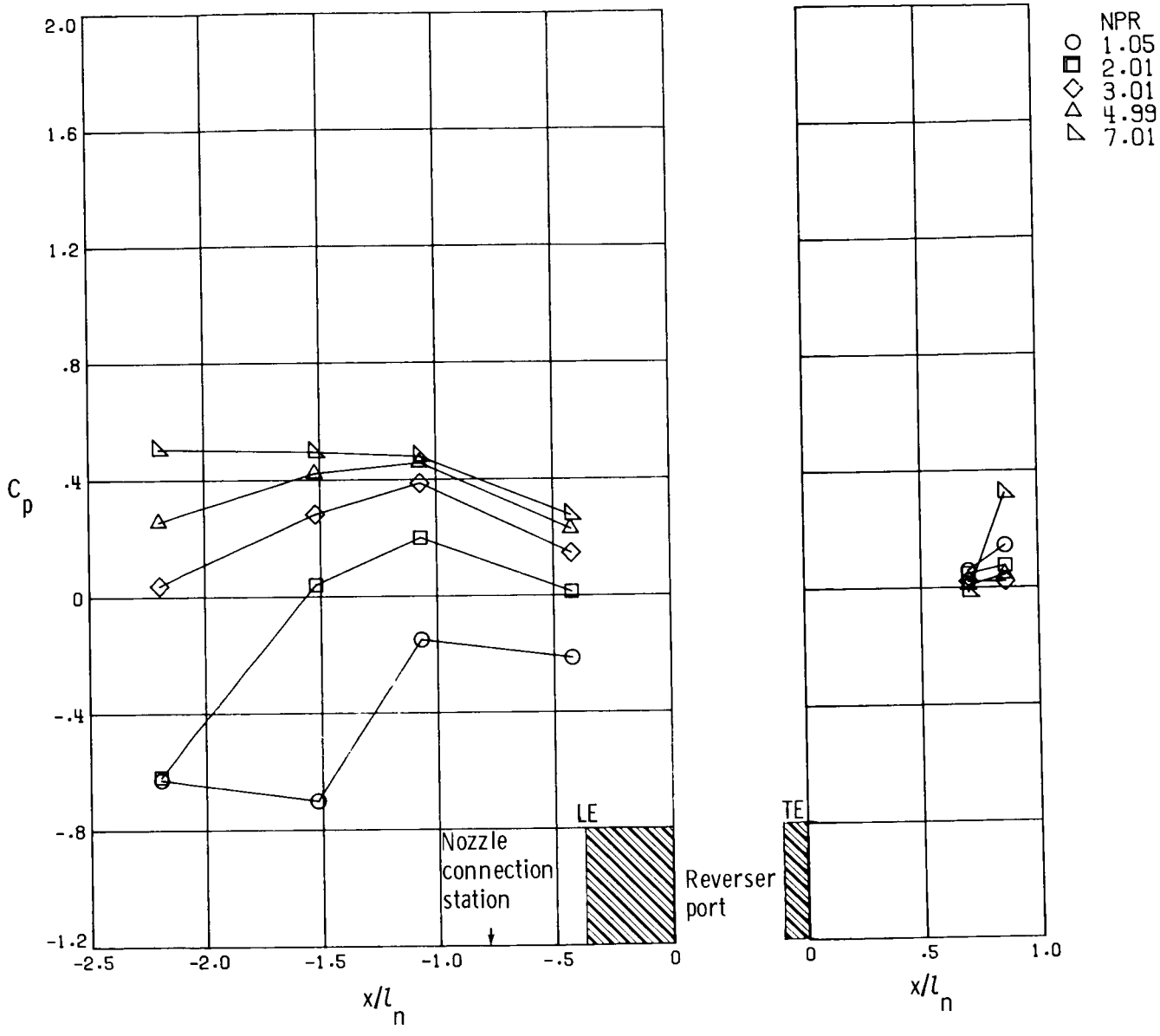

(b) M = 0.90.

Figure 44.- Continued.

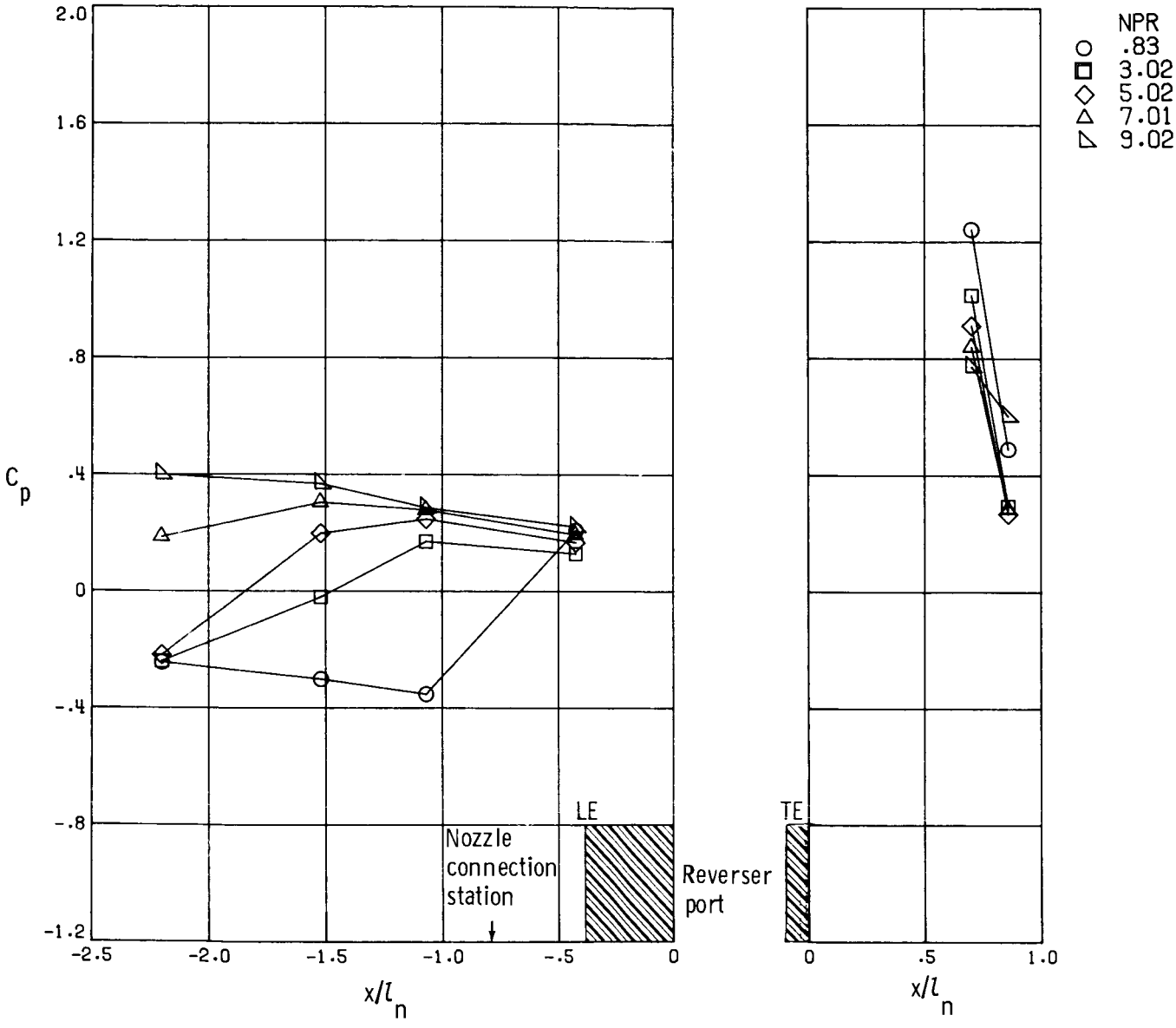

(c) M = 1.20.

Figure 44.- Concluded.

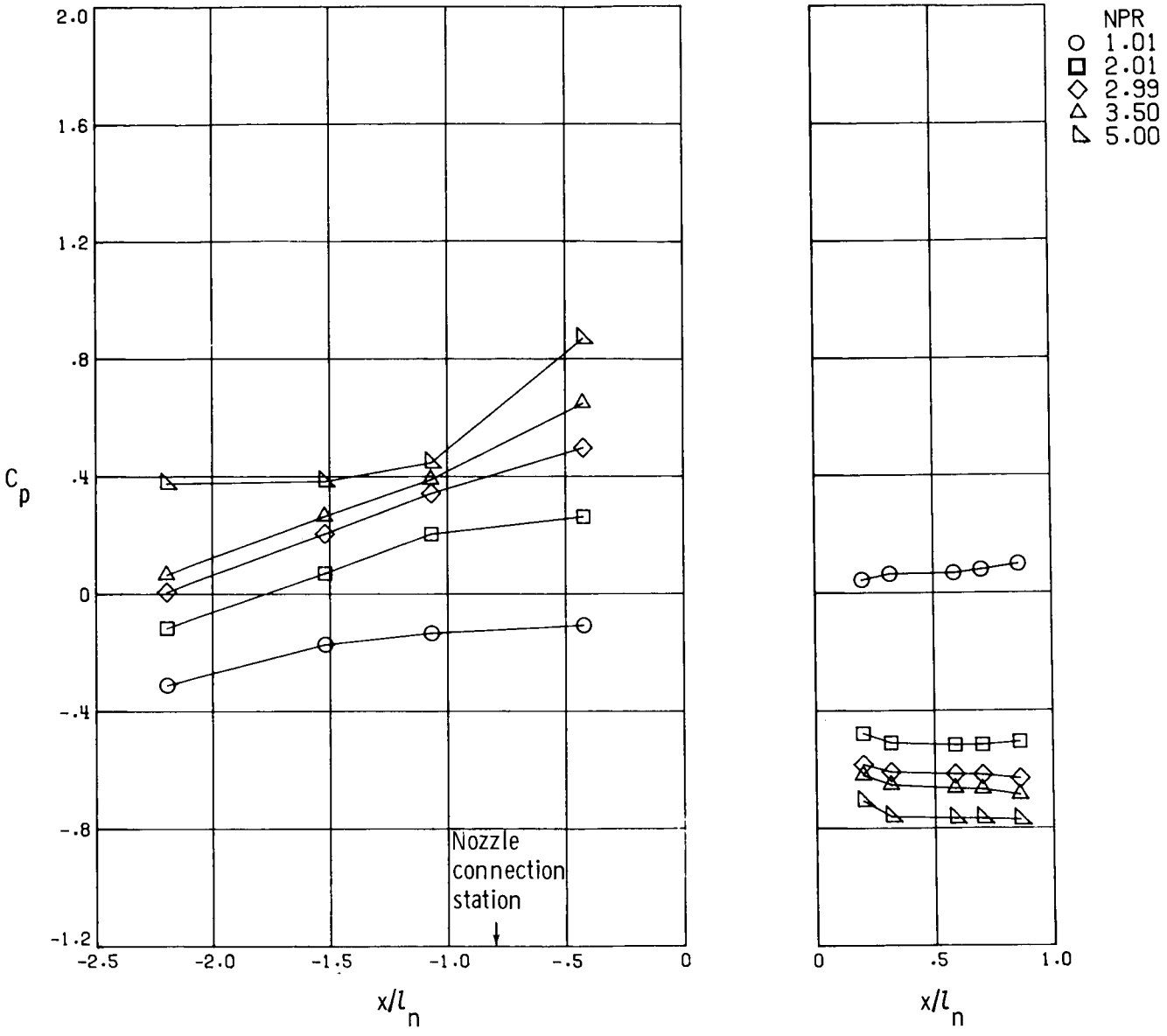

(a) M = 0.60.

Figure 45.- External pressure distribution of 110° reverser-port angle nozzle with short internal passage length.

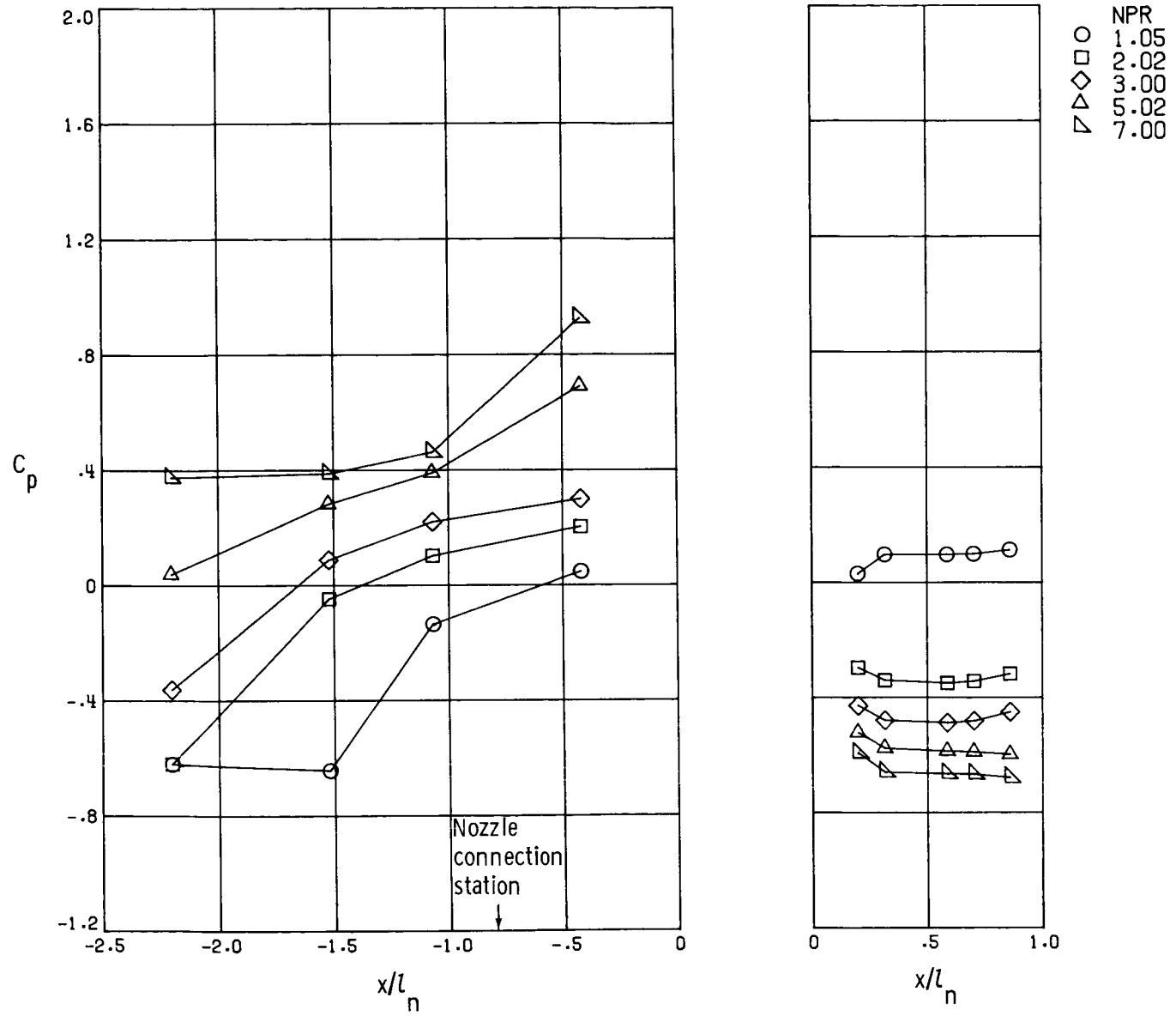

(b) M = 0.90.

Figure 45.- Continued.

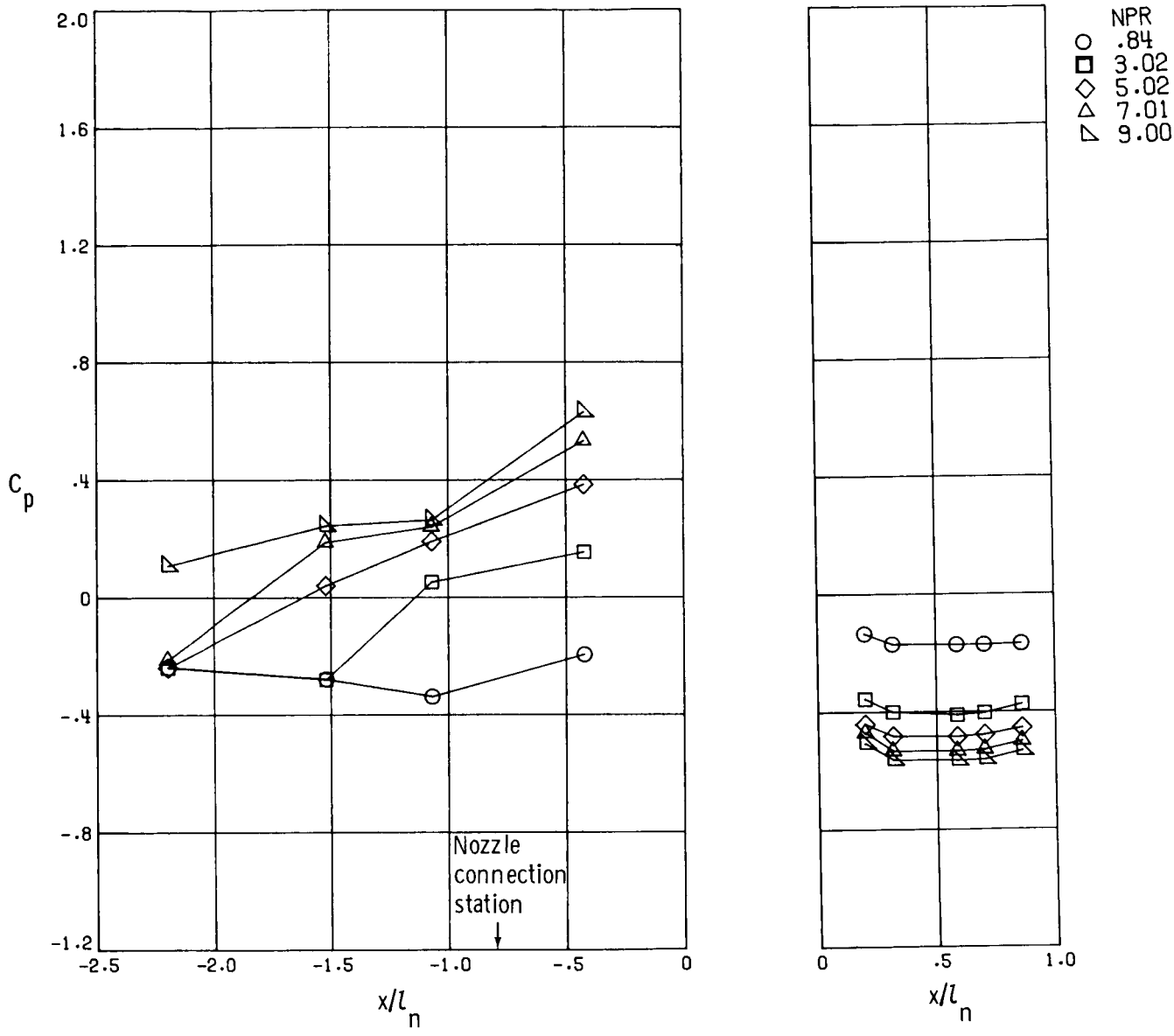

(c) M = 1.20.

Figure 45.- Concluded.

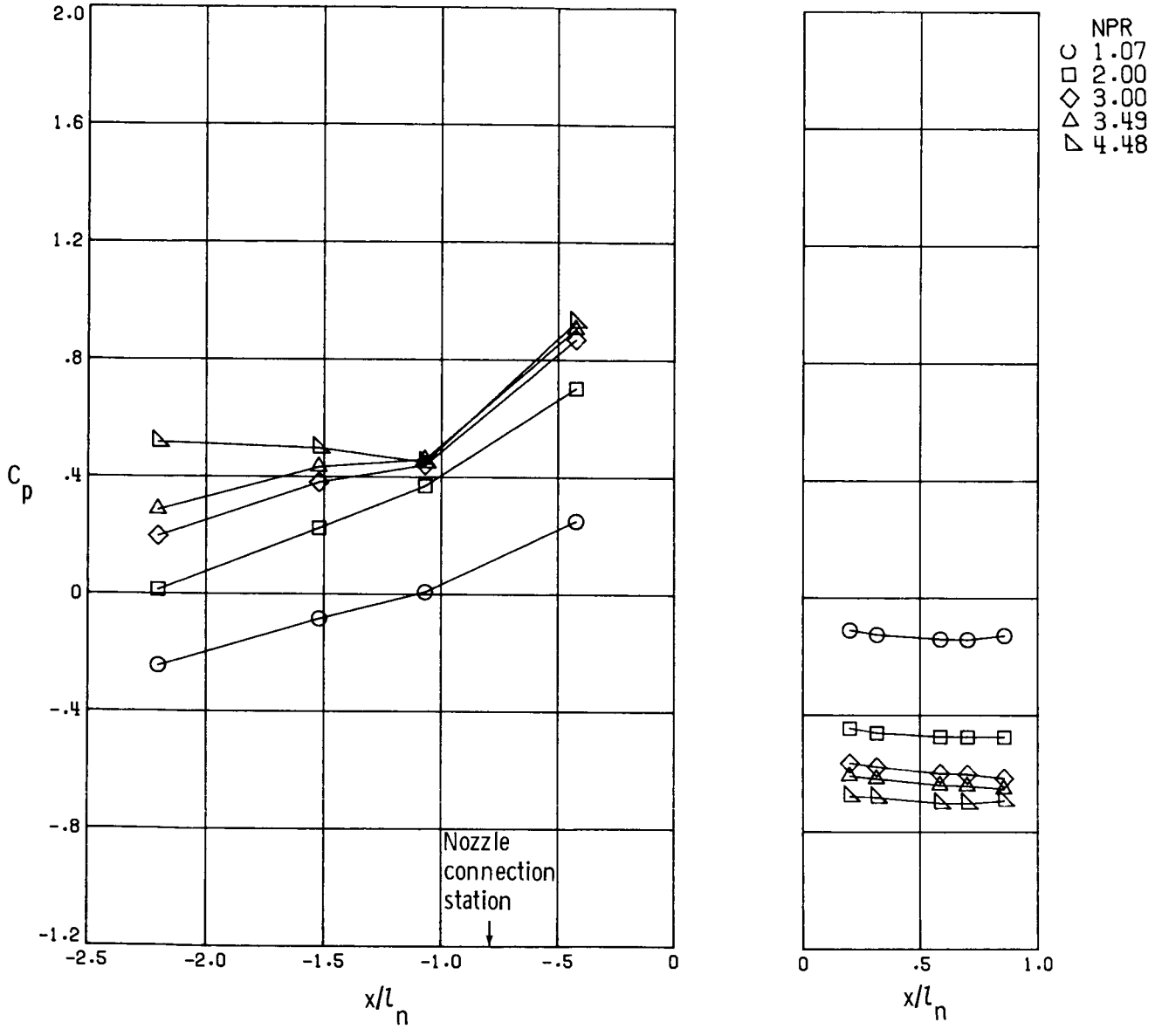

Figure 46.- External pressure distribution of 110° reverser-port angle nozzle with short internal passage length with sidewalls and aft external doors. M = 0.60.

1. Report No.	2. Government Accession No.	3. Recipient's Catalog No.
NASA TP-2306		

4. Title and Subtitle	5. Report Date
AEROPROPULSIVE CHARACTERISTICS OF NONAXISYMMETRIC-NOZZLE THRUST REVERSERS AT MACH NUMBERS FROM 0 TO 1.20	May 1984
	6. Performing Organization Code 505-43-93-07
7. Author(s) George T. Carson, Jr., Francis J. Capone, and Mary L. Mason	8. Performing Organization Report No. L-15724
	10. Work Unit No.
9. Performing Organization Name and Address NASA Langley Research Center Hampton, VA 23665	11. Contract or Grant No.
	13. Type of Report and Period Covered Technical Paper
12. Sponsoring Agency Name and Address National Aeronautics and Space Administration Washington, DC 20546	14. Sponsoring Agency Code

15. Supplementary Notes

16. Abstract

An investigation was conducted in the Langley 16-Foot Transonic Tunnel to determine the performance of nonaxisymmetric-nozzle thrust reversers installed on a generic twin-engine fighter aircraft model. Test data were obtained at static conditions and at Mach numbers from 0.15 to 1.20 with jet exhaust simulated by high pressure air. Results showed that reverse-thrust levels of greater than 50 percent at static conditions and greater than 30 percent at in-flight conditions could be achieved. Internal reverser-port passage length was found to be very important in improving reverse performance. Increasing the reverser-port passage length improved reverse-thrust performance by as much as 28 percent at static conditions and by as much as 17 percent at Mach 1.20.

17. Key Words (Suggested by Author(s))	18. Distribution Statement
Nonaxisymmetric nozzles In-flight thrust reversing Thrust vectoring	Unclassified - Unlimited Subject Category 02

19. Security Classif. (of this report)	20. Security Classif. (of this page)	21. No. of Pages	22. Price
Unclassified	Unclassified	124	A06

For sale by the National Technical Information Service, Springfield, Virginia 22161

NASA-Langley, 1

6 2 1U,A, 840518 S00161DS
DEPT OF THE AIR FORCE
ARNOLD ENG DEVELOPMENT CENTER(AFSC)
ATTN: LIBRARY/DOCUMENTS
ARNOLD AF STA TN 37389